DEVELOPMENT OF A QUADRUPOLE MASS SPECTROMETER

by

CHARLES EDWARD WOODWARD

B.S., Iowa State College
(1957)

S.M., Massachusetts Institute of Technology
(1960)

MASS. INST. OF TECHNOLOGY
JUL 24 1964
LIBRARIES

SUBMITTED IN PARTIAL FULFILLMENT OF THE

REQUIREMENTS FOR THE DEGREE OF

DOCTOR OF PHILOSOPHY

at the

MASSACHUSETTS INSTITUTE OF TECHNOLOGY

June, 1964

Signature of Author .....
Department of Electrical Engineering, May 15, 1964

Certified by .....
Thesis Supervisor

Accepted by .....
Chairman, Departmental Committee on Graduate Students

DEVELOPMENT OF A QUADRUPOLE MASS SPECTROMETER

by

CHARLES EDWARD WOODWARD

Submitted to the Department of Electrical Engineering on May 15, 1964, in partial fulfillment of the requirements for the degree of Doctor of Philosophy

ABSTRACT

The thesis project was the development of electronic circuits for a moderate-resolution quadrupole mass spectrometer intended as a flexible laboratory instrument to cover 1 to 400 amu in four ranges.

Extension of the theory of the quadrupole mass filter showed that high transverse ion momenta pose significant problems in ion collection.

The electronic circuits that supplied voltages to the mass filter were capable of 50:1 spectral range sweeps in 0.1 sec, but resolution over a wide sweep range was limited by nonlinearity in the control of the r-f voltage. Compensation reduced the nonlinearity over a 10:1 sweep range from 4% to 0.4%.

The electron-multiplier ion collector of the spectrometer was operated in a particle-detection mode to eliminate the effects of multiplier gain variations. The theory of coincidence losses in such particle-detection systems was extended to a nonparalyzable counter following a pulse-stretching amplifier. A "delay-line" ratemeter was shown to possess certain signal-to-noise advantages over the conventional R-C output circuit, but practical limitations eliminated these advantages. Pulse circuits with resolving times better than 5×10^{-3} sec were used in the particle-detection system.

Mechanical imperfections in the quadrupole lens limited spectrometer resolution to $m/\Delta m = 40$. The ultimate sensitivity was a partial pressure of 10^{-11} torr.

Thesis Supervisor: Arthur R. von Hippel
Title: Institute Professor; Professor of Electrophysics

ACKNOWLEDGEMENTS

The author wishes to express his appreciation to Professor A. R. von Hippel for his support, advice and encouragement.

Thanks are expressed to Professor C.K. Crawford for initiating and sustaining the quadrupole mass spectrometer project, as well as for designing and constructing all parts of the instrument that are characterized by the term "physical electronics."

Recognition is due Messrs. Jurii Klonizchii and Modesto Maidique for construction of some of the apparatus, to other members of the Laboratory for Insulation Research who have assisted in the project, and to those who helped prepare the manuscript: Messrs. John Mara, Douglas Nicoll, and Michael Hale, who drew many of the figures, and Miss Aina Sils, who typed the text.

TABLE OF CONTENTS

		Page
Abstract		ii
Acknowledgements		iii
List of Figures		vi
List of Tables		viii
I.	The Electric-Quadrupole Mass Spectrometer	1
	A. The mass filter	3
	B. Ion source	7
	C. Ion collector	7
II.	Theory of the Quadrupole Mass Filter	9
	A. Description of operation	9
	B. Equations of motion	9
	C. Mass-filter operation	19
	D. Design considerations	28
III.	Mass Spectrometer Construction	35
	A. Quadrupole lens	35
	B. Ion source	39
	C. Electron multiplier	40
	D. Vacuum system	46
IV.	Electronic Drive Circuits for the Mass Filter	47
	A. Circuit requirements	47
	B. Control generator	49
	C. R-f rod driver	54
	D. D-c rod driver	79
V.	Design Considerations for the Electron-Multiplier Ion Detector	84
	A. Introduction	84
	B. The electron multiplier as a current amplifier	85
	C. The electron multiplier as a particle detector	86
	D. Spectrometer output noise	90
	E. Pulse signal processing	97
	F. Linear signal processing	108

Table of Contents (cont.)

		Page
VI.	Electron-Multiplier Ion Detector	125
	A. System characteristics	125
	B. Pulse system	131
	C. Output processor	161
VII.	Mass-Spectrometer Performance	166
	A. Line shape	166
	B. Resolving power	169
	C. Mass spectra	171
VIII.	Conclusions	175
	A. Summary of work	175
	B. Suggestions for future work	178
Appendix A.	Coefficients in Series Expansion of Solutions of Mathieu's Equation	183
Appendix B.	Tank Coil Design	186
Appendix C.	Symmetric Signals in Balanced, Inductively Coupled Circuits	198
Appendix D.	Self-Checking Balance Detector Algorithm	201
Appendix E.	Pulse-System Test Apparatus	204
References		209
Biographical Note		212

LIST OF FIGURES

		Page
1.1.	The electric-quadrupole mass spectrometer.	2
2.1.	Stable ion trajectories in the mass filter.	10
2.2.	Quadrupole-mass filter electrodes.	11
2.3.	Stability diagram for quadrupole mass filter.	14
2.4.	x and y trajectories.	17
3.1.	Quadrupole lens.	36
3.2.	Ion source.	41
3.3.	Ion-source circuit diagram.	42
3.4.	Electron multiplier.	43
3.5.	Electron-multiplier structure.	44
4.1.	Block diagram of mass-filter circuits.	48
4.2.	Block diagram of control generator.	50
4.3.	Circuit diagram of control generator.	51
4.4.	Circuit diagram of r-f rod driver.	55
4.5.	Deviation of r-f to d-c ratio.	73
4.6.	Circuit diagram of d-c rod driver.	80
5.1.	Distribution in amplitude of ion-electron-multiplier output pulses.	91
5.2.	Probability distribution of pulse amplitudes.	92
5.3.	Performance of counter systems.	100
5.4.	Delay-line ratemeter.	112
5.5.	Response of delay-line ratemeter.	113
5.6.	Impulse response of ratemeter circuits.	123
6.1.	Differentiator-limiter performance.	130
6.2.	Differentiator response.	132
6.3.	Ion-detector pulse system.	133
6.4.	Electron-multiplier circuit.	135
6.5.	Electron-multiplier anode circuit.	139

List of Figures (cont.)

		Page
6.6.	Preamplifier circuit.	144
6.7.	Preamplifier performance.	147
6.8.	Interstage limiting amplifiers.	150
6.9.	Response of preamplifier-amplifier-limiter chain to test pulses.	152
6.10.	Pulse standardizer.	154
6.11.	Pulse standardizer output.	157
6.12.	Response of preamplifier-amplifier-limiter chain to electron-multiplier output pulses.	163
7.1.	Spectral line shape.	167
7.2.	Background-gas mass spectra.	172
8.1.	Proposed high-linearity rectifiers.	181
B.1.	Tuned coupling transformer circuit.	186
B.2.	Coupled-coil configuration.	193
C.1.	Rod-driver output circuit.	199
C.2.	Output circuit collapsed into simpler form.	199
D.1.	Balance-detector flow graph.	201
E.1.	Pulse-system test apparatus.	205
E.2.	Pulse baseline cleaner.	207
E.3.	Test pulse source.	208

LIST OF TABLES

		page
4.1.	Buffer-output r-f transformers.	56
4.2.	Output tank coils.	57
6.1.	Pulse-system resolving times.	160
7.1.	Relative amplitude of spectral lines.	173

I. THE ELECTRIC-QUADRUPOLE MASS SPECTROMETER

The purpose of this thesis was the development of a small mass spectrometer of modest resolving power $m/\Delta m$ (perhaps 500) but with sufficient flexibility to permit it to be easily applied to such diverse problems as the thermal decomposition of dielectric materials and the study of electron-ionization cross sections of the vapor states of solids. The instrument was to be capable of sweeping wide spectral ranges (up to 50:1) in relatively short time (as little as 0.1 second). An electric-quadrupole mass filter (which had been used by previous workers only in feasibility studies and as a background-gas analyzer) was selected for this application and incorporated into a complete spectrometer system as shown in Fig. 1.1. Ions from an ion source are mass selected by the filter and then detected by an ion collector. The mass spectrum is recorded on an oscilloscope or other recording device.

This thesis was part of a joint project with Professor C.K. Crawford. Those parts of the spectrometer involving physical electronics (e.g., the ion source, quadrupole lens, ion collector, and vacuum system) were the responsibility of Professor Crawford; the associated electronic circuits were the responsibility of the author.

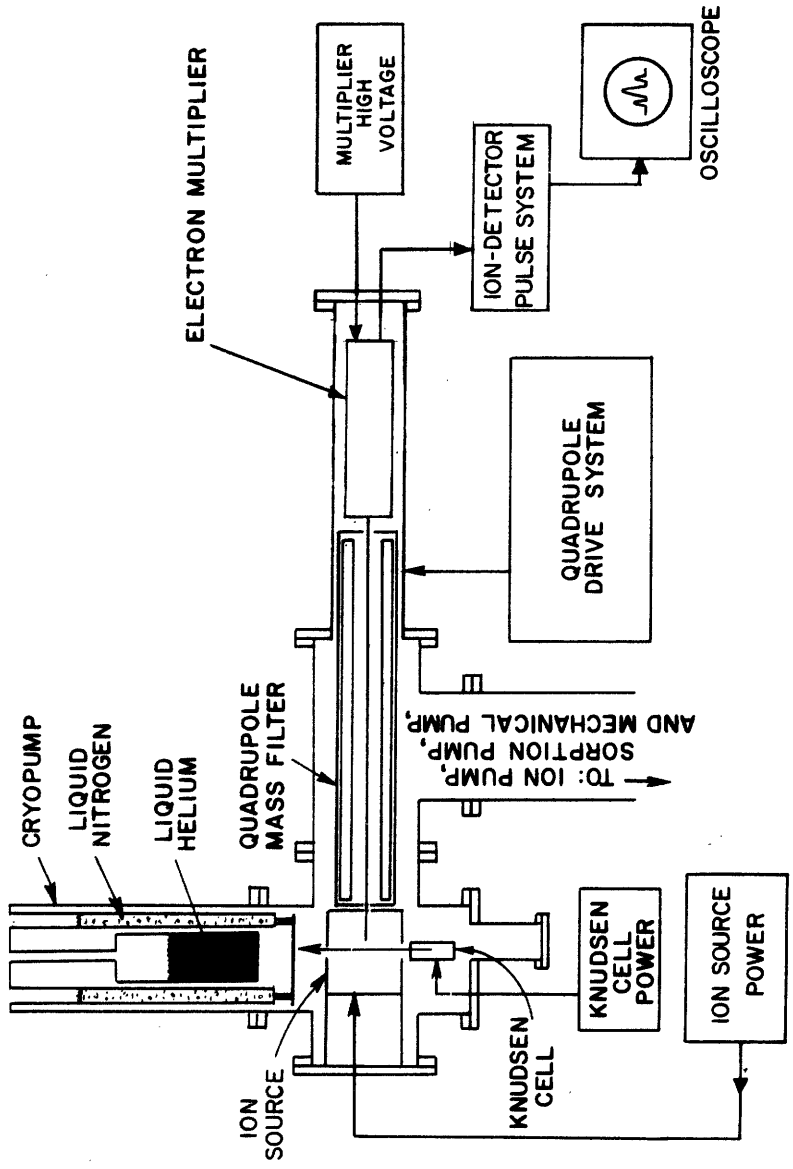

Fig. 1.1. The electric-quadrupole mass spectrometer.

A. The Mass Filter

Principles of Operation

The mass-separation element of the spectrometer is the electric-quadrupole mass filter invented by Paul and his co-workers at Bonn University.[1-3] It consists of four long, parallel cylindrical electrodes, usually circular rods, with d-c and r-f voltages applied. Ions to be mass selected are injected along the axis of the electrode assembly. By a proper choice of applied voltages, ions in a specified mass-to-charge-ratio range (the pass band of the filter) traverse the quadrupole lens and are collected at the output end; other mass-to-charge-ratio ions are deflected sidewise. For operation as a mass spectrometer, the electrode voltages are varied so as to sweep out a mass spectrum as a function of time.

The mechanical precision of the quadrupole lens sets an upper limit on resolving power, but the precision of the quadrupole voltages is the practical limitation on the resolving power of a wide-range instrument. A major part of this thesis work was the development of circuits to provide precise voltages over wide mass-spectral ranges.

Comparison with other Mass Filters

Any new mass spectrometer has to compete with existing ones. While many different types exist, only two have gained wide acceptance as laboratory instruments: the magnetic-deflection

spectrometer (single or double focussing), and the time-of-flight spectrometer, which operates by measuring the times required for isoenergetic ions to traverse a drift tube.

The magnetic-deflection and electric-quadrupole instruments use dispersion in space: All ions except those of the desired m/e ratio are discarded at some location other then the ion collector. In principle these two types of mass filters are interchangeable; the quadrupole could be replaced by a magnetic sector. The time-of-flight, in contrast, uses dispersion in time: All ions reach the collector; distinction is made by arrival time.

The great advantage of a time-of-flight instrument is that each mass spectrum is obtained in a short time (100 μsec in one commercial instrument). Hence spectra may be taken at a high rate (10^4/sec) and rapidly change spectra, as from fast chemical reactions, observed. On the other hand, because the source gas is ionized in a low duty cycle (0.25 μsec per 100 sec collecting time), the effective sensitivity is lower than that of a spatial-filter instrument. This "sampling in time" also makes impractical experiments with modulated ion beams. Finally, at least at the present state of the art, the time-of-flight mass spectrometer has a resolution too low to permit distinction between masses differing by a fraction of a mass unit.

If one compares the two spatial-filter instruments in resolving power, the severe requirements on mechanical tolerances of the

quadrupole filter probably make it inferior. Resolving power up to $m/\Delta m = 8000$ has been achieved with great difficulty with the quadrupole,[4,*] while 500,000 has been reported for a magnetic instrument.[5] Commercial double-focussing magnetic instruments offer resolutions of 15,000, a value beyond the capability of a practical analytical-laboratory quadrupole instrument.

At high background-gas pressure the quadrupole may be potentially superior in resolution because collisions of ions with background gas in the magnetic filter disturb the orbits and cause resolution degredation ("pressure broadening"). In the quadrupole filter such collisions are less disturbing; an ion that should be rejected still has an unstable orbit after collision, and will be deflected to the side of the remaining length of the filter.[6,7]

A potential advantage of the quadrupole instrument in some applications is ease of resolution adjustment. In a magnetic filter a mechanical adjustment of the slit widths is required; in the quadrupole filter only a simple electrical adjustment. In fact, in the instrument described in this thesis, it is possible to change resolution systematically while sweeping a mass spectrum.

---

* In this as in all other work at Bonn resolution is based on full line width at half maximum amplitude, which yields numerical values at least twice as high as from the more usual definitions based on line width near the base. For a better comparison with other instruments, all resolving powers reported by the Bonn group have been divided by 2 when used in this thesis. This has involved appropriate modification of a number of equations in the theory of the mass filter.

The quadrupole filter is extremely tolerant of the axial momentum of entering ions, requiring only that it be below some limiting value that ensures the ions stay in the filter long enough for mass selection. In a practical instrument this usually means an axial momentum corresponding to 100 volts or less. The instrument is considerably more demanding with respect to transverse momentum (typical upper limit < 1 volt). However, in contrast to incorrect momenta in a magnetic filter, a transverse momentum even in excess of the limit degrades not the instrument resolution, but only the transmitted intensity. The quadrupole filter, in short, is more tolerant with respect to entrance conditions than the single-focussing magnetic instrument.

The absence of magnetic fields in the quadrupole filter permits greater freedom in source design, e.g., permits experiments with low-energy electrons, and makes it easier to use electron multipliers as ion detectors.

The final test of the quadrupole mass spectrometer is the market place. The question is: Can a quadrupole instrument be manufactured with a resolution comparable to that of a large single-focussing magnetic spectrometer (500 to 1000), but smaller and more convenient to use and not higher in cost? Results in the literature and in this thesis seem to give an affirmative answer to all but the last question. Cost comparison must await full commercial development of a quadrupole mass spectrometer of

analytical quality.

B. Ion Source

A conventional electron-bombardment source serves as ion source for the spectrometer. The material under study is vaporized in a Knudsen-cell oven and ionized by a transverse electron beam. Ions are extracted from the source region and injected into the mass filter.

Much more elaborate sources have been built,[8] but were not used in the work of this thesis.

C. Ion Collector

The ion current from the quadrupole filter could be collected by a Faraday cup at the exit and measured by an electrometer. In that case instrument sensitivity and response speed are limited by the electrometer with its large time constant (order of seconds) given by input resistance and stray capacitance. The sensitivity limitation is tolerable, but the response speed, since the instrument should allow sweeps of mass spectral lines in milliseconds, is not. The slow response can be overcome by use of an electron multiplier as the ion collector. Its gain of more than 10^5 can yield an output large enough to drive a recording device directly and its bandwidth of more than 100 Mc is high enough for any response speed.

Unfortunately, the electron multiplier has its own drawbacks. The gain suffers slow degredation because of dynode surface con-

tamination, and, even more serious, the yield of the first dynode depends on ion species, so apparent mass discrimination may be introduced. These difficulties can be overcome, at least for the lower values of ion current, by using the multiplier not as a current amplifier but as a single-particle detector: Each ion incident on the first dynode produces a pulse of output current that is amplified and either counted by digital devices or standardized in amplitude and width. The average current of the standard pulses is a signal proportional to the input ion current.

The maximum ion current, or count rate, that can be handled by a particle-detecting electron-multiplier system is limited by the response speed of the pulse-processing circuits. A major part of the work of this thesis was the development of an analog-output system handling rates up to 5×10^6 ions/sec.

Because the ion currents detected by a particle-detector system are necessarily small, shot noise is a significant problem. It is therefore important to choose an output system that will provide a maximum ratio of signal to noise. Work in this thesis showed that the conventional resistance-capacitance low-pass filter is the best practical output network, although - idealized - some other linear systems provide slightly superior performance.

II. THEORY OF THE QUADRUPOLE MASS FILTER

A. Description of Operation

In principle, the mass filter operates as follows: Ions are injected through an entrance aperture (Fig. 2.1) along the axis of a quadrupole lens (four parallel cylindrical electrodes; cf. Fig. 2.2) to which d-c and r-f voltages are applied. Ions with mass-to-charge ratios outside a passband determined by electric-field specifications have unstable orbits and are ejected from the sides of the filter. Ions with masses inside the passband follow complicated but bounded trajectories through the quadrupole to an ion collector at the output (Fig. 2.1). The exact trajectory of an ion depends upon entrance conditions, but for a suitably limited entrance displacement and velocity, all trajectory envelopes lie within the quadrupole dimensions (y direction, Fig. 2.1). However, it is possible that some trajectories exceed filter dimensions, so that some ions of passband mass are lost by collision with the electrodes (x direction, Fig. 2.1).

Some of the theory necessary for the design of a quadrupole mass filter will be developed in this chapter.

B. Equations of Motion

In idealized form the quadrupole mass filter consists of four parallel electrodes of hyperbolic cross section, to which voltages

$$\phi_o = \pm (U + V \cos \omega t) \qquad (2.1)$$

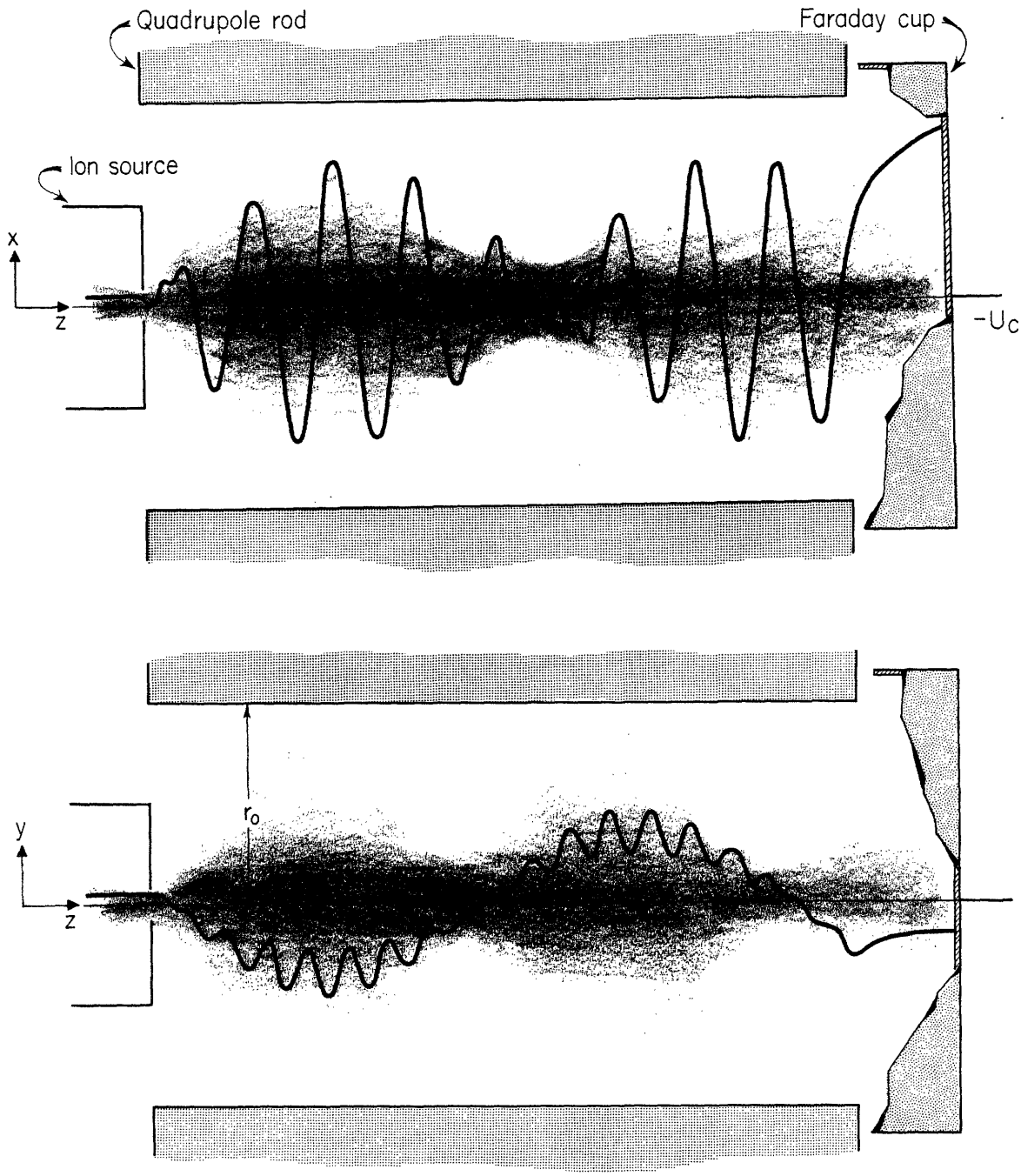

Fig. 2.1. Stable ion trajectories in the mass filter. Typical trajectories (for $\beta_x = 0.9, \beta_y = 0.13$) plotted from the approximations of Eqs. 2.18 and 2.20, with the assumption of an abruptly terminated quadrupole field. Shaded areas indicate distribution of trajectory envelopes for random input conditions.

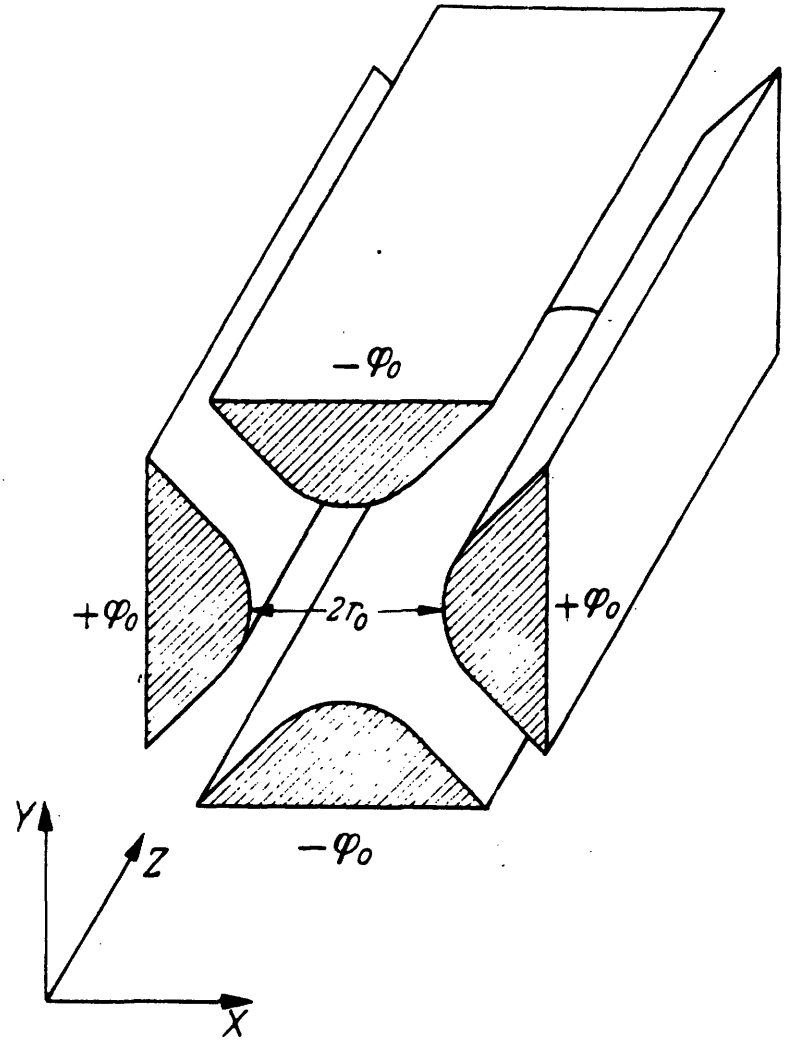

Fig. 2.2. Quadrupole mass filter electrodes. From Paul, et al.[6]

are applied (Fig. 2.2).* The potential at any point in the field region is

$$\phi = \frac{x^2 - y^2}{r_o^2} (U + V \cos \omega t), \tag{2.2}$$

where r_o designates the inscribed radius of the hyperbolic electrodes. The equations of motion for an ion of charge e, mass m are

$$m\ddot{x} + \frac{2ex}{r_o^2} (U + V \cos \omega t) = 0, \tag{2.3}$$

$$m\ddot{y} - \frac{2ey}{r_o^2} (U + V \cos \omega t) = 0, \tag{2.4}$$

$$m\ddot{z} = 0. \tag{2.5}$$

Mathieu's Equation

An ion injected along the z direction will continue with its velocity in that direction unchanged (Eq. 2.5). In the x-y plane, however, the ion trajectory is more complicated and described by Mathieu's equation: The transformations

$$\omega t = 2\xi , \tag{2.6}$$

$$a = \frac{8eU}{mr_o^2\omega^2} , \tag{2.7}$$

$$q = \frac{4eV}{mr_o^2\omega^2} , \tag{2.8}$$

---

* Cf. Ref. 6. This entire chapter is based extensively on this paper; hence statements made without proof refer to it.

reduce the x-y equations of motion to

$$\frac{d^2x}{d\xi^2} + (a + 2q \cos 2\xi)\, x = 0 \qquad (2.9)$$

and

$$\frac{d^2y}{d\xi^2} - (a + 2q \cos 2\xi)\, y = 0, \qquad (2.10)$$

which correspond, except for signs, to the standard form of the Mathieu equation:[9]

$$\frac{d^2x}{d\xi^2} + (a - 2q \cos 2\xi)\, x = 0. \qquad (2.11)$$

All solutions to any of the three preceding equations can be represented in the form

$$x = \alpha' e^{\mu\xi} \sum_{-\infty}^{\infty} c_{2m} e^{j2m\xi} + \alpha'' e^{-\mu\xi} \sum_{-\infty}^{\infty} c_{2m} e^{-j2m\xi} \quad . \qquad (2.12)$$

The solutions are stable (i.e., bounded) for all initial conditions only for $\mu = j\beta$ (purely imaginary), with β not an integer.

The characteristic exponent (μ) depends only on a and q, i.e., is independent of initial conditions. The range of values for a and q for which the solution is stable for each of the Eqs. 2.9 and 2.10 can be plotted as a sequence of regions in the a-q plane; only the one closest to the origin is of interest for mass-filter operation. The operating point (a,q) must lie in a stable region of the a-q plane for both the x and y equations. The combined region of stability is the curvilinear triangle in Fig. 2.3.

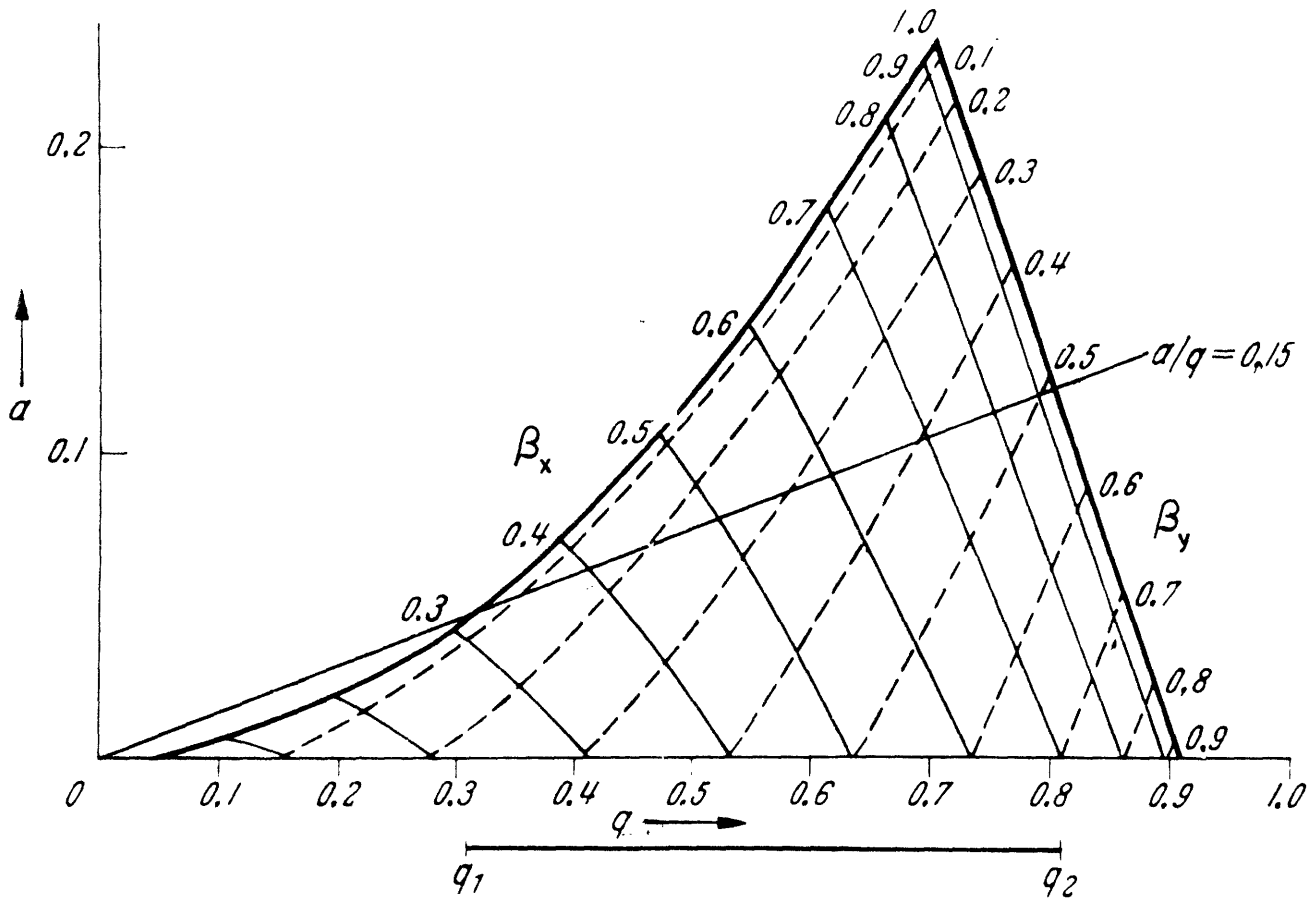

Fig. 2.3. Stability diagram for quadrupole mass filter. From Paul, et al.[6]

If the field specifications (r_o, ω, U, and V) are held constant, the locus of operating points on the stability diagram as a function of mass is a straight line through the origin (cf. Fig. 2.3). The distance from the origin on this locus varies inversely with ion mass. The ion trajectories will be stable only for the range of masses with operating points lying within the stability region - the passband of the filter. As the ratio of d-c to r-f voltage, U/V, is increased, the slope of the a/q line increases, and the range of the stable interval is reduced, until finally ions of only one mass have stable trajectories; all others are ejected sidewise.

Particle Orbits

Within the stable region the solutions of the equations of motion have the form

$$x \text{ or } y = \alpha_I \sum_{-\infty}^{\infty} c_{2m} \cos(m + \tfrac{\beta}{2})\omega t + \alpha_{II} \sum_{-\infty}^{\infty} c_{2m} \sin(m + \tfrac{\beta}{2})\omega t$$

$$= A \sum_{-\infty}^{\infty} c_{2m} \cos\left[(m + \tfrac{\beta}{2})\omega t + \theta\right], \qquad (2.13)$$

where α_I and α_{II} or A and θ are determined by initial conditions and c_{2m} and β by a and q, hence by ion mass and field conditions.

Some insight into the particle trajectories is gained by considering the truncated form of the series Eq. 2.13: by convention $c_o = 1$,

$$x \text{ or } y = A\left\{\cos\left(\frac{\beta}{2}\omega t + \theta\right) + c_{-2}\cos\left[\left(-1 + \frac{\beta}{2}\right)\omega t + \theta\right] + c_2\cos\left[\left(1 + \frac{\beta}{2}\right)\omega t + \theta\right] + \cdots\right\} . \quad (2.14)$$

For $y(t)$ a continued-fraction expansion of the coefficients (Appendix A) gives

$$c_{-2} \approx c_2 \approx -\frac{q}{(2 + \beta_y)^2 + a} , \quad (2.15)$$

and Eq. 2.14 may be rewritten as

$$y(t) \approx A_y \cos\left(\frac{\beta_y}{2}\omega t + \theta_y\right)\left[1 + 2c_2 \cos \omega t\right] . \quad (2.16)$$

Near the vertex of the stability diagram of Fig. 2.3, $\beta_y \ll 1$, $a \approx 0.23$, or

$$c_2 \approx -\frac{q}{4} . \quad (2.17)$$

thus

$$y(t) \approx A_y \cos\left(\frac{\beta_y}{2}\omega t + \theta_y\right)\left[1 - \frac{q}{2}\cos \omega t\right] . \quad (2.18)$$

This equation, also obtained from direct physical reasoning by Brubaker,[10] predicts that the motion of the ion in the y direction will be a low-frequency sine wave to which the second term adds a moderate perturbation at the frequency of the quadrupole drive. This is precisely the form of solution shown in Fig. 2.4b obtained by numerical integration of the original force equation (Eq. 2.10).[10]

A somewhat different approach must be taken for the approximate solution of the x equation because $1 - \beta_x$ is $\ll 1$ for operation near the vertex (cf. Fig. 2.3). Only the first two terms of

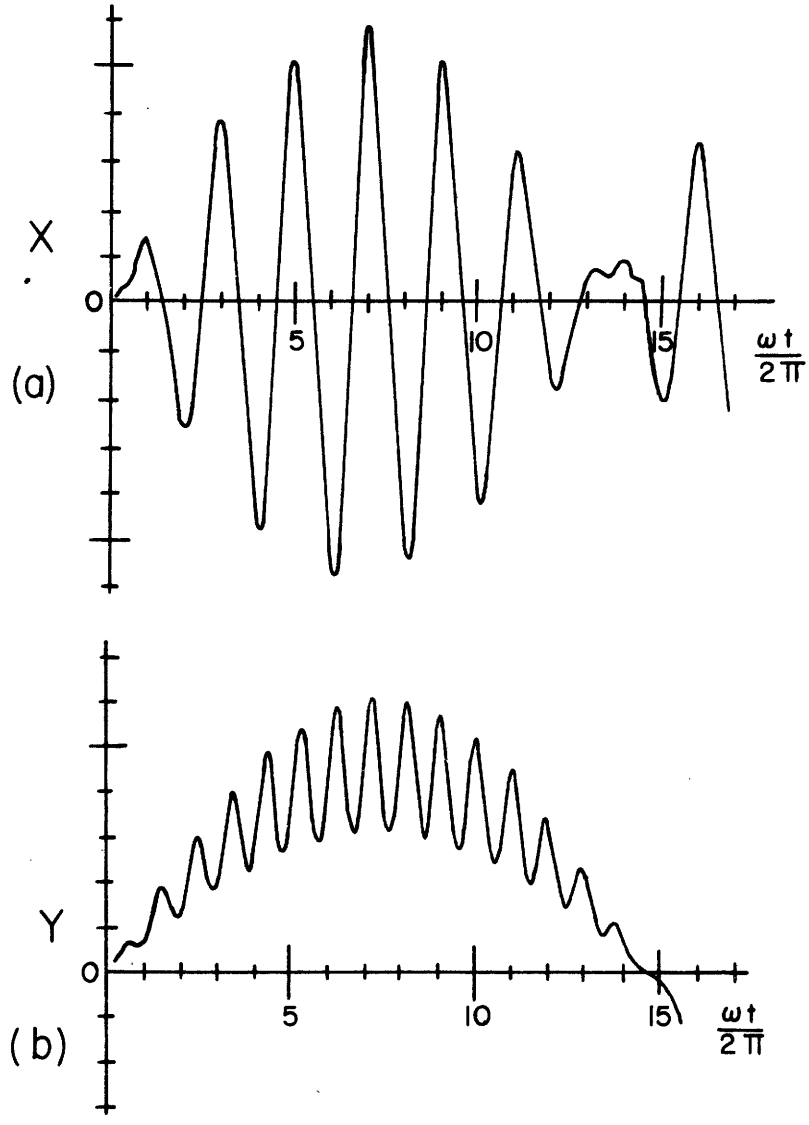

Fig. 2.4. x and y trajectories for a = 0.231, q = 0.7038.
After Brubaker.[10]

Eq. 2.14 are used because (as shown in Appendix A) c_2 is small. Thus

$$x(t) \approx A_x \left\{ \cos \left[\left(\frac{1}{2} - \frac{1 - \beta_x}{2} \right) \omega t + \theta_x \right] + c_{-2} \cos \left[\left(-\frac{1}{2} - \frac{1 - \beta_x}{2} \right) \omega t + \theta_x \right] \right\},$$

i.e.,

$$x(t) \approx A_x \left\{ (1 + c_{-2}) \cos \frac{\omega}{2} t \cos \left[\frac{1 - \beta_x}{2} \omega t - \theta_x \right] \right.$$

$$\left. + (1 - c_{-2}) \sin \frac{\omega}{2} t \sin \left[\frac{1 - \beta_x}{2} \omega t - \theta_x \right] \right\} . \qquad (2.19)$$

Because $c_{-2} \approx 1$ (Appendix A), the first term of Eq. 2.19 dominates:

$$x(t) \approx A_x' \cos \frac{\omega}{2} t \cos \left[\frac{1 - \beta_x}{2} \omega t - \theta_x \right] . \qquad (2.20)$$

The motion of the ion in the x direction is a sine wave at half the quadrupole drive frequency (a subharmonic oscillation) modulated by a low-frequency sinusoid. An exact numerical solution is shown in Fig. 2.4a.

For any individual ion the trajectory in the x-z or y-z plane has the same form as the trajectory plotted against time, because

$$z = \dot{z}(t - t_o), \qquad (2.21)$$

where $\dot{z}$ is the z-direction velocity and t_o the entrance time. The description of all possible spatial trajectories for a given ion species and set of quadrupole voltages is difficult, because the individual trajectories are a function of 5 random variables: two input displacements, two input velocities, and the input time. However,

if $\dot{z}$ is constant, all will be contained within constant-wavelength sinusoidal envelopes. These envelopes can shift in position, but are constrained to low amplitude at the quadrupole entrance aperture and so at subsequent half wavelengths. For example, the input ensemble consisting of ions entering on the axis with finite velocity has a generalized x-z trajectory of the form

$$x(z) \approx A_x' \cos \frac{\omega}{2} \left(t_o + \frac{z}{\dot{z}}\right) \sin \frac{(1 - \beta_x)\omega}{2\dot{z}} z \ , \qquad (2.22)$$

which has envelope nodes at $z = \left[2\pi\dot{z}/(1 - \beta_x)\omega\right]n$, where n is an integer. There exist, then, standing waves of ion-trajectory amplitudes. The range of possible envelopes for one particular set of operating conditions (i.e., one set of a, q values) is indicated by the shaded areas of Fig. 2.1.

C. Mass-Filter Operation

Mass Spectra

A spectrum is swept by variation of one or more electrical parameters. For example, with voltages U and V constant, change of frequency moves the operating point for any specific mass m along a straight line that passes through the origin and intercepts a section of the stability region (cf. Fig. 2.3). The distance from the origin varies inversely with frequency. Increase of frequency causes the operating points of a sequence of decreasing masses to traverse the stability region and the corresponding ions to pass through the filter.

If frequency is held constant and the voltages U and V are varied simultaneously so that their ratio is constant (γ), a straight line through the origin is again traversed, this time with the distance from the origin proportional to the voltage. Increase of voltage makes a sequence of increasing masses traverse the stable region and pass through the filter.

Fractional Transmission

In the discussion above it was assumed that all ions on "stable" orbits traverse the mass filter and are collected at the exit end, while those with "unstable" orbits are ejected. This is not precisely true; some ions may have orbits which, while nominally stable, are so large that they extend beyond the electrodes (cf. Fig. 2.1, x-direction trajectory). Such ions will be lost from the filter.

The exact ion trajectory depends both on the operating point in the a-q diagram and initial conditions. For suitably limited entrance conditions there will be a section well within the stability region for which all ions, regardless of individual entrance conditions, describe orbits in the confines of the mass filter (condition of "unity transmission"; Paul's Region I). In the remainder of the stability region ions will be either transmitted or lost, depending on the size of the initial-condition-determined orbit (condition of "fractional transmission"; Paul's Region II). If the mass-spectrum locus line traverses the inner section of the stability

region the resulting mass lines are trapezoidal in shape, the flat top corresponding to "unity transmission," the sloping sides to "fractional transmission." However, if the locus line crosses the stability region near the vertex, above the inner section, operation is always under conditions of "fractional transmission" and the mass lines are triangular in shape.

Resolution

If the sides of the stability region of Fig. 2.3 are regarded as straight lines, a simple relation can be found between the mass range for stable ion orbits, the passband Δm, and the mass m corresponding to the center of the stability region:

$$\frac{m}{\Delta m} = \frac{0.178}{0.23699 - a_{0.706}} \quad ; \qquad (2.23)$$

$a_{0.706}$ is the ordinate of the mass line in the stability diagram for q = 0.706. In terms of mass-spectrometer operation this is a resolution equation, with line width Δm measured at the base of the mass line.*

Maximum Orbit Size

For any given set of entrance conditions - displacement and velocity - the ion trajectory depends upon the phase of the r-f quadrupole voltage at the instant of ion entrance. When all possible entrance phase angles are considered, the maximum x or y displace-

---

* Cf. footnote on page 5.

ment of the ion, x_m or y_m, for either injection parallel to the axis at a fixed displacement x_o or y_o, or injection at the axis with a radial velocity $\dot{x}_o$ or $\dot{y}_o$, varies inversely as $1 - \beta_x$ or β_y, respectively. If straight-line approximations are made for the constant-β lines in the stability diagram (Fig. 2.3), the maximum displacements can be expressed in terms of the resolving power of Eq. 2.23:

$$\left\{\begin{matrix} x_m \\ \text{or} \\ y_m \end{matrix}\right\} < \left\{\begin{matrix} x_o \\ \text{or} \\ y_o \end{matrix}\right\} \quad 2.5\sqrt{\frac{m}{\Delta m}} \ , \qquad (2.24)$$

$$\left\{\begin{matrix} x_m \\ \text{or} \\ y_m \end{matrix}\right\} < \left\{\begin{matrix} \dot{x}_o \\ \text{or} \\ \dot{y}_o \end{matrix}\right\} \quad \frac{9}{\omega}\sqrt{\frac{m}{\Delta m}} \ . \qquad (2.25)$$

Since for unity transmission all ions must have maximum amplitudes less than r_o, the inscribed radius of the hyperbolic electrodes, Eqs. 2.24 and 2.25 can be used to postulate maximum input displacement and velocity.

Transverse Exit Velocity

If the ion collector of the mass spectrometer is a sufficiently large Faraday cup placed near the end of the mass filter, it will collect almost all the ions coming out of the filter even if they have high transverse exit velocities. On the other hand, if the ion collector is the relatively small first dynode of a commercial elec-

tron multiplier placed some distance from the end of the filter, ions with high transverse exit velocities may not be collected. This lowers apparent mass-filter transmission, and, if the exit-velocity effect is mass selective, can produce false ion-abundance ratios. The transverse exit velocities are therefore of some interest.

The maximum exit transverse velocity is just the maximum transverse velocity of the ion within the mass filter and can be estimated from the approximate trajectories (Eqs. 2.18 and 2.20). These can be regarded as high-frequency (ω or $\omega/2$) sinusoids with slowly varying amplitudes. Differentiation of the high-frequency part of Eq. 2.18 gives for the velocity

$$\dot{y}(t) \approx A_y \frac{q\omega}{2} \cos\left(\frac{\beta_y}{2}\omega t + \theta_y\right) \sin \omega t \ ,$$

and if a displacement amplitude y_m is assumed, the velocity amplitude is

$$\dot{y}_m \approx \frac{y_m \omega q}{2 + q} \ . \tag{2.26}$$

Differentiation of Eq. 2.20 for the x direction similarly gives

$$\dot{x}_m \approx \frac{x_m \omega}{2} \ . \tag{2.27}$$

Because $q \lesssim 0.7$ (cf. Fig. 2.3), the velocity amplitude in the y direction is about half that in the x direction (under the assumption of the same displacement amplitude). For the most pessimistic performance characteristic one need, therefore, consider only

the x-direction motion.

Maximum velocity amplitude occurs when displacement amplitude is a maximum. It must therefore be obtained separately for each of the three limiting values of displacement:

(1) In fractional-transmission operation ions with orbits larger than electrode boundaries are lost; the maximum displacement amplitude of those that remain is r_o. Thus the velocity amplitude of Eq. 2.27 can be squared and express as a transverse "voltage" (U_{tm}):

$$eU_{tm} \approx \frac{mr_o^2\omega^2}{8} \quad .$$

Substitution from Eq. 2.8, which relates r_o and ω to the radio-frequency voltage V, gives

$$U_{tm} \approx \frac{V}{2q} \quad . \qquad (2.28)$$

Since $q \approx 0.7$, the maximum transverse exit momentum, expressed as a voltage, is

$$U_{tm} \approx 0.7\ V \quad . \qquad (2.29)$$

(2) In unity-transmission operation the ion orbits are limited by entrance conditions. If the limit is given by input displacement confined to an aperture of diameter d, the maximum orbit amplitude is given by Eq. 2.24 and the maximum transverse exit momentum, expressed as a voltage, is

$$U_{tm} \approx \frac{0.8}{q}\left(\frac{d}{r_o}\right)^2 \frac{m}{\Delta m}\ V \quad ,$$

or, after the usual approximation for q,

$$U_{tm} \approx 1.2 \left(\frac{d}{r_o}\right)^2 \frac{m}{\Delta m} V \ . \qquad (2.30)$$

(3) If, in unity-transmission operation, maximum displacement results from the transverse entrance momenta of the ions, the maximum orbit amplitude is given by Eq. 2.25 and the maximum transverse exit momentum expressed as a voltage, is

$$U_{tm} \approx \frac{18\ m}{\Delta m}\ U_{to} \ , \qquad (2.31)$$

where U_{to} is the voltage corresponding to the transverse entrance momentum. It is to be understood that Eqs. 2.30 and 2.31 apply only when they yield a voltage lower than that of Eq. 2.29.

Heretofore only the maximum velocity occurring along the filter has been discussed. The transverse exit velocity of a particular ion depends upon its individual entrance transverse velocity, displacement, and time, and upon its transit time in the filter. The entrance time is purely random, the entrance displacement and transverse velocity are widely distributed in some statistical fashion, and even the transit time has some statistical spread because of a slight variation in entrance longitudinal velocity. A statistical treatment is necessary to determine effective output momenta.

The standing-wave amplitudes along the filter are fairly deterministic, depending most strongly upon the precisely known β for the ion species and upon longitudinal velocity. The transverse velocities at the exit, then, could be expected to rise and fall

with change in β in the scan of a mass line, as the standing wave-lenghts change and amplitude loops and nodes alternately pass the exit.

Any more precise treatment requires evaluation of probability distribution functions of all input variables. Because output displacement and velocity are directly proportional to entrance displacement or velocity, an average over entrance conditions will give the mean output velocity with respect to those variables. For example, if the input ion beam is either perfectly collimated and contained by a circular aperture, or perfectly focussed on the axis with velocities uniformly distributed to some upper limit, the mean magnitude in one direction is $4/3\pi$ of the maximum. An average over entrance time (t_o) is more difficult; the approximate solutions for the equations of motion (Eqs. 2.18 and 2.20) are not suitable for such computation (e.g., they predict infinite amplitudes as a result of certain entrance times) while more exact solutions are so complicated as to require machine calculation. For lack of a better means, the effect of entrance time can be estimated from the approximate solution for the special case of entrance on the axis (Eq. 2.22), which says output displacement (hence output velocity) is a sinusoidal function of entrance time. The mean magnitude of output velocity is then $2/\pi$ of the maximum.

The overall mean magnitude of one component of the velocity is then, by crude estimate, $8/3\pi^2$ of the maximum at that point along

the filter. If the effects of simultaneous entrance velocity and displacement, and of y-axis motion as well as x-axis, were considered, the mean would be higher.

To summarize: The absolute maximum transverse momentum of ions at the exit of the mass filter is given by whichever of Eqs. 2.29 through 2.31 applies. The actual maximum is constrained by the relative amplitude of the standing wave of ion displacements at the exit point. The mean transverse momentum must be obtained by an average over both directions of motion, all input times, and all possible input conditions; it can be assumed to be more than 30% of the maximum.

An estimate of the actual effect of the transverse exit momentum can be made by assuming that the region between the mass filter and the collector has plane-parallel geometry, with a separation of distance ℓ between the collector, assumed to be at a voltage of magnitude U_c, and the mass-filter end plane. This is not a totally unrealistic assumption if shielding grids are placed over the output of the mass filter and input of the ion collector. The ion trajectory in the transition region is a parabola, and if the initial axial momentum is negligible, the additional transverse displacement of the ion at the collector will be

$$b = 2\ell\sqrt{\frac{U_t}{U_c}} . \qquad (2.32)$$

Because, according to Eq. 2.29, U_t can be in the low kilovolt

range, there is a need for a high collection voltage to keep the ions confined within a reasonable radius.

It should be noticed that because U_t varies with the selected mass in a voltage-swept spectrometer (Eqs. 2.29 to 2.31), any loss of ions caused by b > collector radius will be mass discriminatory.

D. Design Considerations

Basic Design Equations

For convenience, the most pertinent mass-filter design equations are summarized here.

Consider a quadrupole mass filter with electrode voltage

$$\phi_o = U + V \cos 2\pi\nu t, \qquad (2.33)$$

where r_o is the inscribed radius of the electrode assembly and $\nu = \omega/2\pi$ is the r-f frequency.

The condition for transmission of a singly charged ion of mass m at infinite resolution, that is, at the peak of the stability diagram, may be reduced to

$$V = 7.219\ m\ (\text{amu})\nu^2\ (\text{Mc})\ r_o^2\ (\text{cm})\ [\text{volts}], \qquad (2.34)$$

$$U = 1.212\ m\ (\text{amu})\nu^2\ (\text{Mc})\ r_o^2\ (\text{cm})\ [\text{volts}], \qquad (2.35)$$

and

$$\frac{U}{V} = \frac{1}{5.9581} = 0.16784. \qquad (2.36)$$

Equation 2.34 is also a good approximation in the case of finite resolution. The idealized resolution, based on the width at the foot of the mass line, is approximately

$$\frac{m}{\Delta m} \simeq \frac{0.126}{0.16784 - \frac{U}{V}} \quad . \tag{2.37}$$

The maximum injection-aperture diameter, so that all ions injected with zero transverse momentum will be contained in a circle of radius r_o (the condition for unity transmission), is

$$d \simeq 0.8 \sqrt{\frac{\Delta m}{m}}\ r_o \text{ (cm) } [\text{cm}] \quad . \tag{2.38}$$

The maximum transverse injection momentum so that all ions injected on the axis of the quadrupole will be contained in a circle of radius r_o is, when squared and expressed as a voltage,

$$U_{to} \simeq \frac{V}{30}\ \frac{\Delta m}{m}\ [\text{volts}] \quad . \tag{2.39}$$

It is found experimentally that ions must remain in the mass filter $5\sqrt{m/\Delta m}$ cycles to be mass selected; the maximum axial injection momentum to ensure this is, expressed as a voltage,

$$U_a \simeq 2.1 \times 10^2 \nu^2 \text{ (Mc) } L^2 \text{ (m) m (amu) } \frac{\Delta m}{m}\ [\text{volts}] \quad , \tag{2.40}$$

where L is the length of the quadrupole lens. The maximum transverse exit momentum, expressed as a voltage, is

$$U_{tm} \simeq 0.7\ V \text{ (volts) } [\text{volts}] \quad . \tag{2.41}$$

For resolution $m/\Delta m$, the required dimensional accuracy and r-f frequency stability are $1/4\ (\Delta m/m)$; the required stability of the applied voltages is $1/2\ (\Delta m/m)$.

The r-f voltage is almost invariably taken from a tank circuit; the r-f power required is that taken by losses in the

tank, or

$$P = \frac{(2V)^2 2\pi\nu C}{2Q} \quad , \qquad (2.42)$$

where C is the end-to-end capacitance of the tank circuit, including the mass-filter rods, and Q the "Q" associated with the tank. Substitution from the resonance condition (Eq. 2.34) gives

$$P = 6.5 \times 10^{-4} \frac{C\ (pf)\ m^2\ (amu)\nu^5\ (Mc)\ r_o^4\ (cm)}{Q}\ [watts] \quad . (2.43)$$

Momentum-Limited Transmission

The limit on transverse momentum (Eq. 2.39) is usually the most restrictive entrance condition. If the limit is exceeded, transmission must be less than unity; if the limit is a function of the mass selected, transmission will also be a function of mass. Possible methods of elimination of mass-dependent transmission will be considered in this section.

Equation 2.39 with the r-f amplitude (V) eliminated by use of the resonance condition (Eq. 2.34) becomes

$$U_{to} \simeq 0.24\nu^2\ (Mc)\ r_o^2\ (cm)\Delta m\ (amu)\ [volts] \quad . \qquad (2.44)$$

The design problem is to make the right-hand side of either Eq. 2.39 or 2.44 independent of selected mass. One solution is constant V and constant $m/\Delta m$ (Eq. 2.39), which in turn requires constant U/V (Eq. 2.37). Because both voltages must be held constant, operation in this manner requires the mass range to be swept by a change of frequency.

An alternative solution, due to Professor C.K. Crawford, is constant ν and constant Δm (Eq. 2.44). The mass range is then swept by change of voltage, with a relationship between the r-f and d-c voltages of the form

$$U = \gamma V - \delta, \qquad (2.45)$$

where γ and δ are constants. Substitution in the resolution equation (Eq. 2.37) yields a line width

$$\Delta m \approx 7.94\,(0.16784 - \gamma)m + \frac{1.10\,\delta}{\nu^2\,(\mathrm{Mc})\,r_o^2\,(\mathrm{cm})} \quad \text{amu} . \qquad (2.46)$$

If $\gamma = 0.16784$, Δm is independent of the selected mass.

Both the resolution equation (Eq. 2.37 or Eq. 2.23) and the transverse-momentum equation (Eq. 2.39 or 2.25) are based on straight-line approximations to curves in the stability diagram. In addition, the latter equation is also based upon a further approximation of orbit amplitudes in terms of β_x and β_y. All these approximations fail at low values of $m/\Delta m$, although the errors from the first two tend to cancel. It would therefore be expected that Eq. 2.46 would fail at low values of resolution and that line width would not remain constant, even with $\gamma = 0.16784$.

Two advantages accrue to the constant-Δm mode of operation in addition to the elimination of transmission variation caused by input transverse ion momentum. First, it is possible to operate at lower r-f voltages for a given selected mass without losing transmission at the low end of the mass range; this saving in r-f volt-

age and power can be important at the high end. Second, the uniform width of the mass lines makes comparison of peaks somewhat easier.

Operation at constant Δm does introduce some complications, however. The maximum injection-aperture diameter for unity transmission is inversely proportional to the square root of the mass selected (Eq. 2.38). To avoid mass discrimination, the entrance aperture must be small enough so that no ions are lost because of input displacement even at the very highest resolution. This may impose a severe limit on aperture size.

Operation at constant Δm also enhances mass discrimination in loss of ions by transverse exit momenta, for in Eqs. 2.29 through 2.31 the transverse "voltage" varies as a high power of selected mass with Δm constant than with $m/\Delta m$ constant.

Mass-Filter Design

The parameters of the mass filter incorporated in the quadrupole mass spectrometer were not chosen in one clear and decisive operation, but rather evolved historically, as various filter elements were modified to yield improvements in the most economical fashion. The size of the quadrupole field was originally determined primarily by convenience of mechanical construction. Frequency-swept operation of the filter was considered, but abandoned because of formidable engineering difficulties. A fixed-frequency, voltage-swept system was used instead, with a

choice of frequencies for different mass ranges and provision for introduction of an incremental d-c voltage δ for operation at constant Δm. The r-f frequencies were chosen so that an early version of the quadrupole, using stainless-steel rods, could operate at unity transmission with Δm = 4 amu on an 0-400 amu mass range for ions with input transverse momenta corresponding to 0.9 volt, a value that encompasses 99% of Maxwellian-distributed ions of $2000^{o}K$.[11]

The stainless-steel quadrupole has been replaced by a metallized-ceramic one that has, for reasons of constructional simplicity, slightly different dimensions. The mass filter then no longer exactly complies with the original design requirements. The new quadrupole has an inscribed radius r_o = 0.807 cm and a length L = 0.51 m.

The mass filter has four ranges, 0 to 50, 100, 200, and 400 amu. The r-f frequencies are given by

$$\nu = \sqrt{\frac{50}{M}} \times 3.2103 \quad [\text{megacycles}] , \qquad (2.47)$$

where M is the upper mass of the range being used. The r-f voltage is

$$V = \frac{50}{M} \times 48.5 \text{ m} \quad [\text{volts}] , \qquad (2.48)$$

for a maximum value of 2420 v on all ranges. The maximum transverse momentum for unity transmission, expressed as a voltage, is

$$U_{to} \simeq \frac{50}{M} \times 1.6 \, \Delta m \quad [\text{volts}] . \qquad (2.49)$$

The maximum axial injection momentum for mass selection, expressed as a voltage, is

$$U_a \approx \frac{50}{M} \times 560\ \Delta m\ \text{[volts]} \quad . \tag{2.50}$$

The maximum transverse exit momentum is, expressed as a voltage,

$$U_{tm} \approx 1700\ \frac{m}{M}\ \text{[volts]} \quad . \tag{2.51}$$

III. MASS SPECTROMETER: CONSTRUCTION

Those parts of the quadrupole mass spectrometer that lie in the realm of physical electronics were designed and constructed by Professor C. K. Crawford, and so were not a part of the work of this thesis per se: they are the quadrupole lens, the ion source, the electron multiplier, and the vacuum system.

A. Quadrupole Lens

The quadrupole lens* consists of four metal-coated-alumina rods, 0.760 inch in diameter and 22.5 inches long, ground after metallizing to be round to 0.0001 inch, and mounted in a titanium holder (Fig. 3.1). The nominal inscribed radius was 0.318 inch. Specifications called for the rods to be straight to within 0.0001 inch after grinding. Unfortunately, because of an error in manufacture, the rods are actually quite crooked: deviations of more than 0.002 inch have been measured. The variation in inscribed radius (r_o) produced by this crookedness held spectrometer resolution to low levels.

The original design of the lens called for slots to be cut into the metal surface of each rod to electrically isolate a 270° sector 1.25 inches long on each end. The isolated sectors were to be gripped in two precision-bored end plates, while the remaining

---

* Kindly furnished by the Alloyd Corporation.

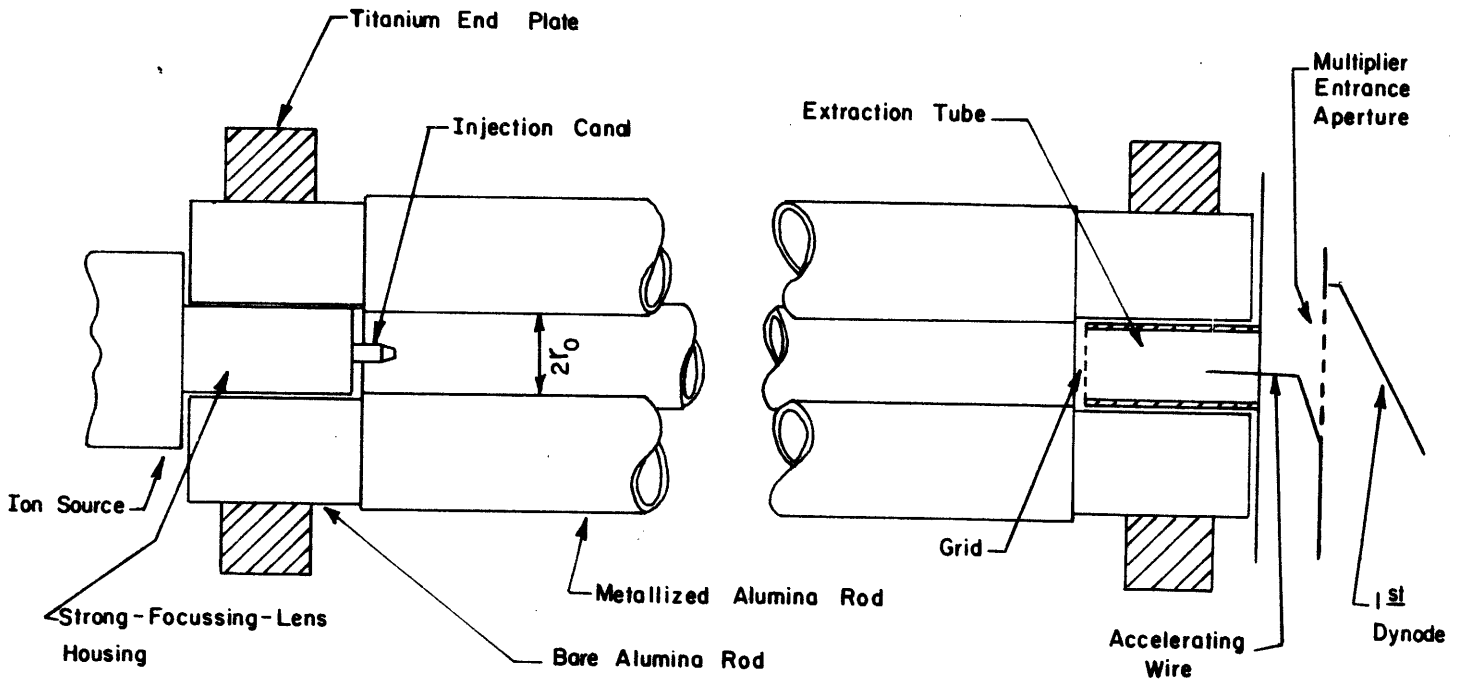

Fig. 3.1. Quadrupole lens. Cross-sectional view with one rod cut away.

90° sectors would extend the quadrupole field to the end of the rods. Because the 270° sector would have been concentric with the main metal surface of the rod, mounting accuracy would have been high. Unfortunately, because of another error in manufacture, the 270° and 90° sectors did not adhere to the ceramic. It was therefore necessary to grind the exposed ceramic end as accurately concentric with the electrode surface as possible, and mount the ceramic stubs in the end plates. This alternative arrangement lowered mounting accuracy, but errors were masked by the gross crookedness of the rods.

The major difficulty with the makeshift mount is that the quadrupole field ends $1\frac{1}{4}$ inches inside the mechanical lens assembly. At the input end this could be described as annoying; it requires a strong-focussing lens to transport ions $1\frac{1}{4}$ inches from the source to the small injection channel (used to minimize end effects). At the output end it is almost catastrophic. If ions at the exit with transverse momenta given by Eq. 2.51 for a mass at the upper limit of a range ($U_{tm} \simeq$ 1700 v) were to be accelerated in a uniform field by a typical accelerating voltage U_c = 10 kv, then (by Eq. 2.32) after traversing $1\frac{1}{4}$ inches they would be contained in a circle of radius 1.4 inches - well beyond the actual exit radius of 0.3 inch. This means that if no special precautions were taken, there would in fact be a large and mass-selective loss of ions between the end of the electrodes and an ion collector

mounted beyond the end of the rods.

The most obvious cure for the exit problem, extra metal electrodes slipped over the ceramic rod ends to extend the field region, is impractical because such electrodes can not be positioned with sufficient accuracy. Instead, the ion collector was extended inside the rod ends. A beryllium-copper-lined metal tube with a high-transmission grid on its input end was slipped into the end region almost up to the quadrupole electrodes, and the first electron-multiplier dynode mounted directly behind it. This extraction tube, which is maintained at the full ion-accelerating potential of the electron-multiplier ion detector, brings the collecting potential close to the end of the quadrupole to cut down the skew of the exit trajectories of the ions and increase the fraction that impinge upon the multiplier first dynode. It also serves as a "zeroth" multiplier dynode: Those ions that strike the inner walls of the tube release secondary electrons that are accelerated by a potential of a few hundred volts to the nominal multiplier first dynode.

The corrective measures for the mounting difficulty were an attempt to save time and money, although it was known that the final arrangement would still be not as satisfactory as a large ion collector butted closely against the end of a correctly constructed quadrupole. Unfortunately, the corrections themselves took enough time (most of an academic year) to prevent both thorough tests of other parts of the spectrometer system and use of the spec-

trometer for a study of thermal decomposition of solids as a part of this thesis project. (It was only at the end of this period that the crookedness of the rods - the one obviously uncorrectible difficulty in the lens - was discovered.)

The use of circular rods to approximate the hyperbolic electrodes of the ideal quadrupole leads to higher-order perturbation terms in the electric potential. Symmetry considerations show that the lowest of these is a twelve-pole term, i.e., one varying as $r^6 \cos 6\phi$, where r and ϕ are polar coordinates. Paul, et al. recommended a ratio of quadrupole rod radius to inscribed radius of 1.16 to minimize this term.[6] The quadrupole lens described above has a ratio of radii of 1.20, hence a non-minimal twelve-pole term that could conceivably introduce a fine structure into observed spectral lines, and possibly even cause multiple ttansmission bands.[12] However, no such line degredation has been observed in instruments with radii ratios of 1.00, so the much smaller deviation of this one is considered unimportant.[2,13]

It should be pointed out that the radii ratio of 1.16 does not really apply to a structure of four circular cylinders. It was obtained by minimizing the twelve-pole term for a quadrupole magnet that used as pole pieces sectors of circular cylinders.[14] Calculations for complete circular cylinders are yet to be done.

B. Ion Source

The ion source, constructed of "Electron-Atom-Ion" standard

parts[8] (Fig. 3.2), is shown schematically in Fig. 3.3. Gas molecules enter the grid-enclosed ionization chamber in paths perpendicular to the paper. It was intended that they come from a solid vaporized in a Knudsen cell immediately below the ionization chamber, but such operation was not achieved; only background gas was analyzed.

Electrons from a tungsten-rhenium filament injected into the ionization chamber (by source V_{elect}) ionize the gas molecules. A small electric field (produced by $V_{chamber}$) accelerates the ions out of the chamber into a strong-focussing lens that conveys them to the injection canal. From the canal they are injected into the quadrupole lens, with a longitudinal momentum corresponding to the aceelerating potential V_{ion}.

The voltages (and even the circuit connections) on the diagram are only typical; they are set to optimum values for any particular experiment.

C. Electron Multiplier

The electron multiplier (Fig. 3.4) has 20 stages of beryllium-copper dynodes with a structure shown schematically in Fig. 3.5. The first dynode was made large (2.5 cm limiting aperture) with the intent that, when placed near the end of a quadrupole it would accept ions with skew trajectories. The last 17 dynodes are identical with those used in the 14-stage RCA C-7187J electron mulitplier, which

---

* Kindly furnished by the Radio Corporation of America.

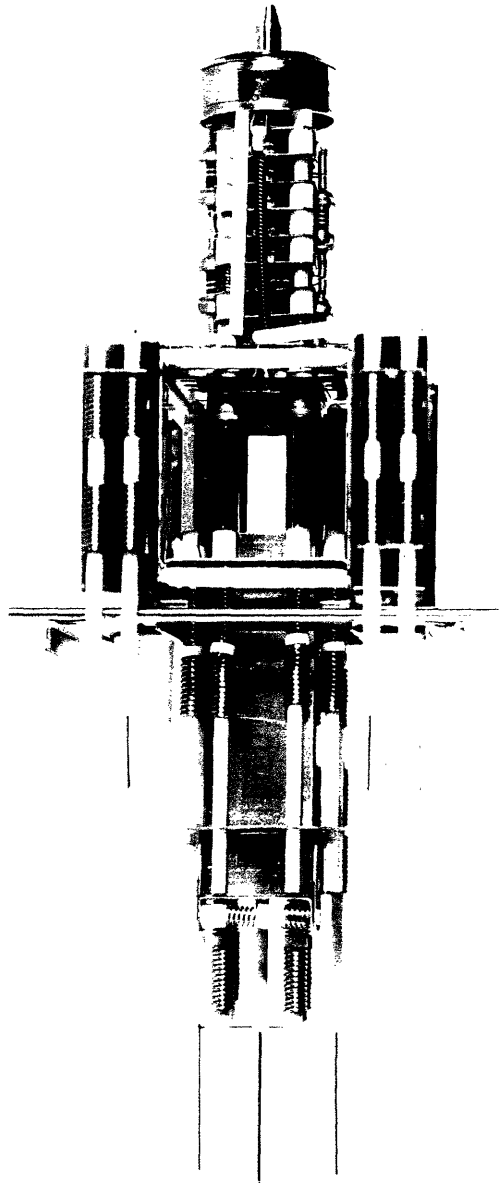

Fig. 3.2. Ion source.

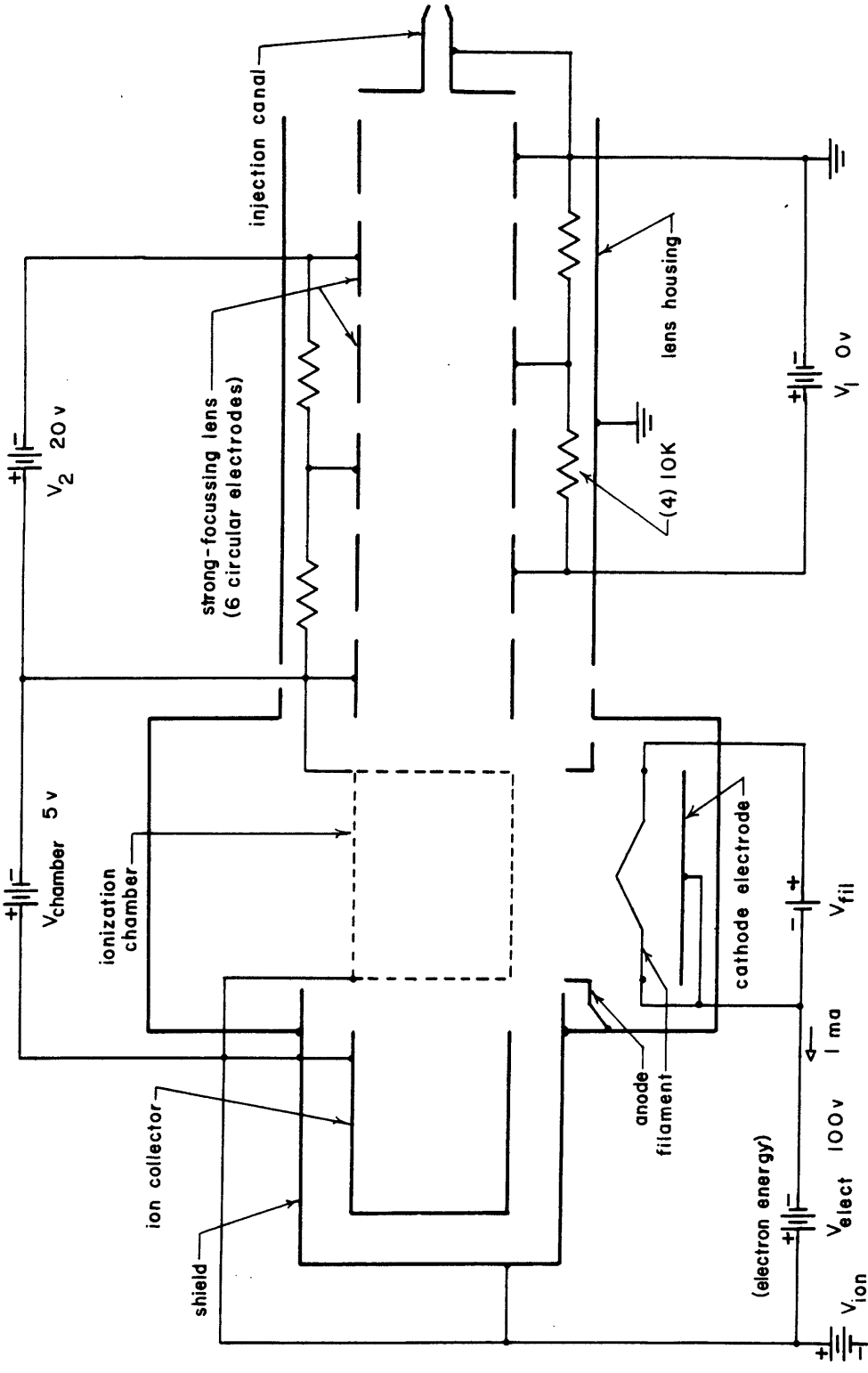

Fig. 3.3. Ion-source circuit diagram.

(a)

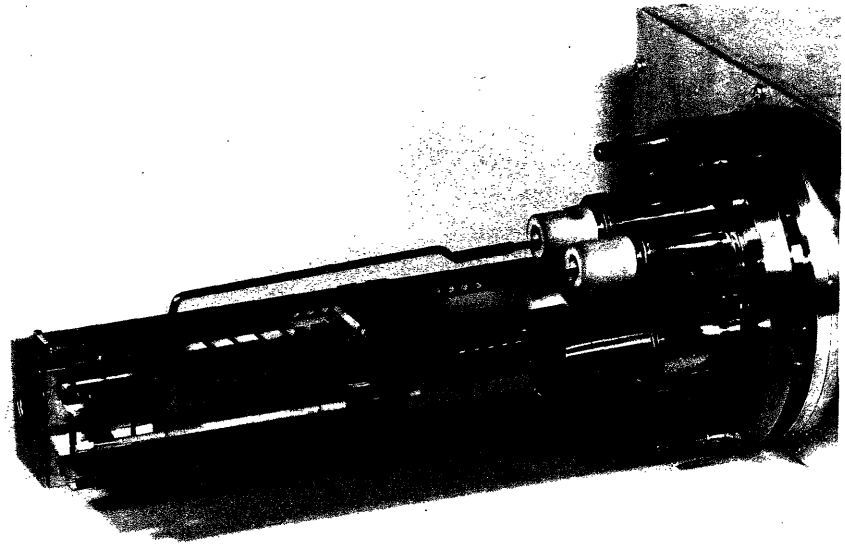

(b)

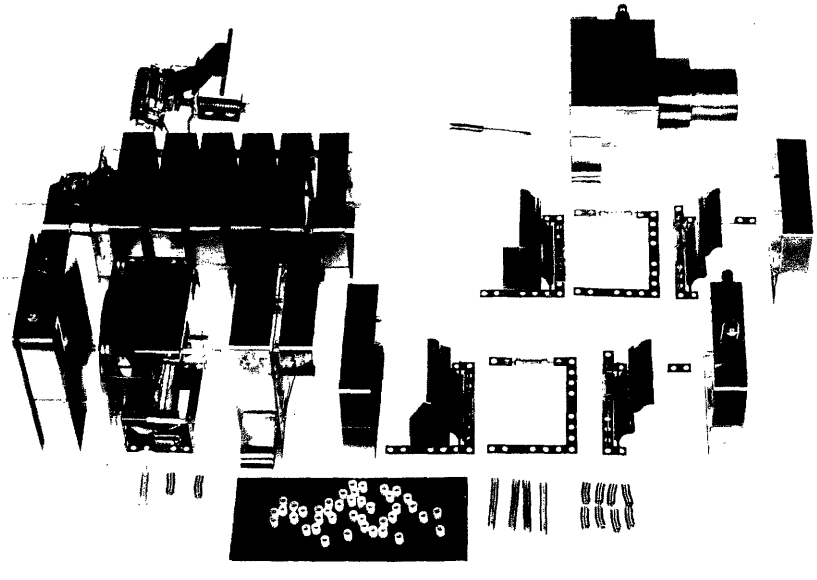

Fig. 3.4. Electron multiplier: (a) on mounting flange, (b) partially disassembled.

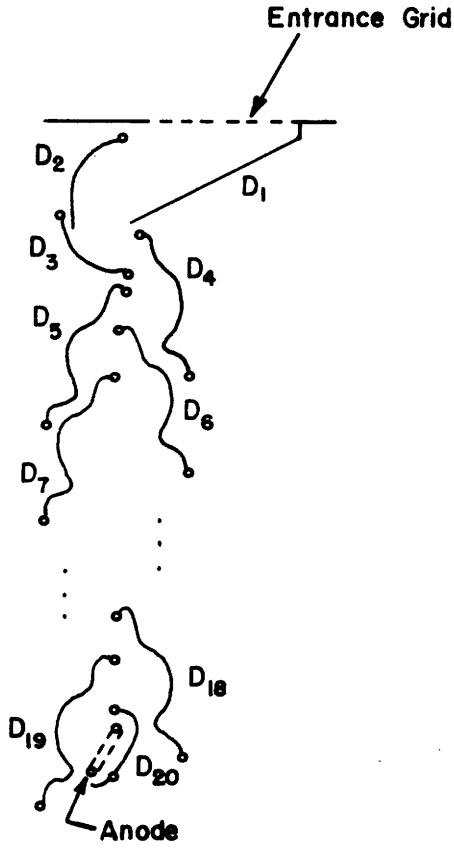

Fig. 3.5. Electron-multiplier structure. D_1 through D_{20} are dynodes.

in turn is identical in structure to the multiplier in the 6810A photomultiplier tube. The second and third dynodes were designed to provide a transition between the large first dynode and the small RCA dynodes. The anode is a grid structure mounted between the 19th and 20 dynodes.

Not shown in either the photograph or the diagram is the "zeroth" dynode, the extraction tube slipped into the space between the ceramic quadrupole rod extensions. The entrance grid for the first dynode is placed within a centimeter of two of the output end of the tube, and a small wire (0.010-inch diameter) run axially up the tube to introduce an accelerating field.

The dynodes were given no sensitization treatment before use. Gain, originally 3×10^8 with 8 kv across 20 dynodes, dropped only slightly over a period of several months. Then a number of internal arcs, brought about by an open connection, reduced it by several orders of magnitude, so sensitization was attempted. The arm of the vacuum system containing the mulitplier was baked for 24 hours at temperatures of about $400^{\circ}C$ and a pressure on the order of 10^{-5} torr. With temperature held constant at $400^{\circ}C$, oxygen was admitted (at a pressure somewhat above 1 torr) for 20 minutes and the system pumped down to about 10^{-5} torr and cooled under vacuum. The resulting multiplier gain was quite high - an estimated 10^8 at only 5 kv applied voltage - but one exposure to the atmosphere reduced it greatly, e.g., to 2×10^7 at 8 kv.

D. Vacuum System

The vacuum system was designed to avoid organic contaminants, which may degrade electron-multiplier gain, form insulating films that can cause erratic potentials on surfaces, and yield a continuum background spectrum. The system is made of stainless steel, with copper-gasket seals at all demountable joints. Oil-free rough vacuum is provided by an alumina-trapped mechanical pump and a zeolite absorption pump. The principal high-vacuum pump, a 90-liter/sec ion pump, was found inadequate to handle bursts of gas produced by evaporation of materials in Knudsen-cell sources, and was therefore augmented during such operation by a liquid-helium cryopump.

The entire system was designed to be baked at temperatures up to 400°C, although this has not yet been done. The vacuum typically obtained in the unbaked system, without use of the cryopump, is about 10^{-6} torr.

IV. ELECTRONIC DRIVE CIRCUITS FOR THE MASS FILTER

A. Circuit Requirements

The quadrupole mass filter requires for its two sets of rods a pair of voltages, balanced about ground, of the form

$$\pm\phi_o = U + V \cos 2\pi\nu t \ . \qquad (4.1)$$

The selected mass is proportional to the r-f amplitude, V. Since the range of masses should be swept over a time suitable for oscilloscopic presentation, starting at any arbitrary mass in the sweep range, the most general form for the r-f amplitude should be

$$V = \alpha t + \beta \ , \qquad (4.2)$$

where α may be adjustable to vary the sweep rate and may even be zero if the filter is to select a single mass line continuously, and β is of course adjustable. The sweep may be either repetitive (a sawtooth) or single shot.

For a constant resolving power, $m/\Delta m$, U should be a fixed fraction of V, but for constant line width, Δm, U should in addition contain a negative constant. The most general form required for the d-c voltage is therefore

$$U = \gamma V - \delta. \qquad (4.3)$$

The electronic drive circuitry that produces voltages described by these equations can be broken into three major parts (Fig. 4.1): The first is the control generator, which produces a voltage of the form $\alpha t + \beta$. The second is the r-f rod driver, whose output, applied in balanced form to the mass filter, is proportional

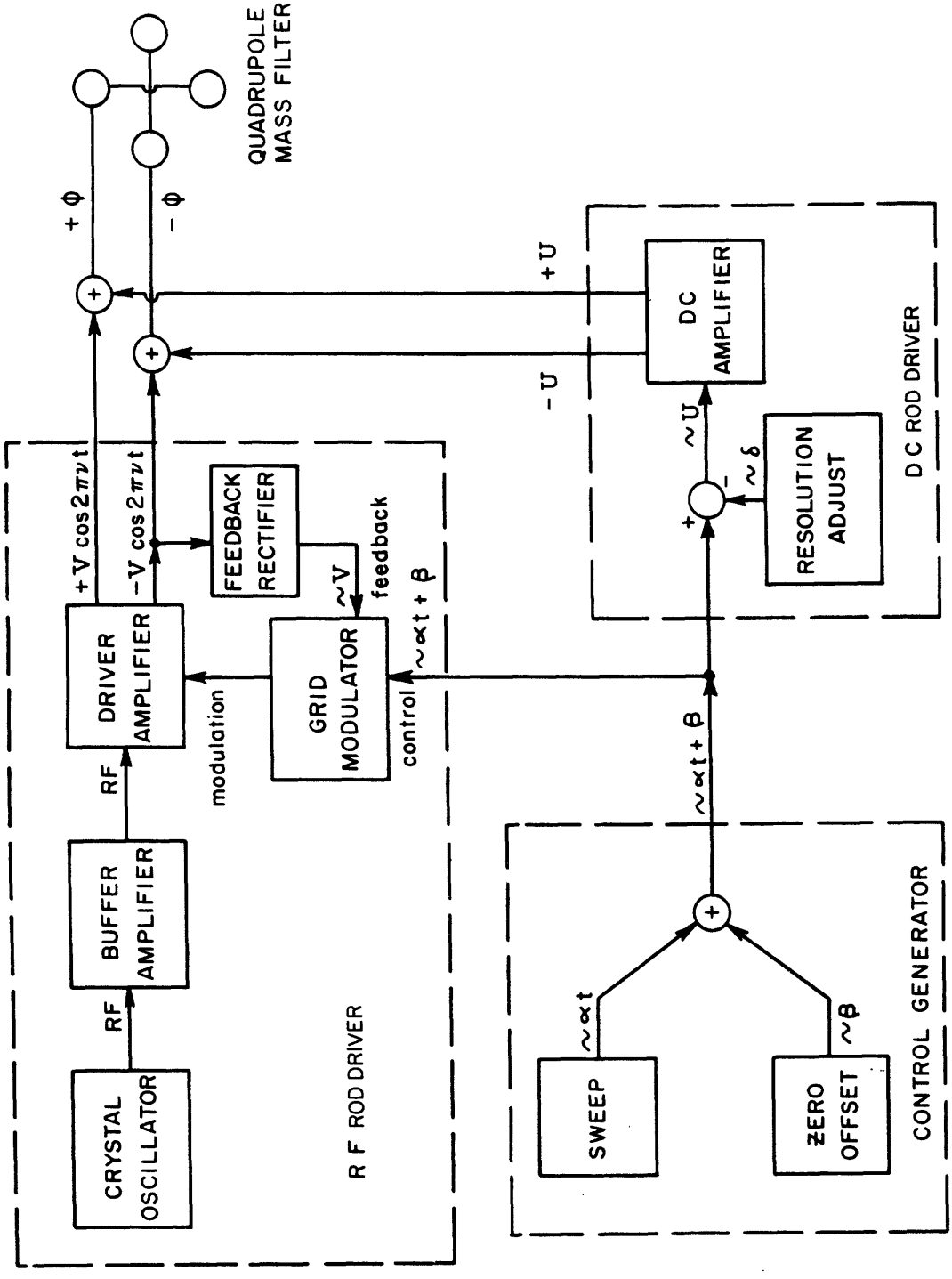

Fig. 4.1. Block diagram of mass-filter circuits.

in amplitude to the input from the control generator. The third is the d-c rod driver, a balanced-output d-c amplifier for the control-generator signal, with provision for the addition of a resolution-compensation voltage.

B. Control Generator

A more complete block diagram of the control generator is shown in Fig. 4.2, and a schematic diagram in Fig. 4.3. The sweep source is a phantastron sweep generator that produces a voltage ramp on either a recurrent or a single-shot basis. This is followed by a pair of operational amplifiers, the first of which inverts signal polarity, while the second provides an amplitude control for the sweep. The sweep signal is then passed through a "sweep zero clamp" that holds the voltage at zero during non-sweep periods. Finally the sweep signal (proportional to αt) is added to a d-c "zero offset" voltage (proportional to β) in a final operational-amplifier stage.

The phantastron sweep generator (tubes V_1 and V_2 and associated circuitry) provides recurrent 0.1- and 1-sec sweeps and manually triggered, single-shot 1- and 10-second sweeps. In the single-shot mode the circuit is quite conventional,[15] but the recurrent mode does have one unusual feature: the recovery delay is generated internally by an R-C circuit involving a regenerative connection of the 6AS6 screen and suppressor.

The rectangular-wave voltage of the phantastron screen

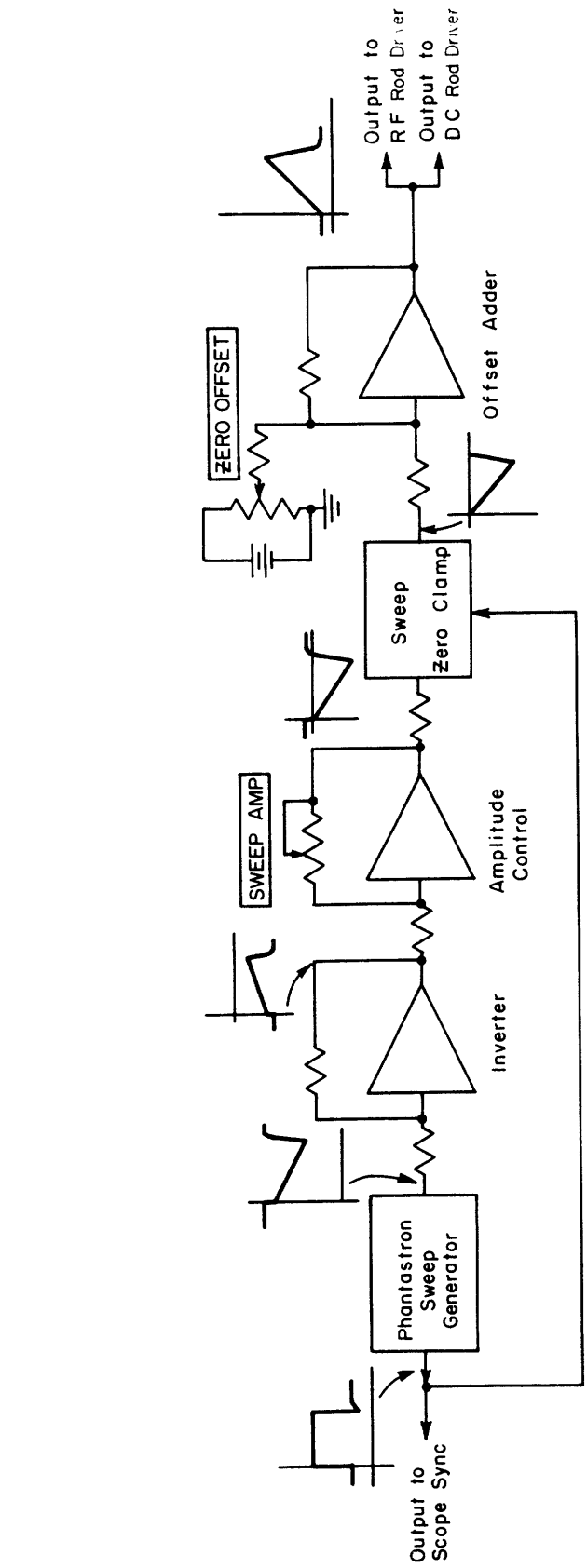

Fig. 4.2. Block diagram of control generator.

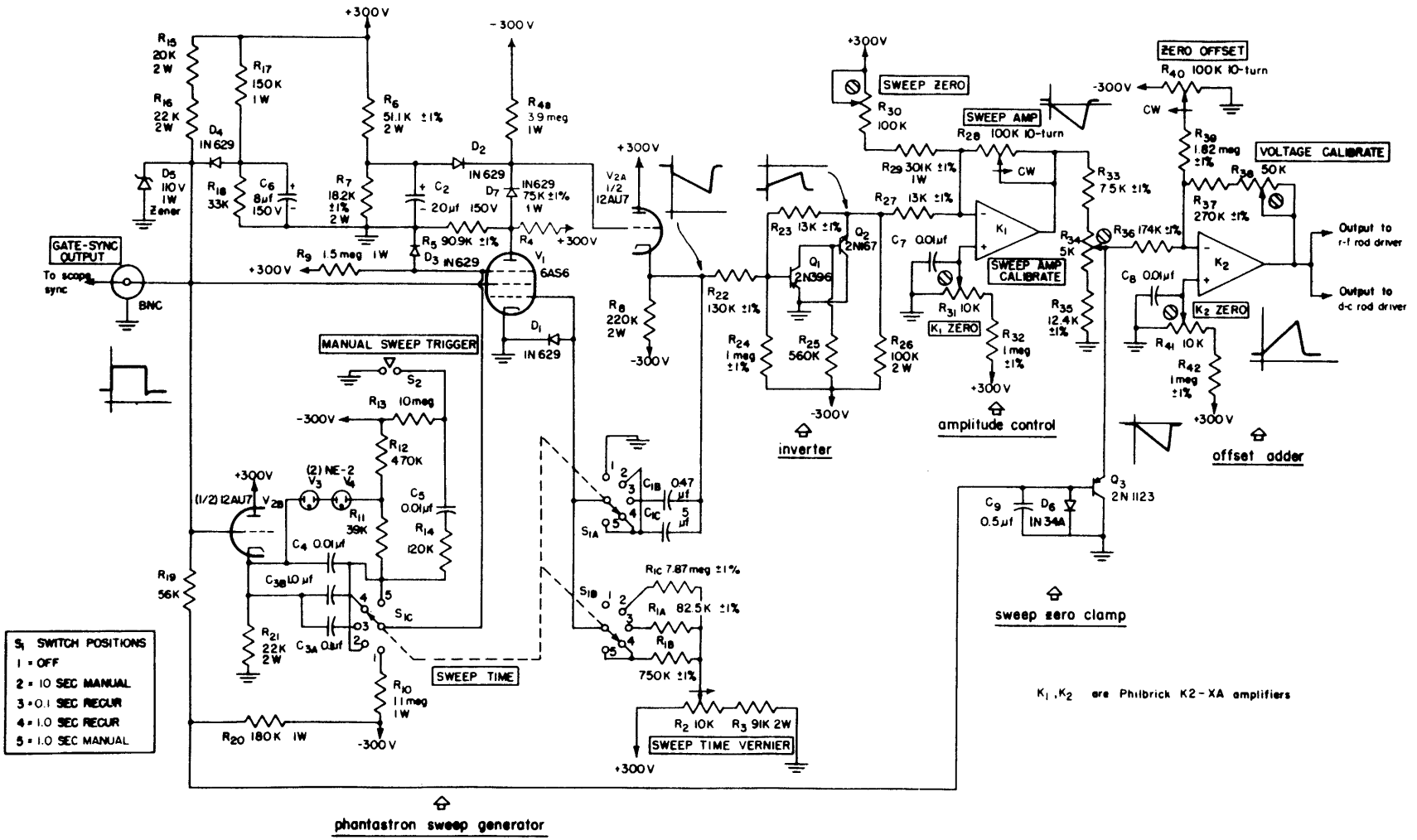

Fig. 4.3. Circuit diagram of control generator. All resistors are ± 5%, 1/2 w, unless otherwise noted.

provides a synchronization signal for the oscilloscope used to display the mass spectrum, and also drives the sweep zero clamp.

The free-running phantastron was chosen because it seemed to provide all the needed sweep services with only two tubes. An alternative sweep circuit considered at the time of the original design involved a transistor current source feeding a capacitor, a Schmitt trigger sweep-limit sensor, a one-shot-multivibrator recovery timer, and a "crowbar" circuit to short the sweep capacitor during the recovery period, for a total of at least 7 transistors. Despite this disparity in active devices it is now felt that the phantastron was a poor choice; it yields a signal with far too many spurious features.

The phantastron, like all Miller integrator circuits, has inherent in its output signal a step preceding the ramp. If this function were applied to the r-f and d-c rod drivers it would excite serious transients in the mass-filter rod voltages at the start of the sweep.

A clamp (transistor Q_3) was installed to short the sweep voltage to zero during the non-sweep period; this did not completely eliminate an initial transient because of a delay caused by difference in rise time of the plate and screen steps.

Another shortcoming of the phantastron sweep circuit lies in voltage and time instabilities. The phantastron generates a highly linear sweep with a rate accurately controlled by the supply voltage and the passive components of the charging circuit (R_1 and C_1).

However, the voltage range over which the phantastron sweeps, and thus the sweep time, depends on less stable circuit elements. The initial sweep voltage in the manual mode, in which plate current is truly zero until the start of the sweep, is not the same as in the recurrent mode, in which there is finite plate current at the start. There is even some difference in starting voltage between different sweep-time settings.

The rest of the control generator consists of operational-amplifier feedback amplifiers. The phantastron ramp is inverted by a simple two-transistor amplifier. The next amplifier (a Philbrick K2-XA) provides a highly linear sweep-amplitude control and adds a d-c component to remove the d-c offset of the phantastron signal. The last amplifier, also a K2-XA, adds the sweep voltage (αt) and a zero-offset voltage (β). The output is calibrated at 50 volts full scale for either sweep amplitude or zero offset. The sum can go to 100 volts, but this overloads the r-f and d-c rod drivers. A neon warning lamp, not shown in the diagram, lights when the total output voltage exceeds 50 volts.

The unstabilized operational amplifiers suffer from appreciable voltage drift. In one test the filament power was turned on for two minutes, plate power for another ten, and stability observation begun. The output of the control generator drifted 55 mv in the first 7 minutes, 145 mv in the first 70 minutes. After d-c power had been removed for 5 minutes (with filament power on) and then reapplied, the output shifted back 73 mv but immediately

resumed a drift in the original direction. A drift of 145 mv amounts to 0.145 amu on an 0-50 mass scale, 1.2 amu on an 0-400 scale; this cannot be tolerated in high-resolution operation.

The control generator therefore suffers from both voltage and time instability in the phantastron circuit and voltage instability arising in the operational amplifiers. For optimum performance it should be completely redesigned and rebuilt. The sweep generator could probably be based on a Miller integrator using one of the small low-drift, commercial transistor operational amplifiers now available, with retrace and control functions handled by transistor multivibrators. Two operational amplifiers are necessary to control sweep amplitude and add zero offset. (A third one might be advisable to produce a zero offset signal that was a more linear function of potentiometer setting.) The transistor operational amplifiers should be satisfactory for these applications also, although it would be necessary to add an additional amplification stage on the output to achieve 50-volt signal levels. (Operation at lower voltage levels would not be satisfactory because a nonlinear network in the input of the r-f rod driver requires rather large voltages for proper operation.)

C. R-F Rod Driver

The r-f rod driver, shown in block-diagram form in Fig. 4.1, schematic-diagram form in Fig. 4.4, must produce rather large r-f voltages variable over an extremely wide amplitude range - at least

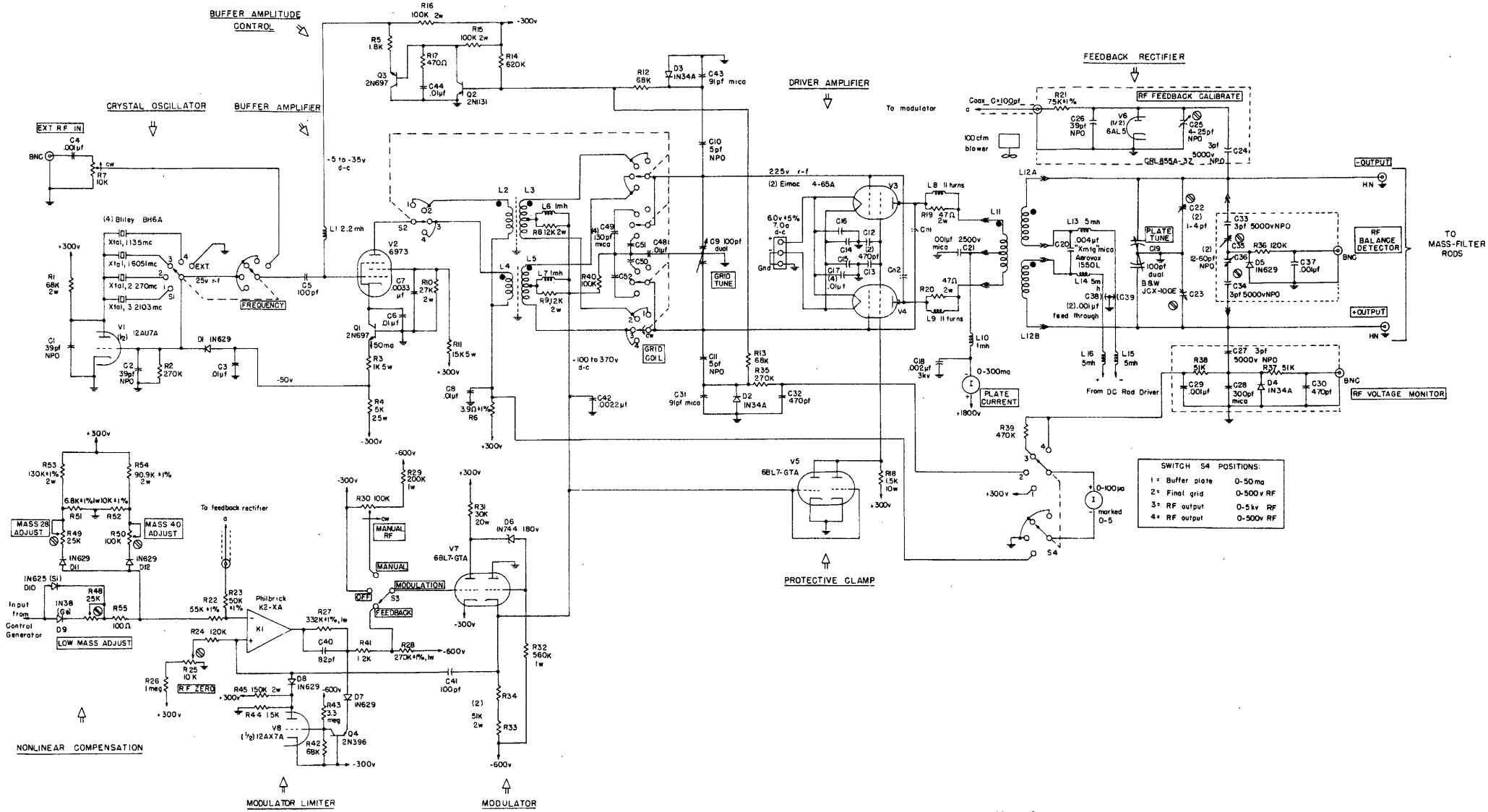

Fig. 4.4. Circuit diagram of r-f rod driver. Unless otherwise noted: (1) all resistors ± 5%, 1/2 w; (2) potentiometers, Allen Bradley Type J; (3) capacitors, high-K ceramic.

Table 4.1. Buffer-Output R-F Transformers.

The 1-inch-diameter primary and $1\frac{1}{4}$ -inch-diameter secondary coils are coaxial, concentric, and wound as a right-hand screw. The secondary is center tapped. The Faraday shield, which lies between the coils and is coaxial and concentric with them, is made of No. 34 bare copper wire wound 40 turns/in. on $1\frac{1}{8}$ -in. o.d. $\frac{1}{32}$ -in. wall phenolic tubing. Every turn is soldered to a longitudinal ground bus and is cut diametrically opposite the bus.

<u>High-frequency transformer</u>: 3.2103 and 2.2700 Mc.

Primary: L_2 = 13 μh. 26 turns, 32 turns/in., B and W "Miniductor.:

Secondary: L_3 = 37 μh. 42 turns, 32 turns/in., B and W "Miniductor."

M = 15 μh.

Faraday shield $1\frac{1}{4}$ in. long.

<u>Low-frequency transformer</u>: 1.6051 and 1.1350 Mc.

Primary: L_4 = 42 μh. 64 turns, 32 turns/in., B and W "Miniductor."

Secondary: L_5 = 143 μh. 110 turns No. 30 HF, 40 turns/in., wound on $\frac{1}{8}$ -in.-wall phenolic tubing.

M = 57 μh.

Faraday shield $2\frac{1}{2}$ in. long.

High- and low-frequency assemblies are mounted at right angles to minimize stray coupling.

Table 4.2. Output Tank Coils.

The coils resonate with ≈155 pf, including the capacitance of 3 1/2-ft of RG-11/U cable and 81-pf quadrupole capacitance. They are coaxial, concentric, and wound as a right-hand screw. The primary is center tapped, the secondary in two halves with a gap between halves for the primary center-tap lead. Unless otherwise noted the coils are commercial air-wound coil stock (Illumitronic Engineering Corporation, Sunnyvale, California) with Lexan insulation.

3.2103 Mc.

Primary: L_{11} = 12 μh. 14 turns No. 16 wire, 2 1/2-in. diam., 10 turns/in.

Secondary: L_{12} = 16 μh. 18 turns No. 12 wire, 3-in. diam., 6 turns/in., 1-turn gap between sections.

M = 9.4 μh. Q = 170.

2.2700 Mc.

Primary: L_{11} = 20 μh. 20 turns No. 16 wire, 2 1/2-in. diam., 10 turns/in.

Secondary: L_{12} = 32 μh. 26 turns No. 14 wire, 3-in. diam., 8 turns/in., 1-turn gap between sections.

M = 18 μh. Q = 170.

1.6051 Mc.

Primary: L_{11} = 51 μh. 32 turns No. 14 wire, 3-in. diam., 10 turns/in., polystyrene insulation.

Secondary: L_{12} = 65 μh. 28 turns No. 14 wire, 4 1/8 -in. diam., 9 turns/in., 2-turn gap between sections. (Modified B and W 3252.)

M = 37 μh. Q = 160.

1.1350 Mc.

Primary: L_{11} = 66 μh. 26 turns No. 20 bare wire, spaced own diameter on 3 1/2-in. o.d., 1/8-in.-wall phenolic tube. Length = 1.66 in.

Secondary: L_{12} = 135 μh. 42 turns No. 18 bare wire, spaced own diameter on 3 1/2-in. o.d., 1/8-in-wall phenolic tube. 1/8-in. gap between sections, each section 1.69-in. long.

M = 65 μh. Q < 170.

100 to 1 to sweep all masses of interest between 1 and 50. The simplest circuit, a modulated oscillator, is ruled out because it is difficult to get an oscillator to stay in oscillation over such a wide modulation range and because the amplitude modulation is accompanied by an undesirable frequency modulation. The output of the r-f driver is therefore obtained from a modulated push-pull Class-C amplifier, the "driver" amplifier.

Grid modulation was chosen for the driver amplifier over such alternatives as plate modulation or combined plate-screen modulation obtained by a series-tube regulator because it offers fewer problems in voltage-level shifting and confines problems of high power to the modulated amplifier. Only one difficulty was encountered: at high negative grid bias, when low r-f output is to be obtained, the r-f amplifier plate conduction time is very low, and harmonic distortion of the output is enhanced.

A grid-modulated amplifier requires a "stiff" r-f driving voltage because the input power demand increases rapidly with grid conduction at high output levels. A feedback-controlled buffer amplifier was therefore chosen to supply the r-f input to the driver amplifier. The buffer amplifier was in turn driven by a crystal-controlled oscillator, which produces a signal of good frequency stability with simple circuitry.

The mass filter requires the relation between the r-f and d-c voltages to be maintained with a high degree of precision.

No r-f modulation scheme is sufficiently linear in direct operation to maintain that relation, but adequate linearity over most of the amplitude range is obtained by a feedback-control system in which a fraction of the r-f voltage is rectified and summed, at the input of an operational amplifier that drives the grid modulator, with the signal from the control generator. Nonlinearity, introduced by the rectifier is reduced by a nonlinear compensation network in the control system input.

Because the required r-f power is directly proportional to the total tank-circuit capacitance (Eq. 2.42), the latter should be kept as small as possible. The entire r-f rod driver might have been placed at the vacuum system next to the mass-filter terminals, to eliminate the capacitance associated with a coupling cable from the driver to the mass filter. This was not done primarily because of mechanical problems involved in mounting it on equipment that may be subject to bakeout. Instead the driver was placed in a rack-mounted chassis and coupled to the mass filter by high-voltage coaxial cable. Total circuit capacitance was about 155 pf, so by Eq. 2.42 the maximum required power is $3.7 \times 10^4/Q$ watts. For a reasonable value of Q, say Q = 200, this is on the order of 200 watts.

Remote mounting of the rod driver may have been in error, because it encourages high-order harmonics in the output. Since the coil admittance becomes negligible at frequencies appreciably above the operating frequency, the entire tank circuit becomes,

in effect, a pair of capacitances on either end of a length of cable. This transmission-line circuit resonates at various frequencies, some of which necessarily lie very close to harmonics of the operation frequency. For the apparatus actually constructed, substantial amounts of 7th to 12th harmonics were observed.

Crystal Oscillator

The crystal oscillator is a single triode (V_1) in a Pierce configuration. The output is taken from the triode grid because the signal amplitude there can be closely controlled (at 25-v peak amplitude) by limiting action. Frequency stability was not measured, but experience with crystal oscillators has shown them to have a stability of better than 1 part in 10^4 under almost any conditions of operation, which is better than required for mass-filter operation.

Buffer Amplifier

The buffer amplifier is a single pentode (V_2) with the output inductively coupled to the grids of the driver amplifier. The output amplitude is regulated by a "buffer amplitude control" feedback circuit that grid modulates the buffer to maintain constant r-f voltage on the driver-amplifier grids despite changes in load caused by grid conduction.

A type 6973 beam-power pentode was chosen for the amplifier because it combines appreciable power-handling capability in a small

envelope with a favorable plate-to-screen current ratio under conditions in which screen voltage exceeds the plate voltage.

If the output tank circuit of the buffer amplifier were to be badly detuned, the amplitude-control circuit would attempt to maintain full r-f output by bringing the pentode grid bias as close to zero as possible. If no special precautions were taken this would result in excessive d-c plate current, excessive plate dissipation, and damage to the tube. Transistor Q_1 prevents this by limiting pentode cathode current to 50 ma. Under ordinary operating conditions (cathode currents of 10 to 40 ma) the transistor is in saturation and holds the cathode essentially at ground potential.

The output circuit is one of two switch-selected r-f transformers with a tuned, balanced secondary (Table 4.1; Appendix B). Mica padding capacitors make possible resonance at the lower of the two frequencies for each transformer.

The buffer amplitude control consists of a diode detector that applies to a transistor amplifier a d-c current proportional to the r-f voltage on the driver-amplifier grids. The output of the transistor amplifier grid modulates the buffer amplifier so as to hold the output constant despite load changes.

The diode detector consists of two capacitively coupled, shunt-diode, half-wave rectifiers (D_2 and D_3), one for each side of the balanced r-f circuit. Each such rectifier has in its out-

put an r-f current equal in amplitude to the d-c current, but the balanced arrangement makes it unnecessary to use the customary low-pass filter with its accompanying phase shift that enhances feedback instability problems. The current applied to the input of the transistor amplifier is the sum of the outputs of two rectifiers whose d-c components add arithmetically, but whose r-f components are 180° out of phase and so subtract arithmetically. If the circuit were perfectly balanced and the RC time constant infinite, the current applied to the amplifier would be pure d-c. In fact there is some residual r-f current of frequency ω, caused by circuit unbalance, and some ripple of frequency 2ω. The residual ripple is of amplitude $\pi/\omega RC$ relative to the d-c, or essentially that which would be obtained from a full-wave rectifier with a simple R-C filter.

The feedback amplifier consists of a common-emitter stage (Q_2) followed by an emitter follower (Q_3) that gives the amplifier the capability of supplying appreciable output current when there is buffer-amplifier grid conduction. The amplifier bias was chosen so that under closed-loop conditions the r-f output of the buffer amplifier is about 225 v.

The buffer amplifier output voltage varies less than 2% as the operation frequency is switched over all four available values or as load is increased from zero to the value that causes current-limiting action by protective transistor Q_1. The maximum power output ranges from 3.2 to 3.8 watts, depending on frequency, 30% beyond the require-

ments of the driver amplifier.

Driver Amplifier

The driver amplifier consists of a pair of 4-65A tetrodes in a push-pull Class C arrangement, with r-f input applied to the grids in series with d-c bias from the modulator, and a secondary-tuned, transformer-coupled output.

The amplifier is neutralized to compensate for direct capacitive coupling of r-f energy from the tube grids to the tube plates, which would make it impossible to reduce the output voltage below ca. 10 volts, even with the tubes cut off. Neutralization is accomplished by capacitors C_{n1} and C_{n2}, each of which consists of a short length of wire extending up from a chassis feed-through, connected to the grid of one tube and "looking" at the plate of the other.

The 4-65A filaments are heated with 6.0 volts d-c to eliminate hum modulation of the r-f output. When the filaments were run from the usual filament transformer the hum modulation was on the order of 0.5 volts, even with the most careful hum-bucking arrangements. This was caused by a strong third-harmonic component in the 60-cps line voltage, in conjunction with a frequency response in the feedback circuitry controlling the r-f amplitude so poor for noise introduced in the driver amplifier stage that it was unable to reduce significantly the 180-cps modulation produced.

The protective clamp circuit (V_5) was intended, in case of bias

failure, to drop the 4-65A screen voltage to such a low value that the tetrode plates and screens would be protected from overdissipation. However, the 4-65A is so insensitive to screen voltage that the plate can be overdissipated even with zero screen voltage, so the clamp offers little protection. There is still a need for some arrangement that will sense any of the conditions that may lead to overdissipation, such as bias failure or plate-tank detuning, and remove voltages from the 4-65A's to prevent damage.

The d-c plate-supply voltage of 1800 volts is the minimum with which the driver amplifier can produce full output at 3.2103 Mc. Operation at lower plate voltages and higher plate currents requires more grid drive than the buffer amplifier can supply.

The r-f output of the rod driver is taken from the tuned secondary of one of four plug-in output tank coils (Table 4.2; Appendix B).

The two-winding output transformer has substantial advantages over the autotransformer used in the earlier version of the rod driver.[16] First of all, the d-c voltage for the quadrupole rods can be applied at the center of the transformer secondary, thus eliminating the high-loss r-f isolating chokes and one of the bulky d-c isolating capacitors necessary in the autotransformer arrangement. (One large mica capacitor is still necessary to complete the r-f path across the gap in the secondary winding.)

Second, the amplitude of the harmonic distortion that appears in a symmetric mode in the output (as contrasted to the antisymmetric fundamental) is greatly reduced. Elementary theory, which assumes an output transformer with unity coupling between primary and secondary, predicts no inductive coupling of symmetric-mode signals into the output, but, as is shown in Appendix C, there is such coupling because of flux leakages. Experimentally it is found that the two-winding output transformer nearly eliminates the second-harmonic symmetric signal and substantially reduces the amplitudes of higher harmonics.

The r-f output of the rod driver is supposed to be perfectly antisymmetric, that is, balanced with respect to ground. The condition of balance is determined by the self-checking balance detector; any unbalance in the output is indicated by a d-c output voltage. The balance of the detector itself is determined by reversing it in its socket, according to the balancing algorithm (Appendix D). Output balance is achieved by simultaneous adjustment of capacitors C_{22} and C_{23}, so as to keep end-to-end capacitance constant. A single adjustment would suffice if C_{22} and C_{23} were replaced by a single capacitor consisting of three parallel plates; two widely separated stators, one connected to each side of the r-f output, and a single grounded plate that could be moved between them. Adjustment of the movable plate would change the end-to-ground capacitances, but leave the end-to-end capacitance essentially constant.

The driver-amplifier output capability on all frequencies

ranges from a minimum of a few tenths of a volt, set by imperfectly neutralized r-f leakage from the grids to the plates, to beyond the full design output of 2400 volts. At 3.2103 Mc, the most demanding output frequency, full output requires 180 ma d-c plate current, about 225 volts and 2 watts of grid drive, and about 2 watts screen power. The dissipation of each 4-65A plate at this output, as measured by observation of plate temperature with an optical pyrometer, is about 38 watts. Because the efficiency of a grid-modulated amplifier drops at lower output levels, maximum plate dissipation occurs at an output of 1500 v; it is 48 watts, well within the 65-watt rating of the tube.

The output of the driver amplifier contains harmonics of the operation frequency in both symmetric and antisymmetric modes. If the driver amplifier were perfectly balanced the symmetric-mode harmonics would be even-order, the antisymmetric-mode odd order. In fact, the observed symmetric-mode voltage does consist primarily of even-order harmonics, from the second to the twelfth, with the fourth predominating at most operation frequencies; the antisymmetric-mode voltage consists primarily of odd-order harmonics, with the third predominating. The seventh harmonic of 3.2103 Mc appears strongly in both symmetric and antisymmetric fashion, indicating both that there is a transmission-line resonance near that frequency and that the driver amplifier is slightly unbalanced. (The conclusion of amplifier unbalance is supported by the observation that

the dissipations of the two 4-65A plates are not quite the same.) It might be advisable in any circuit redesign to include more elaborate balancing features in the driver amplifier - perhaps a balance adjustment for r-f drive in the grid circuit, or individually adjustable tube grid biases, or both.

The amplitude of the symmetric-mode harmonic output is relatively small, ranging typically from about 0.5% of the output voltage at low outputs, ca. 100 volts, to 0.05% at the full 2400-v output. The amplitude of the antisymmetric third harmonic ranges from 0.2% to 0.1% of the output voltage, the amplitudes of the other antisymmetric odd harmonics considerably smaller.

The effect of the harmonic distortion of the r-f signal on the mass-filter operation is a matter of some concern. The only effect of the symmetric-mode voltage is a modulation of the axial momentum of ions entering the filter. Since this is noncritical, the symmetric-mode voltages should have little effect. On the other hand, the antisymmetric harmonics are applied between the quadrupole rods in the same fashion as the fundamental, and might be expected to have a significant effect, but such is not the case; at most they produce a slight shift of the stable region on an a-q diagram.[2,12]

The harmonics in the output, both symmetric and antisymmetric, do have an adverse effect on the r-f rod driver itself: because they are amplitude dependent, they tend to reduce the linearity of

the feedback rectifier for the fundamental component. In addition, the symmetric-mode signal can also be capacitively coupled to the anode of the electron-multiplier ion detector, and, if the multiplier is used in particle-counting fashion, appear in the output of the broad-band amplifiers following the multiplier. (In practice it has been found possible to eliminate this trouble by careful shielding of the multiplier rods.)

It may be concluded that, in general, the presence of harmonics in the r-f voltages applied to the mass-filter rods caused no difficulties. However, because harmonics increase the problem of nonlinearity of r-f amplitude control, for a very high resolution mass spectrometer it might be advisable to minimize them by mounting the rod-driver output tank circuit as close as possible to the rods, and to operate the driver amplifier so that plate conduction times are a maximum.

Feedback-Controlled Modulator

The amplitude of the r-f rod driver is controlled, in mass-spectrometer operation, by a feedback-control system consisting of a high-gain modulator that modulates the r-f driver amplifier and a diode rectifier that returns to a summing point at the modulator input a d-c signal proportional to the r-f output.

The modulator is a commercial operational amplifier driving a cascaded triode amplifier and cathode follower, capable of supplying output voltages from -100 v to -370 v and driver-amplifier grid cur-

rent up to 20 ma. For circuit tests, the feedback loop can be broken by a switch and the modulator either controlled by a potentiometer (so-called "manual" operation) or set to a fixed voltage cutoff r-f output.

A limiter circuit (transistor Q_4 and triode V_8) constrains the output of the operational amplifier to the range of voltages necessary for modulator action. In essence, the limiter works by closing a subsidiary feedback loop, involving the "+" input of the operational amplifier, any time the amplifier output is positive enough to produce grid conduction in the triode amplifier.

The transmission of a mass filter is a critical function of the ratio of the d-c and r-f voltages. Differentiation of Eq. 2.37 gives the change of line width as a function of change in the voltage ratio:

$$\delta(\Delta m) \approx 8m\delta \left(\frac{U}{V}\right). \qquad (4.4)$$

At high masses a small change in the voltage ratio produces a large change in effective line width. Because in fractional-transmission operation transmission is roughly proportional to line width, a large change in apparent ion abundance is also produced.

Because the d-c rod voltages can be maintained with great accuracy by conventional feedback circuitry, it is the r-f voltage that is of concern. Its amplitude can be controlled with no more precision than it can be measured by the rectifier in the control

circuit. Hence the rectifier is the most critical single element in the quadrupole rod drivers.

Two distinct troubles can beset the control rectifier. The first is instability, a change with time of d-c output for a fixed r-f input. This can be kept small by careful choice of critical elements, such as capacitors and resistors, and by such special precautions as operation of heaters of vacuum-tube diodes from regulated supplies. The second problem is nonlinearity, which is simply an expression of the fact that the rectifier output is not strictly proportional to the r-f input, nor even proportional to within an additive constant. Over a wide range of inputs, such as the 100-to-1 range of a mass spectrometer sweeping from below mass 1 up to mass 50, the nonlinearity produces significant change of the r-f output relative to the control signal, and therefore a change in mass-spectrometer resolution and transmission as the mass range is swept. Nonlinearity of the control rectifier therefore imposes a fundamental limit on the "(resolution) x (mass-range)" product of the mass spectrometer.

A single shunt-vacuum-diode, peak-reading rectifier coupled to the r-f output by a capacitive voltage divider was used as the control rectifier because it gives the best linearity realizable with present-day devices and conventional circuits. The most obvious alternative, a semiconductor-diode rectifier, is slightly inferior. One improvement could easily be made in the present rectifier, how-

ever: the single diode could be replaced by two diodes in a balanced configuration, as in the buffer-amplitude-control circuit. Such an arrangement would, of course, do nothing for rectifier nonlinearity, but would make possible improvement of the modulation frequency response, just as it did in the buffer amplitude control, and also reduce the sensitivity of the system to unbalance in the rod-driver output voltage.

A study of rectification techniques was made in an attempt to obtain a more linear rectifier. It was found that more elaborate circuits involving slide-back or comparison techniques are no better than a simple peak-reading detector unless they use a threshold detector (nonlinear element with a sharp break in its voltage-current curve) better than a conventional diode. A slide-back detector using the extremely sharp knee available in some selected avalanche diodes was extensively investigated, but proved impractical because of the noise inherent in such diodes at low current levels and because the extremely high junction capacitance (100 pf typical for a small diode) made 3-Mc operation impossible.

A simple alternative to a more linear rectifier, compensating nonlinearity in the input of the amplitude-control feedback loop, is used in the r-f rod driver. The voltage-current characteristic of a 1N625 silicon diode (D_{10}) is such that when the diode is in series with the feedback-modulator input resistor, it approximately compensates rectifier nonlinearity. At moderately low inputs the silicon-diode voltage drop is too high; resistor R_{48} is then an effective

shunt. At the very lowest currents a sharper nonlinearity is necessary: a germanium diode (D_9) in series with R_{48} provides this. Additional small corrections to the 1N625 voltage drop are provided by adjustment currents switched in by diodes D_{11} at all inputs above 15 v (corresponding to mass 15 on the 0-50 scale) and D_{12} at all inputs above 30 v.

The nonlinearity compensator is adjusted by observation of background-gas mass spectra on the two lowest mass ranges of the spectrometer. On the 0-100 range the LOW MASS ADJUST control (R_{48}) is set to give the same fractional transmission at mass 14 as at mass 28, for a constant setting of the DC/AC RATIO control of the d-c rod driver (i.e., a nominally constant γ), and the RESOLUTION control set at zero (i.e., $\delta = 0$). Then on the 0-50 range the MASS 28 ADJUST is set to give the same transmission at mass 28 as at mass 14, and the MASS 40 ADJUST to give the same transmission at mass 40 or mass 44.*

The deviation of the r-f-to-d-c ratio from its value at 14 control volts (mass 14 on the 0-50 range, mass 28 on the 0-100 range) is shown in Fig. 4.5 for both the compensated and uncompensated case. The data were obtained from observations of the d-c rod-driver voltage (as measured by the DC/AC RATIO control) required for 10% transmission of a number of ion species. In

---

* Constant fractional transmission provides a true indication of constant U/V only when ions are lost solely because of entrance displacement; transverse entrance momentum enhances loss at low values of mass even with U/V = constant. However, through it is not exact, simplicity makes constant fractional transmission a good practical test of U/V.

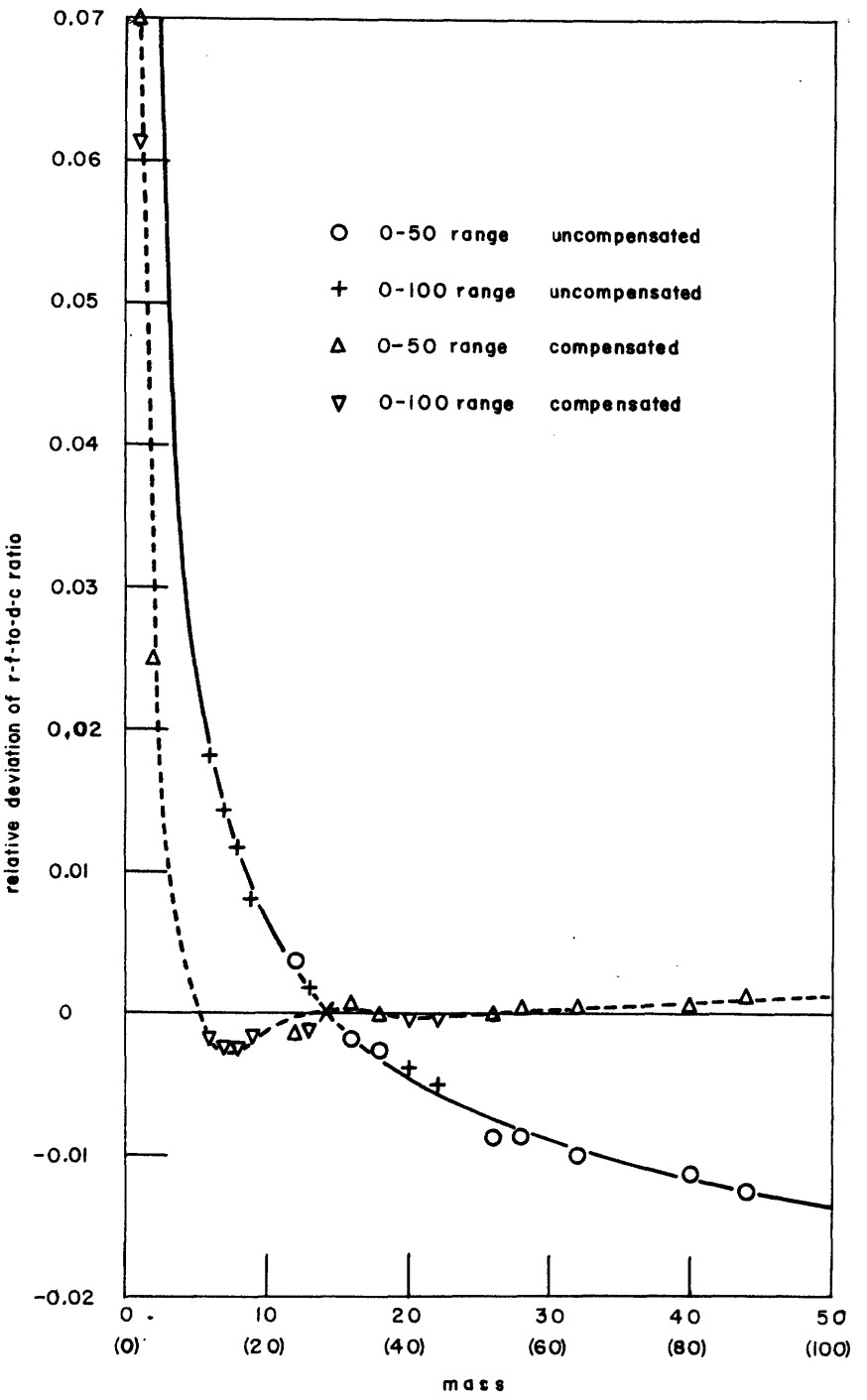

Fig. 4.5. Deviation of r-f-to-d-c ratio as a function of control voltage (or mass).

both the compensated and uncompensated case the r-f voltage is quite high at low mass values (around mass 1 and 2), but while the uncompensated r-f voltage shows a total deviation of some 4% over the upper 90% of the mass range, the compensated voltage shows a deviation of only 0.4%.

The performance of the nonlinearity compensator should not be regarded as the ultimate, for it was intended only to demonstrate the practicability of compensation. It should be possible to design a network to hold the r-f voltage within about 0.1% of the desired value over a 10:1 amplitude range.

Four separate problems arise in the feedback-controlled operation of the r-f rod driver: (1) dynamic stability, (2) transient response, (3) control dead zone, and (4) long-term stability.

(1) Dynamic stability. The problem of dynamic stability was a first consideration in the design of the feedback-control system. With capacitor C_{41} omitted, the open-loop transfer function of the r-f rod driver can be approximated by three poles on the negative real axis of a root-locus diagram, with no compensating zeros. The first of these poles arises from the K2-XA operational amplifier transfer function. The amplifier is designed to have a 6 db/octave falloff over almost the entire useful range of frequencies, with a transfer function

$$K = \frac{K_o \omega_K}{s + \omega_K} ,$$

where $K_o \approx 30{,}000$ and $\omega_K \approx 100$. The second pole, at approximately $\omega_f \approx 2 \times 10^5$, arises from the diode-rectifier low-pass filter. The third pole arises from the bandpass characteristic of the driver-amplifier plate-tank circuit, and is

$$\omega_Q = \frac{2\pi\nu}{2Q} ,$$

where ν is the r-f frequency and Q the tank-circuit "Q". For the frequencies and coil Q's of interest this pole lies between $\omega_Q = 2 \times 10^4$ and $\omega_Q = 7 \times 10^4$.

Under closed-loop conditions two of the three poles migrate to the right-hand plane and cause system oscillation.[17] To prevent this, compensating capacitor C_{41} and associated resistor R_{24} were added to produce a zero in the open-loop transfer function at $\omega = 3 \times 10^4$, which virtually eliminates the pole produced by the tank-circuit bandpass, ω_Q.

(2) Transient response. The closed-loop transient response is a function of the three-open-loop poles, the compensating zero, another zero arising in the feedback rectifier, and open-loop gain. Because one of the open-loop zeros, ω_Q, depends upon the operating frequency and coil "Q", and the small-signal open-loop gain depends upon the steady-state r-f output voltage, there is substantial variation in transient response. Depending upon operating frequency and steady-state amplitude, the response is characterized by either a simple exponential or a slightly underdamped sinusoid. To a first approximation it can be described by a single exponential of

time constant between 30 and 150 μsec, with 50 μsec being the typical value.

The r-f rod driver is required to handle only ramp inputs. The output of an exponential-response system to such an input is, after an initial transient lasting a few time constants, a ramp lagging the input by the exponential time constant (5×10^{-5} sec for the r-f rod driver). This lagging error has little effect on the critical U/V ratio of the mass spectrometer in part because it is small (only 0.05% after 0.1 sec) and in part because the d-c rod driver has a similar lagging response, so that the only first-order effect is a negligible delay in mass sweep.

(3) Control dead zone. One special difficulty arises in a feedback-control system involving a modulated r-f voltage: There can be no "negative" r-f output to correspond to a negative control voltage, so the system has a "dead zone" encompassing the entire negative range. This problem becomes especially severe during sweep retrace to zero. When the input signal drops abruptly to zero the modulator cuts off the 4-65A's completely, but the r-f output drops slowly because of the high Q of the tank circuit. The diode rectifier sends a large error signal to the modulator, driving it to saturation in the cutoff direction. The modulator may or may not recover before the next sweep begins. The modulator limiter circuit previously described tends to prevent gross saturation of the operational amplifier K_1 during such periods, but cannot completely eliminate the problem because there must necessarily be a range of

operational-amplifier output voltage between that necessary for complete r-f cutoff and that at which the limiter goes into operation.

(4) Long-term stability. Because it is necessary to maintain the r-f voltage to within better than one part in 10^3 in order to maintain a satisfactorily precise U/V ratio, the long-term stability, or freedom from drift, of the control circuit is highly important. The stability of the existing r-f control system must be characterized as highly unsatisfactory, primarily because of drift in the input offset voltage of the operational amplifier used for K_1. The K2-XA has a rated drift of 8 mv per day under "optimum" conditions. This would be marginally adequate if it could be achieved in the rod-driver circuits, because 8 mv represents about 0.1% of a typical control voltage of 10 volts. However, "optimum" conditions evidently require operation with supply voltages always on and at temperatures more constant than those in the mass spectrometer equipment racks, for much greater drift has been found. In one test, after filament voltage was applied for 2 minutes and both filament and plate voltages for another 10 minutes, the K2-XA offset voltage still drifted 30 mv in the next 5 minutes of operation, and another 33 mv in the next two hours. After d-c power was removed for 5 minutes (with filament power on) and then reapplied, the zero-offset voltage returned to nearly the value it had at the start

of the test and began another drift cycle. Because plate power is frequently removed and reapplied in the operation of the mass spectrometer, this sensitivity to power removal is particularly unfortunate.

The K2-XA should be replaced by a more stable operational amplifier, probably because of the output voltages required, a chopper-stabilized vacuum-tube amplifier, which should reduce drift some three orders of magnitude.

A more stable operational amplifier would undoubtedly reveal a number of other sources of d-c drift. The most obvious of these is a zero-offset current flowing in the vacuum-diode r-f detector even when the r-f voltage is zero, because of the thermal velocities of electrons emitted from the diode cathode. This current is appreciable in magnitude (approximately 1 μa in the present circuit, corresponding to a voltage offset of about 50 mv), highly dependent upon heater voltage, and subject to long-term drift. The effect of fluctuations in this current could be greatly reduced by injection into the summing point of the operational amplifier a compensating current obtained through a resistor from the cathode of a grounded-anode vacuum diode.

A second obvious source of drift is the deposited-carbon resistors and carbon-composition potentiometers used in the control circuit. These should be replaced by the more stable metal-film resistors and wire-wound potentiometers.

The nonlinearity-compensation circuit in the input of the

control circuit is a potential source of drift from temperature fluctuations because it uses semiconductor-device voltages. It might be necessary to place this circuit in a temperature-regulating oven.

Incorporation of all these recommended changes should make it possible to hold long- and short-term drifts in the r-f voltages to less than one part in 10^3.

D. D-C Rod Driver

The d-c voltages for the mass-filter rods can be obtained most easily by rectification of the r-f voltage.[6] In as much as the rectifier is linear, the d-c voltage would be proportional to the r-f amplitude. However, if d-c voltages are obtained from separate amplifiers, it is much simpler to obtain high-speed sweeps, to add a resolution-broadening voltage δ, and to compensate for nonlinearities in the r-f rod driver.

The d-c rod driver consists of a pair of cascaded inverting feedback-controlled amplifiers (Fig. 4.6). The first provides gain for the control-generator output signal adjustable from 0 to 10 by the DC/AC RATIO control. Its output is applied to one of the pairs of mass filter rods as the negative or "d-c" signal, and is also passed through a 1:1 inverter whose output is the positive, or "d-c+" signal. A "self-checking" balance detector that uses the same principle as the r-f balance detector - reversible connections - ensures that the rod voltages are balanced with respect to ground.

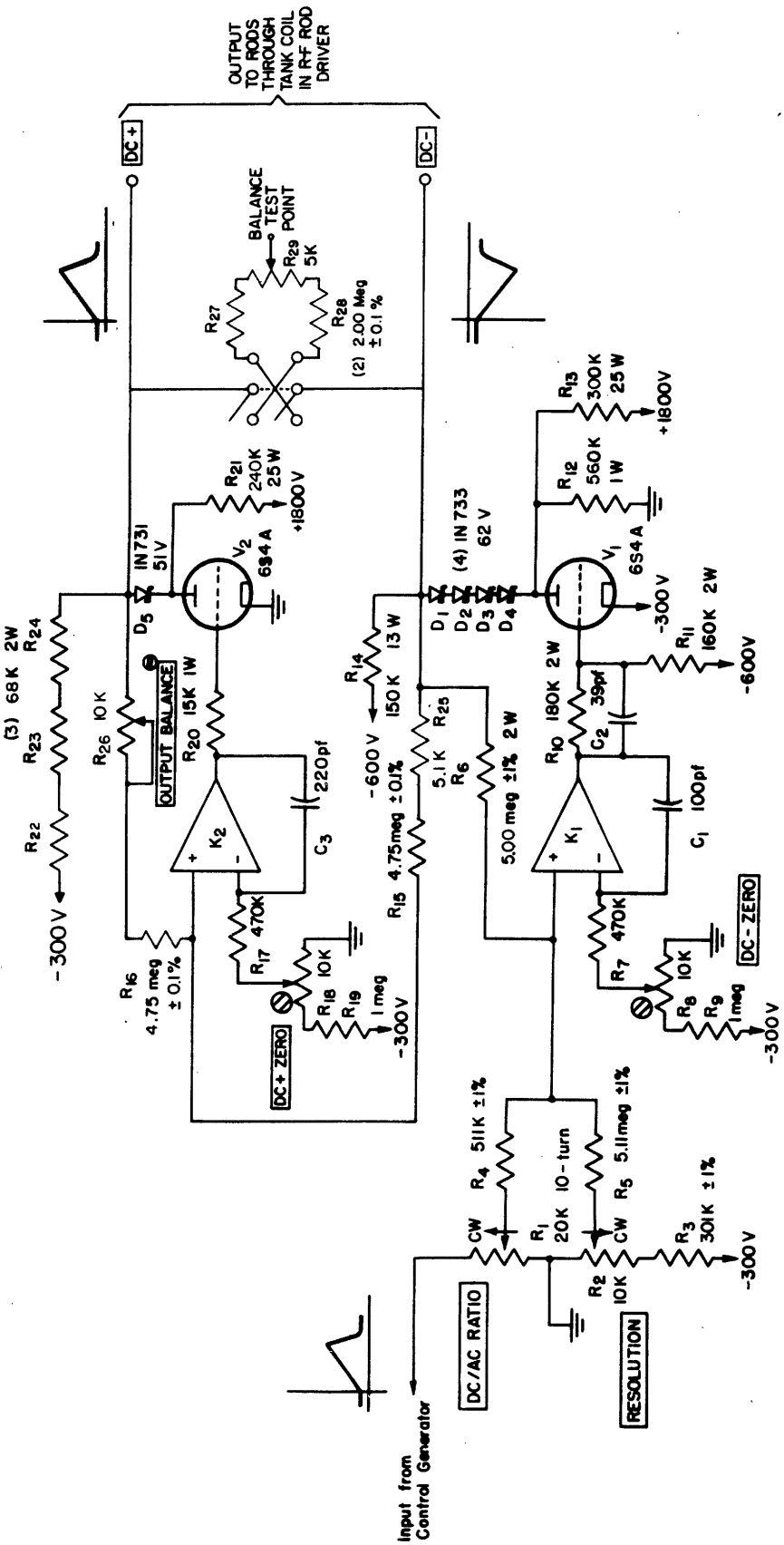

Fig. 4.6. Circuit diagram of d-c rod driver. Unless otherwise noted, all resistors are ± 5%, 1/2 w.

Because the r-f rod driver produces a signal whose amplitude V is 48.46 times the control signal amplitude, the 0-to-10 gain range of the d-c rod driver gives U/V ratios up to approximately 0.2. However, since the maximum U/V ratio for transmission through the mass filter is 0.16784, the highest voltage required from the d-c rod driver is not 480 v but 0.16784 x 2420 = 407 v. The actual dynamic ranges of the two amplifiers exceed 0 to 450 v.

The resolution-broadening voltage δ, added to the control-generator signal at the input to the first amplifier stage, can be varied from 0 to approximately 10 volts by the RESOLUTION control. If the DC/AC RATIO control is set at the "infinite resolution" value of 0.16784 and the RESOLUTION control at 10 v, the actual line width on the 0-to-50 mass scale is 1.5 amu.

Each amplifier in the d-c rod driver has two stages, the first a Philbrick K2-XA operational amplifier, the second a 6S4A triode that provides the necessarily large voltage swing. The outputs are series fed to the mass-filter rods through the split-winding output tank coil of the r-f rod driver.

The use of feedback control in each amplifier of the d-c rod driver presents three of the four problems that arose in the r-f rod driver: (1) dynamic stability, (2) transient response, and (3) long-term stability.

(1) Dynamic stability. The open loop transfer function of either of the two amplifiers with the compensating capacitor

C_1 or C_3 omitted from the circuit has three significant poles, all on the negative real axis, and no zeros. The first pole is that arising from the K2-XA transfer function. The second is caused by the combination of high Miller effect input capacitance of the K2-XA at its positive input terminal, some 150 to 200 pf, and the high feedback resistances required by the high-voltage circuitry. This pole is at about $\omega_i = 2300$ for the "d-c+" and $\omega_i = 14000$ for the "d-c-" amplifier. The third pole is caused by the combination of the high open-loop output impedance of the amplifier and the large shunt capacitance necessary in the r-f rod driver, some 0.009 μf effective capacitance from each side to ground. Its location varies with plate voltage as the plate resistance changes, but remains between $\omega_o = 9 \times 10^3$ and $\omega_o = 3 \times 10^4$.

The combination of three low-frequency poles and a high open-loop gain causes closed-loop oscillation of each amplifier. The compensating capacitor (C_1 or C_3) introduces a zero into each transfer function at approximately the same position as one of the original poles and thus eliminates the oscillation.

(2) Transient response. Both the "d-c+" and "d-c-" amplifiers have step responses with slightly underdamped sine-wave ringing, the first with a ringing period on the order of 10^{-5} sec, the second with a period on the order of 10^{-4} sec. The ramp response of the "d-c-" amplifier then has a small initial transient, lasting perhaps a few milliseconds, followed by a lagging error that

varies with amplifier output level, because both system gain and open-loop output impedance are voltage dependent. The error ranges between 2×10^{-4} sec at low voltages to 1×10^{-4} sec at the highest output voltages. The "d-c+" amplifier has a substantially faster response, with transient decay in less than a millisecond, and a delay of about 10^{-5} sec for a ramp input. These transient responses are adequate for the present spectrometer, but in the design of an optimum system care should be taken to minimize "d-c+" delay and to match the "d-c-" and r-f rod-driver delays.

V. DESIGN CONSIDERATIONS FOR THE ELECTRON-MULTIPLIER ION DETECTOR

A. Introduction

The simplest ion detector for a mass spectrometer is a Faraday cup connected to an electrometer that amplifies the minute ion currents. This arrangement has a maximum usable sensitivity of some 10^{-16} amp amd a response time that becomes poor at high sensitivities because of input RC time constants on the order of seconds. Since the quadrupole mass spectrometer was intended for moderately rapid sweeps of mass spectra, in times as short as 0.1 second, as well as for the study of ion beams modulated at several hundred cps, much greater response speed of the ion detector is necessary. This response speed can be achieved, along with improved sensitivity, by use of the high gain-bandwidth capabilities of an electron multiplier in the ion detector.

The simplest way to use an electron multiplier as an ion-detection amplifier is to let its first dynode serve as the ion collector of the mass spectrometer. Secondary electrons emitted upon ion impact are multiplied in the subsequent stages. This technique, used for over a quarter of a century,[18] is summarized in a review article by Akishin.[19] Its principal shortcoming is that it exposes all electron-multiplier dynodes to surface contamination in the mass-spectrometer vacuum system.

An alternate method minimizes the dynode contamination problem by collecting the ions with a scintillator crystal or with a single

dynode whose electron output goes to a scintillator crystal. A commercial photomultiplier tube outside the vacuum system detects light from the scintillator.[20-22] The chief disadvantage of this arrangement, the difficulty of finding a high-speed scintillator suitable for use in high vacuum, was considered prohibitive, so direct ion-electron multiplication was used.

B. The Electron Multiplier as a Current Amplifier

The most obvious method of using the electron mulitplier is as a current amplifier. The ion current is multiplied by the mean electron yield of the first dynode and the mean current gain of the following dynodes, for a typical overall gain on the order of 10^6. While adequate for many applications of the mass spectrometer, variations in electron-multiplier gain make this method unsuited for precise quantitative work, such as a comparison of the relative abundances of isotopes of a given element or of ions of two different elements.

Two distinct variations in gain are troublesome in current-amplifier operation. The first is a variation in electron yield of the first dynode as a function of the species, charge, isotopic mass, energy, and angle of incidence of the ions, and of the nature and condition of the surface of the first dynode. There is no *a priori* way to determine yield, or even relative yield. For example, Barnett, Evans and Stier[23] found that for noble-gas ions incident upon an activated beryllium-copper first dynode, the

secondary-electron yield increased with ion mass for incident energies of appreciably less than 20 kev, but decreased with ion mass for energies appreciably greater than 20 kev. As a further example, Sugiura found that for He^+, Ne^+, and A^+ ions of the same energy (in the range 2 to 3 kev), the yields from an electropolished beryllium-copper dynode were in the ratios 2.45:1.79:1.00, respectively, while the yields from an oxygen-treated dynode of the same material were in the ratios 2.00:1.28:1.00.[24] Results such as these indicate that it is necessary to calibrate the gain of each electron multiplier for each ion species to be studied.

The second variation in gain is that caused by contamination of the electron -multiplier dynodes over a long period of time. If only the second and following dynodes were affected the result would be a simple drop in gain, which could be determined by a single measurement and easily compensated. However, contamination of the first dynode may very well reduce electron yield more for some ion species than for others. The results of Sugiura show that two surfaces freshly prepared by different techniques have different yield ratios; it is prudent to assume a freshly prepared and a contaminated surface would likewise have different yield ratios. This secular, selective change in yield makes long-term calibration of multiplier gain impossible.

C. The Electron Multiplier as a Particle Detector

One method of avoiding the gain variation problems in electron-multiplier ion collectors is to use the multiplier not as a current

amplifier but as a particle detector. Each ion incident on the first dynode produces some 10^6 electrons at the anode; this is a quantity of charge sufficient to be treated in a quantized or digital fashion by subsequent electronic apparatus. The output pulses can be amplified, if necessary, and then passed through a standardizer circuit that yields pulses of a single selected size despite variations in multiplier output pulse amplitudes. This scheme is as old as the use of electron multipliers as ion detectors,[18] and has been carried out successfully many times.[25-28]

There are two methods of processing the output of a pulse standardizer. The pulses may be counted with a digital counter, a technique of value for long-term measurements of a single mass but unsuited for scanning a mass spectrum, or they may be integrated, in what has come to be known as a count-rate meter, to give an average current or voltage that is proportional to the rate at which ions arrive at the multiplier first dynode.

The operation of an electron-multiplier ion collector as a particle detector is, in principle, quite simple. There is, however, one characteristic of electron multipliers that makes particle-detection operation rather difficult in practice: dispersion in output pulse amplitudes from the multiplier caused by statistical variations in the secondary-emission process at each dynode. The pulse circuitry associated with the electron multiplier must be capable of handling not only the variations in output pulse amplitudes caused by

discrimination of ion species at the first dynode and secular changes in gain because of contamination, which together might give one order of magnitude variation in amplitude, but also the statistical dispersion in output amplitudes for a given ion species at a given time, which might amount to an additional two orders of magnitude. The system is therefore required to be insensitive to an extremely wide range of pulse amplitudes to circumvent relatively small variations in gain.

The distribution in amplitude of the output pulses of an M-stage electron multiplier is a function of the distribution in amplitude of electron yield per incident ion on the first dynode and of yields per incident electron on the subsequent M-1 dynodes. It is common to assume that the distribution for an electron-electron secondary emission process is Poisson, that is,

$$p_n = \frac{\lambda^n}{n!} e^{-\lambda} , \qquad (5.1)$$

where p_n is the probability of the emission of n electrons and λ is the mean emission, although Shockley and Pierce were able to show many years ago that noise measurements on electron multipliers indicated that the distribution could not be truly Poisson,[29] and Barrington and Anderson found by direct measurement a non-Poisson distribution for secondary emission from an activated beryllium-copper surface.[30] Nevertheless, careful measurements of output pulse amplitude distributions for single electrons incident on the

first dynodes of a number of commercial photomultiplier tubes has shown a distribution roughly of the form xe^{-x},[31] which corresponds fairly well with that predicted under the assumption of Poisson statistics at each dynode.[32] The Poisson distribution hypothesis, then, remains useful as at least a first approximation to the actual distribution.

No direct studies have been made of the yield distribution for the ion-electron process. However, overall pulse amplitude distributions have been obtained for ion-electron multipliers with both beryllium-copper[23] and silver magnesium[26] dynodes and found to have roughly an xe^{-x} shape. The results of Barnett, et al. are plotted as a probability density function and compared to an xe^{-x} curve in Fig. 5.1.

Johnson, et al.,[33] report a strikingly different amplitude distribution for a multiplier with silver-magnesium dynodes. They found a multi-modal distribution, with the modes spaced as the integers. Apparently the multiplier was more or less faithfully reproducing the yield distribution of the first or ion-to-electron dynode. Two factors may have made this possible: First, the multiplier probably had a rather high gain and low yield dispersion on all stages except the first. Second, the ions incident on the first stage had a low energy, 3 kev, that would give a low electron yield.

The results of Barnett, et al., can probably be taken as more

typical of ion-electron multiplier amplitude distributions. The integral of one set of data of Fig. 5.1, plotted as a probability distribution in Fig. 5.2, shows that in order to respond to all but the smallest 1% of pulses from the electron multiplier the pulse circuits must accept a dynamic range of about 2 orders of magnitude, from roughly 0.05 $\overline{K}$ to 5 $\overline{K}$, where $\overline{K}$ is the mean pulse amplitude or d-c gain of the multiplier.

One other consideration in particle detection operation is the possibility of no output for an input ion, i.e., of a detection efficiency less than unity. If the distribution in amplitude of electron yields from the first dynode is Poisson, with mean λ_I, then by Eq. 5.1 the probability of zero output from that dynode is $e^{-\lambda_I}$: It is therefore necessary to maintain $\lambda_I > 4$ for negligible loss. Barnett, et al., found the probability of zero output from a beryllium-copper dynode vanished for a wide range of incident ion species provided their energy was greater than 10 kev.

D. Spectrometer Output Noise

Noise in the output signal of an electron-multiplier ion collector arises from four distinct sources: background noise, regenerative noise, shot noise from the discrete nature of the input signal, and electron-multiplier noise introduced by the amplitude dispersion in electron-multiplier amplification.

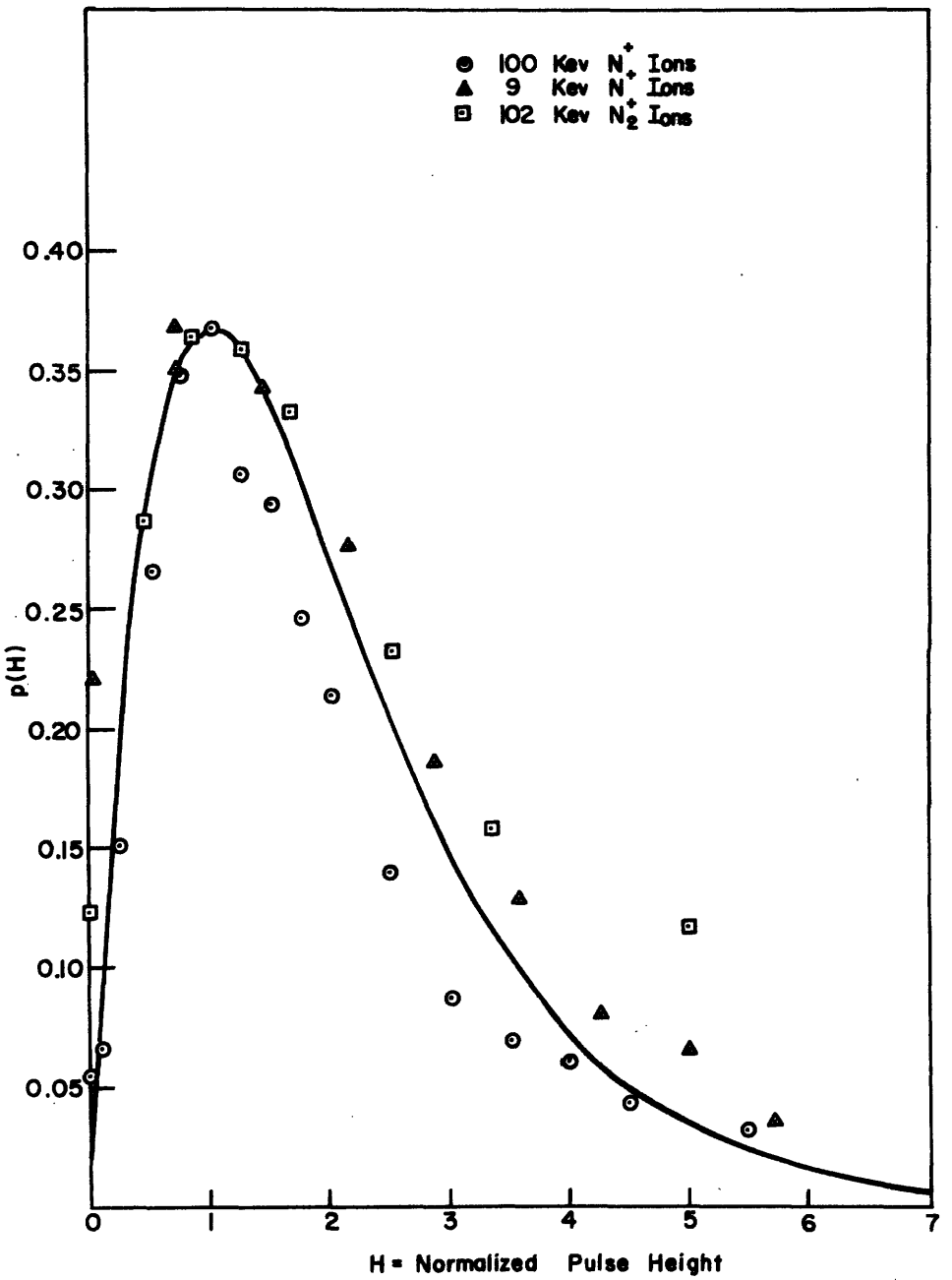

Fig. 5.1. Distribution in amplitude of ion-electron-multiplier output pulses compared with $H\,e^{-H}$ curve. Experimental data (from Barnett, et al.[23]) matched to curve at the mode.

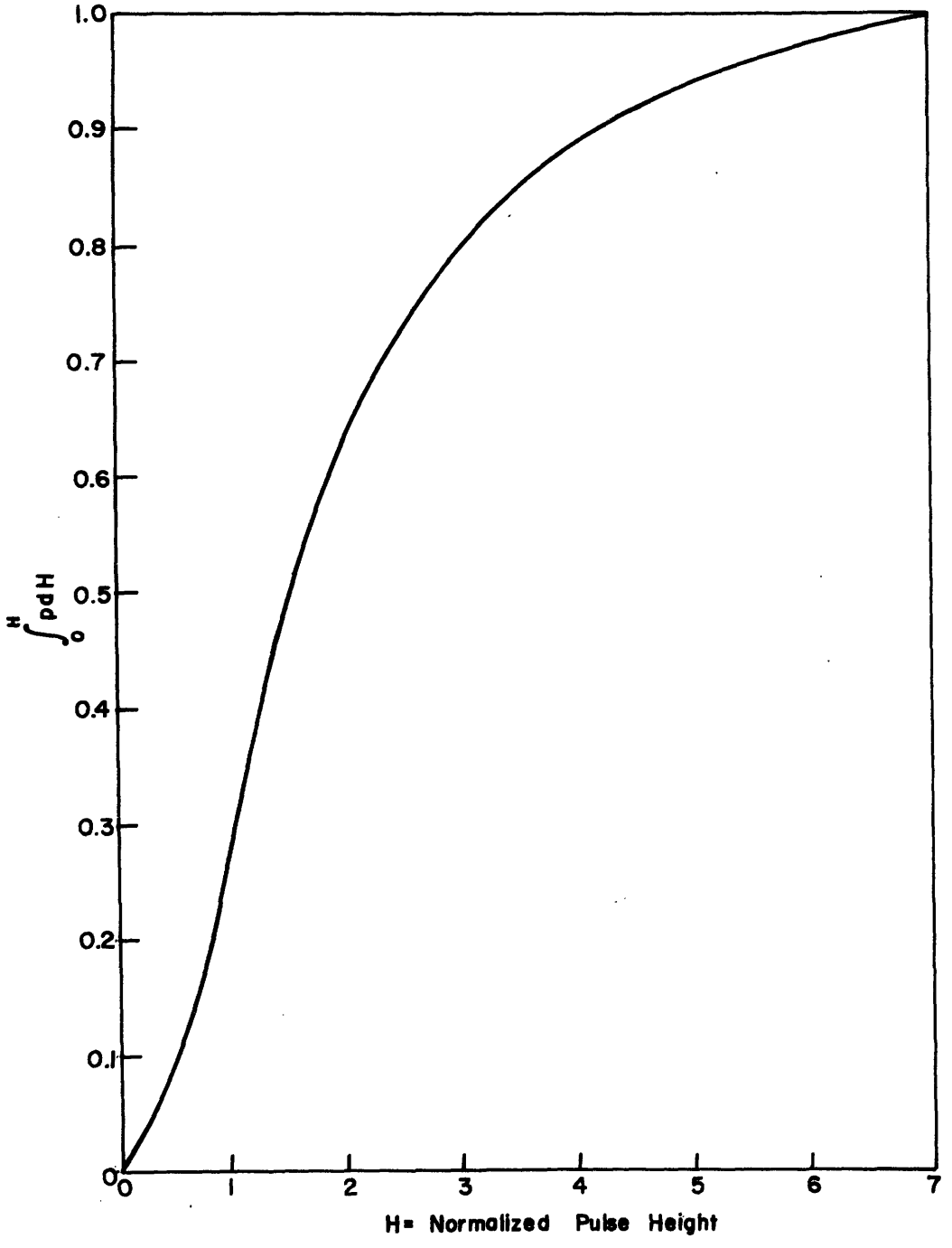

Fig. 5.2. Probability distribution of pulse amplitudes for 100-kev N^+ ions into electron multiplier. Data from Barnett, et al.[23]

Background Noise

Some of the sources of background noise are:

(1) Stray ions generated within the multiplier that impact on one of the first dynodes. These are background-gas molecules ionized by either the high fields or by field-emitted electrons. This noise is kept low by careful construction that minimizes high electric fields, and by maintenance of the highest possible vacuum in the mass spectrometer.

(2) Light from a filament that causes photoemission at the first dynode. This can be minimized by careful light shielding and by use of multiplier dynodes with high work functions.

(3) Soft X rays from electron impacts on source electrodes that causes photoemission. Careful shielding can minimize this noise.

(4) Stray ions produced by the source that leak through or around the mass filter from the ion source to the collector.

With care, background noise from all sources can be reduced to a few counts per second.

Regeneration

A source of noise that is more insidious because it accompanies the signal and so is more difficult to detect is regeneration in the electron multiplier. Electron-impact processes in the latter stages can produce emitted light that causes photoemission from an early dynode, or latter-stage electrons can ionize background-gas molecules,

which then find their way to an early dynode to cause secondary emission of more electrons. In either case there is a second, spurious pulse, following the first one by the transit time of the multiplier (on the order of 0.1 μsec) or by the transit time of the multiplier plus the ion travel time (several μsec), respectively. The regeneration process need not stop at one additional spurious pulse; it can produce two or more, or even become self-sustaining. The cure for regeneration is careful optical and ion shielding of the first stages of the multiplier from the last ones, and operation at the best possible vacuum.

Shot noise

There is inherent in the output of the mass spectrometer shot noise due to the discrete nature of the output - the arrival of individual ions.

To a good approximation the ions arrive at the collector at random times, with the probability of arrival during a given interval statistically independent of the previous intervals. The probability distribution of ion arrival time is then Poisson:

$$P(n,\tau) = \frac{(N\tau)^n}{n!} e^{-N\tau} , \qquad (5.2)$$

where $P(n,\tau)$ is the probability that n ions will arrive in an interval τ, and N is the average number of ions arriving in one second. If for each ion of charge q the current flow is $i_I(t)$, the autocorrelation function of the output is

$$\phi_{II}(\tau) = N \int_{-\infty}^{\infty} dt\ i_I(t) i_I(t+\tau) + (qN)^2, \qquad (5.3)$$

where the first term is the noise and the second is the signal.[34] If the currents i_I are impulses the autocorrelation function becomes

$$\phi_{II}(\tau) = Nq^2 u_o(\tau) + (qN)^2 , \qquad (5.4)$$

where $u_o(\tau)$ is the unit impulse function. The Fourier transform of this is the power density spectrum:

$$\Phi_{II}(\omega) = \frac{Nq^2}{2\pi} + (qN)^2 u_o(\omega). \qquad (5.5)$$

If the output is fed through an ideal low-pass filter with bandwidth Δf, the noise power is

$$P_{noise} = 2N_q^2 \Delta f \qquad (5.6)$$

and the ratio of signal to rms noise is

$$\frac{I_{signal}}{I_{noise}} = \sqrt{\frac{N}{2\Delta f}} . \qquad (5.7)$$

This ratio is the reciprocal of the normalized standard deviation of the output.

Electron-Multiplier Noise

The statistical dispersion in electron-multiplier pulse gain enhances the randomness of the output signal and therefore increases the noise. A simple extension of the process that yielded the autocorrelation function for a shot-noise process gives for the autocorrelation function of the output

$$\phi_{II}(\tau) = \overline{k^2}N \int_{-\infty}^{\infty} i_I(t) i_I(t+\tau)\,dt + (\bar{k}\,qN)^2 , \qquad (5.8)$$

where $\bar{k}$ is the mean pulse gain, $\overline{k^2}$ the mean of the square of the pulse gain, and $i_I(t)$ the input current. It is assumed that there is negligible time dispersion in the electron multiplier. The power-density spectrum is then, under the assumption of impulse inputs:[35]

$$\Phi_{II}(\omega) = \overline{k^2}\,\frac{Nq^2}{2\pi} + (\bar{k}qN)^2 u_o(\omega). \qquad (5.9)$$

Comparison of the power density spectrum with that of the input shot noise shows that the effect of the electron multiplier is to multiply the signal power by the square of the mean gain, the noise power by the mean square gain. The rms signal-to-noise ratio is then multiplied by the factor

$$\sqrt{\bar{k}^2/\overline{k^2}}\,. \qquad (5.10)$$

An idea of the reduction of the signal-to-noise ratio, or enhancement of noise, can be obtained by substitution of typical values of mean gain and mean square gain. If the multiplier-gain probability density function is of the form xe^{-x}, the mean gain is 2!, the mean square gain 3!, and the noise enhancement is by the factor $\sqrt{1.5} \approx 1.2$.

Because the pulse standardizer used in particle-detection operation of the electron multiplier removes the amplitude variations in the electron-multiplier output, it also removes the noise introduced by the electron multiplier. One would expect an improvement in the signal-to-noise ratio by a factor of about 1.2 when the pulse

standardizer is used. This offers an additional reason for use of the electron multiplier as a particle detector for low ion currents.

E. Pulse Signal Processing

Pulse Resolving Time

The finite resolving time of the pulse system, i.e. the fact that the system can respond only to inputs arriving some finite time apart, distorts the output signal and sets an upper limit on the mean pulse rate at which the system can operate.

In the most simple analyses of this distortion it is assumed that the pulse system or "counter" response is controlled by a single element that behaves in one of two very simple fashions:

(1) Non-paralyzable element. If the counter has a dead time ρ after each output pulse, during which it simply ignores all inputs, it is said to be non-paralyzable. The measured mean output rate (N') will be, in terms of the input rate N:[36]

$$N' = \frac{N}{1 + N\rho} . \tag{5.11}$$

(2) Paralyzable element. If after each input event the counter is incapable of responding to another input for a resolving time ρ, it is said to be paralyzable, for it will respond to only the first of a sequence of input events all spaced less than ρ apart. The output rate is:[37]

$$N' = N\, e^{-N\rho} . \tag{5.12}$$

The upper limit on mean particle rate would seem to be that which causes an unacceptable number of pulses, say 10%, to be lost. However, if the resolving time ρ is known, it is possible to use the appropriate equation above to compute the mean rate from the measured one, and so operate at appreciably higher rates. For example, Barton, et al., claim 1% accuracy at a true mean rate of 5×10^6 counts/sec with a non-paralyzable counter with a dead time of 1 μsec.[28] For the correction scheme to work the arrival times of the particles must be truly random, as they are in a mass spectrometer with an electron-bombardment ion source. It is interesting to note that arrival times may very well have not been random in the apparatus used by Barton, because it used a surface ionization source, which tends to give wide fluctuations in the rate of ionization.

Two complicating factors are not considered in the correction equations (Eqs. 5.11 and 5.12). First, there may easily be more than one element in the system that introduces a characteristic resolving time. For example, the pulse system of the quadrupole-mass-spectrometer ion detector used a pulse standardizer preceded by a chain of amplifiers and limiters, each with its own resolving time. Second, the system might not be neatly classifiable as "paralyzable" or "non-paralyzable," but may have some other mode of operation; it may even have resolving times that are functions of the random input pulse amplitudes, and so random variables.

Methods developed by Jost[38] can be used to treat the statistical problems of more realistic models of two or more devices in cascade. A reasonable representation of an ion-detector pulse system that is still tractable for analysis breaks the system into two major components, an amplifier-limiter chain and a pulse standardizer. The amplifier-limiter performance is approximated by an idealized pulse stretcher: for every input pulse there is an output pulse of standard amplitude and width ρ_1; when two pulses overlap, the output amplitude remains unchanged and the pulse continues for time ρ_1 after the last event (Fig. 5.3a and b). The pulse standardizer is assumed to be an ideal non-paralyzable counter element with resolving time $\rho_2 > \rho_1$. There are then two types of performance, depending on how the standardizer responds to the amplifier output. If it senses the level of the output, it will, at the end of a response to a first pulse, respond again if there has been an input in the preceding ρ_1 seconds; the amplifier in effect remembers for the standardizer any input events in time ρ_1 before standardizer recovery (Fig. 5.3c). As a rough approximation, one might guess the output to be that of a single non-paralyzable counter element with resolving time $\rho = \rho_2 - \rho_1$. This obviously cannot hold as $\rho_1 \longrightarrow \rho_2$, because in that limit Eq. 15 would predict that no pulses would be lost. If, on the other hand, the standardizer senses transitions in amplifier output, that is, if it responds to all positive transitions at its

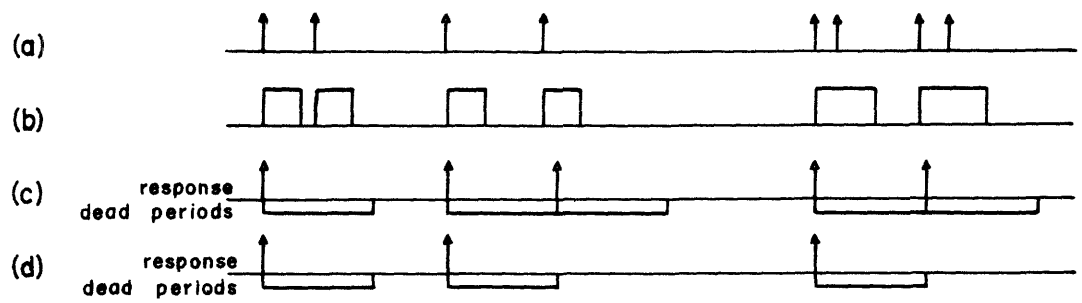

Fig. 5.3. Performance of counter systems:
(a) Input events.
(b) Output of pulse-stretching amplifier.
(c) Response of level-sensing standardizer.
(d) Response of transition-sensing standardizer.

input occurring when it is "live," there is not only no memory of pulses arriving during the dead time, but also a blocking effect: A sequence of pulses starting before the end of the standardizer dead time generates a level that prevents further transitions until the amplifier has recovered after the last pulse (Fig. 5.3d). The amplifier appears as a paralyzable counter element, and the overall system consists of a paralyzable element driving a non-paralyzable one.

Basic Relations in Pulse Processing

Some statistical functions for a sequence of random input events must be defined.[38] Assume that the zeroth event occurs at time t = 0. Then the probability density function for the first event can be defined as P(t); P(t)dt is the probability that the first event lies on the interval t, t + dt. The probability density function for the nth event is then the n-fold convolution of P(t), or $P^{*n}(t)$, defined by

$$P^{*(n+m)}(t) = \int_0^t P^{*n}(\tau)P^{*m}(t-\tau)d\tau \ . \qquad (5.13)$$

One can next define the density of events, F(t); F(t)dt is the expected number of events on the interval t, t + dt. Then

$$F(t) = \sum_{n=1}^{\infty} P^{*n}(t) \ ;$$

from this comes the integral equation

$$F(t) = P(t) + \int_0^t F(t-\tau)P(\tau)d\tau. \qquad (5.14)$$

It will be convenient throughout this analysis to use Laplace transformation, by which convolution is transformed to multiplication. The transform of Eq. 5.14 is

$$f(s) = p(s)\left[1 + f(s)\right] , \tag{5.15}$$

where

$$f(s) = \int_0^\infty e^{-st}F(t)dt ,$$

etc.

It can be shown that the average number of events per unit time is given by[39]

$$N = \lim_{T\to\infty} \frac{1}{T}\int_0^T F(t)dt. \tag{5.16}$$

To obtain N directly from the Laplace transform of F(t) one first defines N(T) to be the function of Eq. 5.16 before the limit is taken. Its transform is then

$$n(s) = \int_0^\infty N(T)e^{-sT}dT = \int_0^\infty dTe^{-sT}\frac{1}{T}\int_0^T F(t)dt = \int_s^\infty \frac{f(s)}{s}\,ds ,$$

and by the final-value theorem,

$$N = \lim_{T\to\infty} N(T) = \lim_{s\to 0} sn(s) = \lim_{s\to 0} s\int_s^\infty \frac{f(s)}{s}\,ds,$$

provided the limit exists. Application of L'Hôpital's rule gives

$$N = \lim_{s\to 0} sf(s) . \tag{5.17}$$

The input pulses to the ion-detection system are Poisson dis-

tributed, and so, from Eq. 5.2, since P(t)dt is the probability of zero pulses in time t and one pulse in time dt, one obtains

$$P(t) = Ne^{-Nt} . \tag{5.18}$$

Laplace transformation of P(t) gives

$$p(s) = \frac{N}{s + N} ; \tag{5.19}$$

use of Eq. 5.15 gives

$$f(s) = \frac{N}{s} \tag{5.20}$$

and

$$F(t) = Nu_{-1}(t), \tag{5.21}$$

where $u_{-1}(t)$ is the unit step function:

$$u_{-1}(t) = 0, \quad t < 0$$
$$= 1, \quad t > 0 .$$

Non-Paralyzable Counter With Arbitrary Input

Consider a non-paralyzable counter element with dead time ρ and input events represented by the characteristic quantities P(t), F(t) and N. The corresponding quantities P'(t), F'(t), and N' that describe the output events can now be determined. The probability of the first output event between t, t + dt, where $t > \rho$, is equal to the sum of the probability of the first input event between t, t + dt and the sum for all n of the probability of the (n + 1)th input event between t, t + dt, given that the nth occurred before $t = \rho$. Then

$$P'(t) = u_{-1}(t - \rho)\left[P(t) + \int_0^{\rho} F(\tau)P(t - \tau)d\tau\right], \qquad (5.22)$$

and application of Eq. 5.14 gives

$$P'(t) = u_{-1}(t - \rho)F(t) - \int_0^{t} u_{-1}(\tau - \rho)F(\tau)P(t-\tau)d\tau. \qquad (5.23)$$

The truncated density function $u_{-1}(t-\rho)F(t)$ will be called $G(t)$ for convenience. Then the Laplace transform of Eq. 5.23 is

$$p'(s) = g(s)\left[1 - p(s)\right], \qquad (5.24)$$

and substitution of p' from this in Eq. 5.15 gives for f'

$$f'(s) = \frac{g(s)}{1 + f(s) - g(s)}. \qquad (5.25)$$

Now

$$g(s) = f(s) - \int_0^{\rho} e^{-st}F(t)dt,$$

so

$$f'(s) = \frac{f(s) - \int_0^{\rho} e^{-st}F(t)dt}{1 + \int_0^{\rho} e^{-st}F(t)dt},$$

and application of Eq. 5.17 gives

$$N' = \frac{N}{1 + \int_0^{\rho} F(t)dt} \qquad (5.26)$$

Level-Sensing Standardizer Driven by Pulse Stretcher

The results of the previous section must be modified for a non-paralyzable standardizer of resolving time ρ_2 that responds to the output level of a pulse-stretching amplifier of resolving

time ρ_1. There is now a finite probability that at the end of the standardizer recovery, at $t = \rho_2$, the system will be "waiting" with a "remembered" pulse, and so will yield another output event. This probability is equal to the probability $L(\rho_1,\rho_2)$ that there were one or more input events in the interval $\rho_2 - \rho_1$, ρ_2. Therefore the probability density of a first output event is equal to the sum of the probability densities of (1) a "waiting" event, (2) a first event at time $t > \rho_2$, and (3) (for all n) an (n+1)th event at $t > \rho_2$, given an nth before $t = \rho_2-\rho_1$. Then

$$P'(t) = L(\rho_1,\rho_2)u_o(t-\rho_2)+u_{-1}(t-\rho_2)\left[P(t)+\int_o^{\rho_2-\rho_1} F(\tau)P(t-\tau)d\tau\right]. \quad (5.27)$$

A solution for the output count rate, N', can most easily be obtained by substitution in Eq. 5.27 of the parameters of a Poisson-distributed input obtained from Eqs. 5.2, 5.18, and 5.21 to give

$$P'(t) = (1-e^{-N\rho_1})u_o(t-\rho_2)+u_{-1}(t-\rho_2)Ne^{N(\rho_2-\rho_1-t)} . \quad (5.28)$$

Laplace transformation of Eq. 5.28 followed by solution of Eq. 5.15 for f' gives

$$f'(s) = \frac{e^{-\rho_2 s}\left[N + s(1 - e^{-N\rho_1})\right]}{N + s - e^{-\rho_2 s}\left[N + s(1 - e^{-N\rho_1})\right]} . \quad (5.29)$$

Application of the limit theorem (Eq. 5.17) gives

$$N' = \frac{N}{e^{-N\rho_1} + N\rho_2} , \quad (5.30)$$

the mean output rate for this system. If the exponential in the denominator is expanded as a power series one has

$$N' \approx \frac{N}{1 + N(\rho_2 - \rho_1)} .$$

Comparison of this with the output rate of the non-paralyzable counter element driven by an ideal Poisson-distributed impulse source (Eq. 5.11) shows that to a first approximation the effect of amplifier pulse stretching is to shorten standardizer dead time by the pulse width, just as was intuitively predicted.

Transition-Sensing Standardizer Driven by Pulse Stretcher

An entirely different approach must be used to determine the mean output rate of a transition-sensing standardizer driven by a pulse-stretching amplifier. This system is equivalent to a paralyzable counter element of resolving time ρ_1 driving a non-paralyzable one of resolving time ρ_2. The output rate of the second stage, N", can be obtained from Eq. 5.26, which, with appropriate notation change, becomes

$$N'' = \frac{N'}{1 + \int_0^{\rho_2} F'(t)dt} , \qquad (5.31)$$

where N' is the output rate and F'(t) the output event density function of the first stage.

The expected number of first stage output pulses in an interval

t, t+dt is zero for $t < \rho_1$. For $t > \rho_1$ it is equal to the sum of the probability of a first pulse in the interval, and the sum for all n of the probability of an (n+1)th pulse, given that the nth pulse occurred before $t-\rho_1$. The output pulse density function of the paralyzable stage is then

$$F'(t) = u_{-1}(t - \rho_1)\left[P(t) + \int_0^{t-\rho_1} F(\tau)P(t-\tau)d\tau\right] . \quad (5.32)$$

The input to the first stage is Poisson distributed in time, so substitution of P(t) and F(t) can be made from Eqs. 5.18 and 5.21 to give

$$F'(t) = u_{-1}(t - \rho_1)N\, e^{-N\rho_1} . \quad (5.33)$$

Then by the average taken over all time, Eq. 5.16,

$$N' = Ne^{-N\rho_1} , \quad (5.34)$$

and by substitution in Eq. 5.31, the mean output rate is

$$N'' = \frac{Ne^{-N\rho_1}}{1 + N(\rho_2 - \rho_1)e^{-N\rho_1}} . \quad (5.35)$$

This is, as might be expected, lower than the output rate of either a simple non-paralyzable counter (Eq. 5.11) or of a level-sensing non-paralyzable standardizer driven by a pulse-stretching amplifier (Eq. 5.30).

F. Linear Signal Processing

The output signal of any mass spectrometer is of necessity subjected to filtering by linear networks, if only the response characteristic of the recording device. The output signals of a particle-detecting ion collector are small enough, some 10^7 events per second or less, that the problem of extracting the signal - the mass spectrum - from the noise is significant. The question arises as to whether or not some sophisticated signal-processing scheme cannot improve upon such time-honored filtering techniques as recorder response times and resistance-capacitance low-pass filters. Unfortunately, as the results in this section show, it seems that it cannot.

Idealized Counting-Rate Meter

The output of the pulse standardizer of a particle-detecting ion collector is fed to a ratemeter circuit that should give an output proportional to the mean pulse rate. Ideally, this ratemeter performs a short-time averaging process on the output of the standardizer to give

$$i_r(t) = \frac{1}{T} \int_{t-T}^{t} i_o(t')dt' \quad . \qquad (5.36)$$

The averaging time T must be short with respect to any variation in the mean rate of input pulses, N, but long with respect to the reciprocal of the rate itself.

In the frequency domain the integration operation becomes

$$I_r(\omega) = \frac{1 - e^{-j\omega T}}{j\omega T} I_o(\omega) , \qquad (5.37)$$

where I_o is the Fourier transform of the standardizer output, I_r the transform of the ratemeter output. If the standardizer output consists of impulses of charge q occurring at random times with a mean rate N , the output of the averager has a power density spectrum obtained by multiplication of Eq. 5.5 by the square of the magnitude of the system function of Eq. 5.37, or

$$\Phi_{rr}(\omega) = (qN)^2 u_o(\omega) + \frac{Nq^2}{2\pi} \frac{\sin^2 (\frac{\omega T}{2})}{(\frac{\omega T}{2})^2} . \qquad (5.38)$$

The first term is the signal (a d-c current, qN), the second, noise. The total noise power, obtained by integration of the second term over all ω, is

$$P_{noise} = \frac{Nq^2}{T} , \qquad (5.39)$$

and the ratio of rms signal to rms noise is

$$\frac{I_{signal}}{I_{noise}} = \sqrt{NT} . \qquad (5.40)$$

R-C Counting-Rate Meter

The most common ratemeter is a simple parallel combination of a resistor and capacitor fed by the pulse source. One can show that this is an approximation to an averaging circuit by writing the equation for the output current in terms of the signal from the pulse

standardizer. The R-C combination has an impulse response of

$$h(t) = \frac{1}{RC}\, u_{-1}(t)\, e^{-t/RC} ,$$

and by convolution with the input signal the output is

$$i_r(t) = \frac{\int_{-\infty}^{t} e^{t'/RC}\, i_o(t')dt'}{RC\, e^{t/RC}} . \qquad (5.41)$$

This rather closely resembles the equation defining the averaging process (Eq. 5.36). The input signal is multiplied by an exponential weighting function and then integrated; the decay of the exponential approximates the lower limit in the exact averaging equation.

The exponential rise and fall characteristic of the R-C circuit introduces error into the observed peak mass line amplitude and puts a long "tail" on the line. The large ratio of observable line amplitudes in a mass spectrum makes the tail the speed-limiting quantity of an R-C ratemeter. If there is to be less than 10% error in a mass line that follows a line 1000 times as large, the tail of the first line must have decayed by a factor of at least 10^4 by the time of the start of the second; thus the RC time constant must be at most 1/9 of the time between lines.

The signal-to-noise ratio for the R-C ratemeter can be computed in the same manner as for the idealized averaging circuit. It is found to be

$$\frac{I_{signal}}{I_{noise}} = \sqrt{2NRC} . \qquad (5.42)$$

Delay-Line Counting-Rate Meter

If the equation defining the averaging process, Eq. 5.36, is rewritten as

$$i_r(t) = \frac{1}{T} \int_{-\infty}^{t} i_o(t')dt' - \frac{1}{T} \int_{-\infty}^{t-T} i_o(t')dt', \quad (5.43)$$

it is obvious that this can be physically realized by an operational amplifier, a delay line, and a differential amplifier (Fig. 5.4). If the components of the circuit all performed ideally, the response of the system to a rectangular input pulse (a very crude approximation to the shape of a line in a mass spectrum) would be as shown in Fig. 5.56. The only signal degredation would be the finite rise and fall time, and the slight increase in the line width at the base.

Any practical delay line degrades the signal because of its inability to discharge all its stored energy into its load terminations within T seconds of the time the input signal is removed. In a transmission-line delay this energy storage would be characterized as mismatch reflections at the terminations. In the lumped-constant lines necessary for the long delays (on the order of milliseconds) required by the averaging circuit, the energy storage and dissipation process is much more complex, but for purposes of analysis can still be assumed to be caused by reflections. Then an input pulse to the line will produce a principal output pulse at time T and a sequence of "reflection" pulses at 3T, 5T, ···, with amplitudes in a decreasing geometric progression with ratio defined as r, where r may be positive

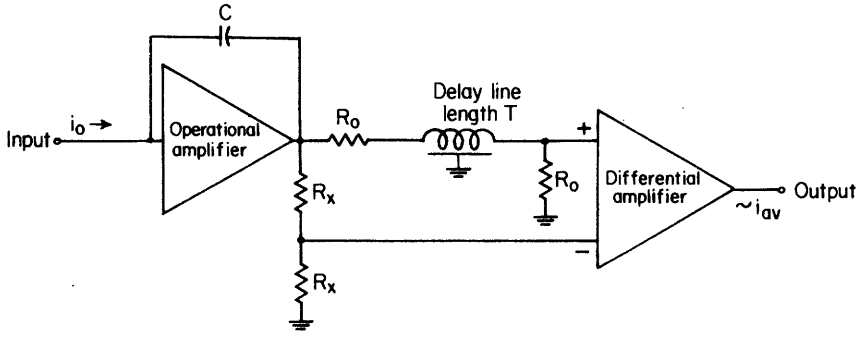

Fig. 5.4. Delay-line ratemeter.

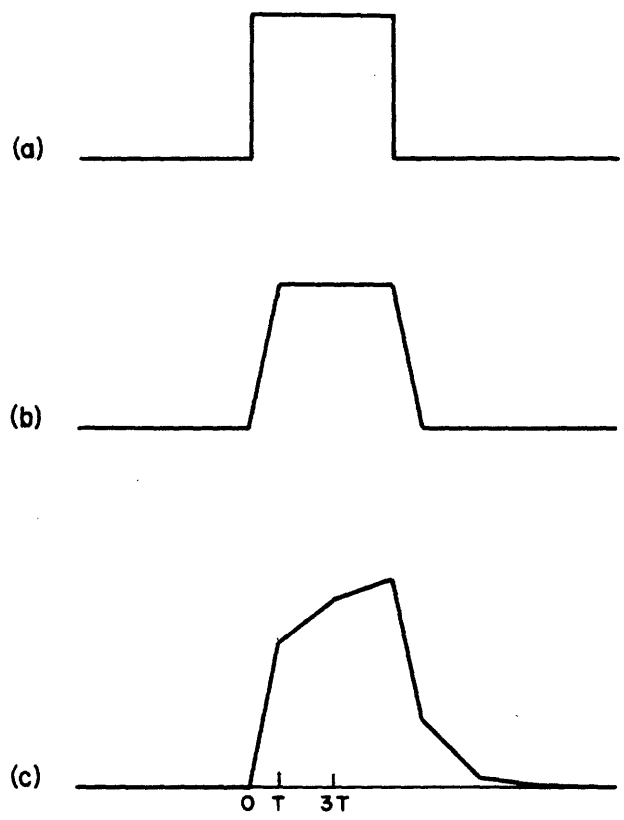

Fig. 5.5. Response of delay-line ratemeter: (a)Input. (b) Output for ideal line. (c) Output for reflecting line, r = 0.2.

or negative.*

An example of the additional signal degredation introduced by delay-line reflections is given in Fig. 5.5c. The distortion of the output is exaggerated, for the sake of clarity, by the choice of the exceptionally high reflection ratio r = 0.2.

The presence of transmission-line reflections changes Eq. 5.36 for the output function to

$$i_r(t) = \frac{1}{T} \int_{t-T}^{t} i_o(t')dt' + \epsilon(t), \qquad (5.44)$$

where the error $\epsilon(t)$ is

$$\epsilon(t) = \frac{r}{T} \sum_{k=0}^{\infty} r^k \int_{t-(2k+3)T}^{t-(2k+1)T} i_o(t')dt'. \qquad (5.45)$$

The effect of this error on output amplitude will be compared with the effect of error of the R-C ratemeter in the next section. Another consequence is a change in the noise properties of the ratemeter. The error of Eq. 5.45 addes a term to the frequency-domain transfer function of Eq. 5.37,

$$\frac{r}{j\omega T} \frac{e^{-j\omega T} - e^{-j3\omega T}}{1 - r\, e^{-j2\omega T}} .$$

Appropriate integration of the square of the magnitude of the total transfer function shows that, for small r, the reflection error

---

* It should be noted that if one side of the output is taken from the input end of the delay line, rather than from a divider as shown in Fig. 5.4, there will also be reflection pulses at 2T, 4T, ···. This more complicated case has not been investigated.

multiplies the output noise by the ratio

$$\frac{\text{noise with reflection}}{\text{noise without reflection}} \approx 1 - 3r, \qquad (5.46)$$

a negligible change for practical values of r.

Another imperfection in practical delay lines is a finite rise time. Because the delay time, T, of the line must be chosen to be not larger than the time in which any change in input signal can occur, and the rise time of any reasonable delay line is much smaller, this finite rise time can have little effect on the system transient response. However, it might have some effect on the noise characteristics. If it is assumed that the line has an exponential rise characteristic with time constant $T_r/2.2$, where T_r is the rise time measured at the 10% and 90% levels, it is easily shown that the signal-to-noise ratio of Eq. 5.40 is multiplied by the factor

$$\frac{1}{\sqrt{1 + \frac{T_r}{4.4T}}}.$$

Since even the poorest commercial lines have $T/T_r > 10$, this effect is negligible.

Comparison of Ratemeters

The R-C ratemeter has all advantages of simplicity and economy over the delay-line circuit, so the latter must give some definite advantages in performance to be considered for practical

applications. Comparisons of the two circuits can be made on the basis of transient response and noise characteristics. The transient response of interest is the response to a step function; this should give some idea of the decay of the "tail" from one mass-spectral line before the arrival of a second, much smaller one. The noise characteristic of interest is the ratio of rms signal to rms shot noise.

To gain some idea of the upper limit of delay-line ratemeter performance, one incorporating an ideal delay line will be compared to the R-C ratemeter. For a step-function input the output of the delay-line circuit reaches full amplitude in time T (Fig. 5.5b) while the output of the R-C circuit has an exponentially decaying error,

$$\epsilon_{RC}(t) = e^{-t/RC} . \qquad (5.47)$$

If RC = T/2, the two ratemeters will, according to Eqs. 5.40 and 5.42, have identical signal-to-noise ratios. Then at time T the delay-line circuit will have zero error, but the R-C circuit will still have an error of $e^{-2} = 0.14$.

A somewhat better comparison might be had by a choice of the RC time constant for some maximum permissible error at time T and the assumption that there is a minimum acceptable signal-to-noise ratio for the ratemeter output. The ratio of the ion count rates that give this signal-to-noise ratio with the two ratemeters can

then be taken as a comparative figure of merit. If the two signal-to-noise ratios, Eqs. 5.40 and 5.42, are equated one obtains

$$\frac{(N_{dl})_{min}}{(N_{RC})_{min}} = \frac{2RC}{T} \quad , \tag{5.48}$$

where $(N_{dl})_{min}$ and $(N_{RC})_{min}$ are the minimum count rates for acceptable signals from the delay-line and R-C ratemeters, respectively. In terms of acceptable error at time T this ratio becomes

$$\frac{(N_{dl})_{min}}{(N_{RC})_{min}} = \frac{2}{\ln \epsilon_{RC}(T)} \quad . \tag{5.49}$$

If one assumes the desired error at time T to be less than 10^{-4}, which might be necessary for an extreme case of a low-amplitude mass line closely following a high-amplitude line, the ratio becomes

$$\frac{(N_{dl})_{min}}{(N_{RC})_{min}} = \frac{2}{4 \ln 10} = \frac{1}{4.6} \quad . \tag{5.50}$$

In the case most favorable to the delay-line ratemeter, that circuit will accept a minimum count rate lower than that of the R-C integrator by a factor of 4.6.

The effect of reflections on the transient response of a delay-line ratemeter must be considered. Application of Eqs. 5.44 and 5.45 to the case of a unit step input to the ratemeter, shows

that the output is a sequence of straight line segments approaching a final value in roughly exponential fashion, with nodes at times $t = (2j + 1)T$, $j = 0, 1, \cdots$, and amplitudes

$$(i_r)_j = 1 + \epsilon_j = 1 + \frac{2r(1 - r^j)}{1 - r} \quad .$$

According to this, long after the input step there is a constant error $2r/(1-r)$; this simple scaling error can be easily eliminated by changing system gain by the factor $(1-r)/(1+r)$, which changes the output to

$$(i_r)_j = 1 + \epsilon_j = 1 - \frac{2r^{j+1}}{1 + r} \quad . \qquad (5.51)$$

Comparison of the performances of the imperfect delay-line ratemeter and the R-C ratemeter is difficult because the two error curves differ in shape, but one can assume a time constant $RC = T/2$, so that the signal-to-noise ratios will be equal, and then compare errors at the particular time at which the delay-line error is largest with respect to the other.

Determination of the time at which delay-line error is relatively largest is a two-step process. The first step involves determination of the point on each line segment in the error function at which the relative error is a maximum; the second involves determination of the line segment in which this error is largest.

In the interval $(j+1)T < t < (j+3)T$ time may be represented by the parameter x_j, defined by

$$t = (2j + 1)T + 2x_j T ;$$

the error in the delay-line ratemeter output is then defined by the line segment connecting the jth and (j+1)th node,

$$\epsilon_{dl} = - \frac{2r^{j+1}}{1 + r} \left[1 - (1 - r)x_j \right] , \qquad (5.52)$$

and if RC = T/2 the error in the R-C circuit output is

$$\epsilon_{RC} = e^{2(2j+1) - 4x_j} . \qquad (5.53)$$

The relative error of the delay-line circuit is then

$$\left| \frac{\epsilon_{dl}}{\epsilon_{RC}} \right| = \frac{2|r^{j+1}|}{1 + r} e^{2(2j+1) - 4x_j} \left[1 - (1 - r)x_j \right] . \qquad (5.54)$$

Differentiation with respect to x_j shows that for small r the maximum relative error occurs at approximately $x_j = 3/4$, and is

$$\left| \frac{\epsilon_{dl}}{\epsilon_{RC}} \right| = \frac{|r|^{j+1}}{2} e^{4j+5} . \qquad (5.55)$$

For $r > e^{-4}$ this diverges at large j, and the delay-line circuit is clearly inferior; for $r < e^{-4}$ the most unfavorable case is j = 0. The error in the delay-line circuit is then a maximum, relative to an exponential of time constant T/2, at $t \approx 5/2\ T$ and is

$$\left| \frac{\epsilon_{dl}}{\epsilon_{RC}} \right| \approx \frac{r}{2} e^{5} . \qquad (5.56)$$

A line with a rather low reflection ratio, $r < 0.014$, is required to make possible any improvement over a simple R-C ratemeter.

One may conclude that because the R-C ratemeter is much simpler, less expensive, and can be easily adjusted for the best compromise time constant for any given input signal, it is still the best choice for most applications.

It is possible to formulate an upper limit for spectral sweep speeds for a mass spectrometer with a particle-detecting ion collector and an R-C ratemeter. The time per spectral line (T_{line}) is the sum of the required decay time (T_1) after one line and the rise time (T_2) of a second. Let D be the spectral dynamic range, i.e., the ratio of largest line amplitude to the smallest, and F the maximum acceptable "interference factor," i.e., the amplitude of the tail of a preceding line relative to the total amplitude of the line under consideration. Then if lines have abrupt rise and fall transitions and the smallest spectral line follows the largest, the minimum time between lines is given by

$$D\, e^{-T_1/RC} = F \,. \qquad (5.57)$$

The RC product is defined in terms of a signal-to-shot-noise ratio and count rate (Eq. 5.42). If the largest line corresponds to a count rate N_{max}, the largest the pulse system can handle, the lowest count rate is N_{max}/D. Let S_{min} be the lowest acceptable signal-to-noise ratio. Then

$$RC = \frac{D\, S_{min}^2}{2\, N_{max}} \,. \qquad (5.58)$$

The line rise time can be taken to be the time for a rising exponential to come within $1/S_{min}$, or one standard deviation, of the final value:

$$e^{-T_2/RC} = \frac{1}{S_{min}} \quad . \tag{5.59}$$

The total time per mass line $(T_1 + T_2)$ is, from Eqs. 5.57 through 5.59,

$$T_{line} = \frac{S_{min}^2 \, D}{2 \, N_{max}} \ln \left[\frac{D \, S_{min}}{F} \right] \quad . \tag{5.60}$$

If, for example, it is assumed that $N_{max} = 5 \times 10^6$, $S_{min} = 10$, $D = 100$, and $F = 0.1$, then

$$T_{line} = 9 \text{ msec},$$

and a spectrum of 100 lines can be swept in 0.9 sec. This result depends strongly on the assumed signal-to-noise ratio; if $S_{min} = 100$, the time for a mass line increases to

$$T_{line} = 1.2 \text{ sec}.$$

Optimum Signal Processing

The comparison of the R-C and delay-line ratemeters is a small part of a much larger question: What linear system attached to the output of the pulse standardizer gives the "best" output signal in the presence of noise?

The word "best" must be defined in terms of some quantitative error criterion that is tractable to an analytical minimization process. One frequently used criterion, mean square error, leads directly to

the synthesis of a linear "optimum" network in terms of signal and noise correlation functions.[40] However, a mean-square error criterion is of little value for mass spectrometric signals because it weights large errors more heavily than small ones, and therefore could easily term optimum a linear network that would give a small error during a mass line but a small but very long tail following the line.

In one attempt to find an optimum signal-processing system the criterion was a minimum rms noise relative to a signal given a fixed mean delay L in the system response.[41] The optimum linear system was found to have an impulse response falling linearly to zero (Fig. 5.6a). The rms signal-to-noise ratio is then

$$\frac{I_{signal}}{I_{noise}} = \sqrt{\frac{9}{4}\ NL}\ , \tag{5.61}$$

compared to

$$\frac{I_{signal}}{I_{noise}} = \sqrt{2\ NL} \tag{5.62}$$

for both the simple R-C ratemeter and the delay-line ratemeter (whose impulse responses are also shown in Fig. 5.6). Because the "optimum" system yields a signal-to-noise ratio only 6% better than a simple R-C circuit, and is rather difficult to synthesize in practice, it was concluded that the R-C circuit was the best practical compromise.

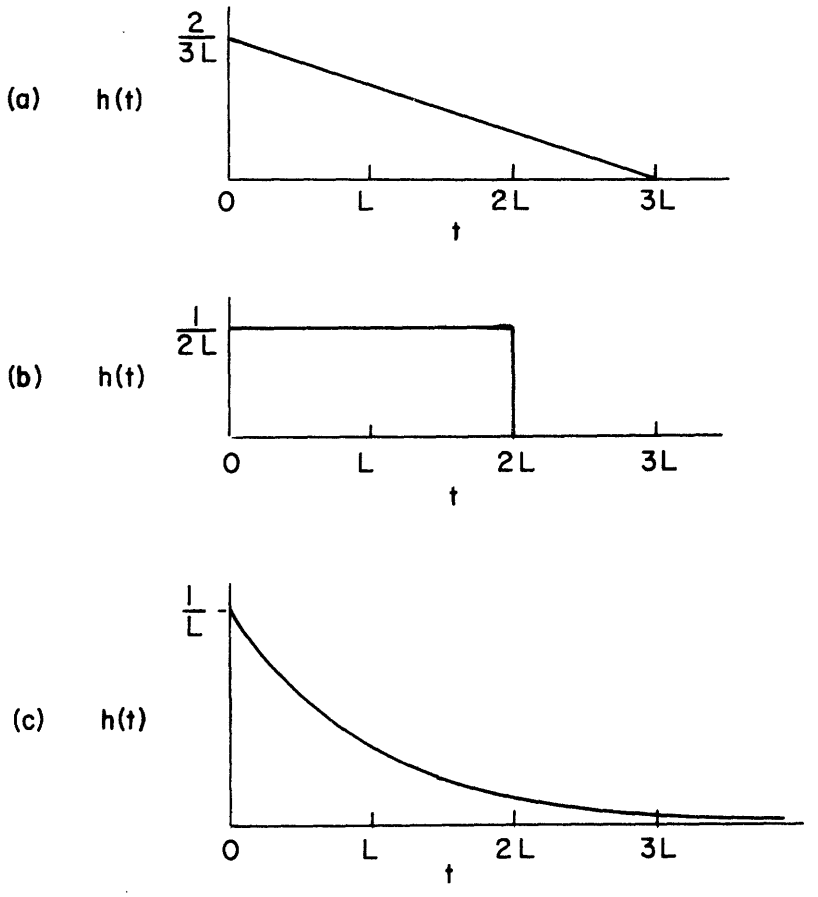

Fig. 5.6. Impulse response of ratemeter circuits:
(a) "Optimum" response.
(b) "Delay-line" response.
(c) Conventional R-C response.
From Vincent.[41]

The delay-line ratemeter satisfies a different optimization criterion - minimum "memory" time, or minimum time for complete response to an input signal. It is interesting that by one criterion, step response, the ideal delay-line circuit shows an appreciable advantage over the conventional R-C circuit, while by another criterion, average delay, it shows no advantage at all. This illustrates just how strongly an "optimum" design depends upon the choice of criteria.

Another work worthy of mention is concerned with the more limited problem of the choice of time constant for an R-C ratemeter. Fröhner[42] has calculated the response of R-C circuits to inputs whose rates vary as the Gaussian function, $e^{-t^2/2d}$, with particular attention to such factors as line broadening, line displacement (delay or lag), and line peak attenuation. He has also computed the "optimum" value of time constant, using as his criterion a maximization of the peak value of the output relative to the rms noise resulting from a constant background-count rate. While this may be a useful criterion for gamma-ray spectroscopy (his intended application) it is of little value in mass spectrometry, where the background may be less than one count per second.

VI. ELECTRON-MULTIPLIER ION DETECTOR

A. System Characteristics

General Requirements

Operation of the electron-multiplier ion detector of the mass spectrometer as a particle detector requires electronic circuits to amplify the pulses of current from the electron multiplier and convert them to pulses of standard amplitude and width. The design requirements may be summarized as follows:

1. Sensitivity. The system must have adequate sensitivity to detect the smallest ion-produced pulses from the electron multiplier.

2. Amplitude range. The system must be capable of accepting at least a two-order-of-magnitude dynamic range of input amplitudes arising from statistical variations in multiplier gain, plus as much as possible of a third order-of-magnitude range coming from secular changes and specific discrimination.

3. Output constancy. The output pulse amplitude and width must be independent of all input variables.

4. Response speed. To make possible operation at high ion count rates, the system response time must be as near the electron-multiplier pulse width (several nsec) as possible. The design goal was a count loss of less than 10% at an input rate of 5×10^6/sec.

5. Rate insensitivity. The ability to respond to closely spaced pulses should be independent of the count rate.

6. Noise insensitivity. Response to random noise, or to extraneous signals such as the r-f voltage applied to the quadrupole, must be negligible.

The requirements of output constancy can be easily met by any one of a number of trigger circuits or pulse standardizers that deliver a standard pulse when their input goes beyond a certain threshold. The response-speed design goal requires a standardizer resolving time of 20 nsec. In order to meet the sensitivity requirement the standardizer must be preceded by an amplifier that will bring the signals up to the trigger threshold; the amplifier must be a broad-band one in order to avoid degredation of the response speed. The requirement on noise insensitivity is rather easily met; the signals from the 20-stage electron multiplier are large enough to be well out of the random noise of amplifier input stages.

Amplitude Range

The requirement on amplitude range presents problems that are not immediately obvious. It would seem that a wide-range system would require only an amplifier capable of bringing the smallest pulse from the electron multiplier up to the standardizer trigger threshold, plus one or more limiting devices to prevent amplifier and standardizer saturation. However, the response of the amplifier system to its input pulse (approximately the system impulse response) will have after the main output a small but finite "tail" of irregular

nature, which will be called "post-pulse noise." If this post-pulse noise is above the trigger threshold at the time of the recovery of the standardizer from the pulse, a second standard output pulse will result - a "double count." If it is substantially below the zero level, it can block detection of a small following pulse - a "lost count." Because of the wide range of input pulse amplitudes, a relatively small amount of post-pulse noise can cause either double or lost counts. For example, if the input dynamic range is three orders of magnitude and the amplifier system is linear, post-pulse noise of 1 part in 1000 from an input of the largest amplitude will be as large as the response to an input of the smallest amplitude. The pulse system must then have a post-pulse noise, measured at the resolving time of the standardizer, better than one part in one thousand. This makes it mandatory to place amplitude limiters in the system at the earliest possible stage, preferably before any amplifiers, so the broad-band amplifier circuits are never confronted with such a wide range in amplitudes.*

Rate Insensitivity

The second system requirement warranting special comment, rate insensitivity, is familiar to all designers of pulse systems. Basically, the problem is this: Any practical wide-band high-gain amplifier in a pulse system must be a-c coupled. This presents no special

---

* This remedy was suggested by Mr. Charles Freed of M.I.T. Lincoln Laboratory.

problem in the amplification of pulses that are either uniformly or widely spaced. If, however, there occur bursts of closely spaced pulses, pulse baseline shift will occur. For example, assume the input consists of a sequence of positive pulses of shape described by $p(t)$, a function with unit peak amplitude, that occur at times t_j with relative amplitudes a_j:

$$v = \sum_j a_j p(t - t_j).$$

If the t_j and a_j are independent random variables, the d-c value of the pulse train is $N\ \bar{a}\ P$, where N is the mean pulse rate, $\bar{a}$ is the mean value of a_j, and $P = \int_{-\infty}^{\infty} p(t)dt$. If the pulse train is passed through a unity-gain a-c-coupled amplifier, the d-c component will be eliminated. The output is then

$$v_o = \sum_j a_j p(t - t_j) - N\ \bar{a}\ P.$$

All those pulses for which $a_j < N\ \bar{a}\ P$ will not even reach zero d-c level and must lie below the detection threshold of the pulse standardizer.

The ion-detector pulse system requires that baseline shift be small enough that no signal pulses be shifted below the standardizer threshold and no noise pulses be shifted above it.

There are several possible cures for the problem of pulse baseline shift. Perhaps the simplest is a single-diode d-c restorer that clamps the most negative point (for positive pulses)

of the a-c coupled waveform to ground.[43] This method is effective only when the signal is substantially larger than the forward drop of the clamp diode. Unfortunately, the signals involved in any wide-band pulse amplifier are small with respect to the forward drop of a high-speed diode, so the diode clamp is ruled out. A second, somewhat more involved system uses a diode rectifier to sense the d-c level of the amplifier output and a low-speed d-c feddback amplifier driven by the rectifier to add the necessary d-c signal to the pulse signal.[44] Problems of diode forward drop are not as important for such a circuit because the diode can be used as a small-signal detector. Another common method of overcoming baseline shift is differentiation of the pulse to remove its d-c level. Ideally, the performance of the differentiator would be as shown in Fig. 6.1a and b. Pulses, assumed triangular for simplicity, are differentiated to yield doublets. These doublets can be passed through a-c coupled amplifiers and symmetrical amplitude limiters without change in wave shape or introduction of any d-c component. Such performance is based upon an assumption of equal rise and fall times of the input pulse. If, as is actually the case, the rise and fall times are unequal, as in Fig. 6.1c, the differentiated doublet has unequal amplitudes and widths for its two lobes. When this is passed through an amplifier and symmetrical limiter, the lobes will have equal amplitude but unequal widths (Fig. 6.1e). There is then a d-c component associated with each pulse, and there

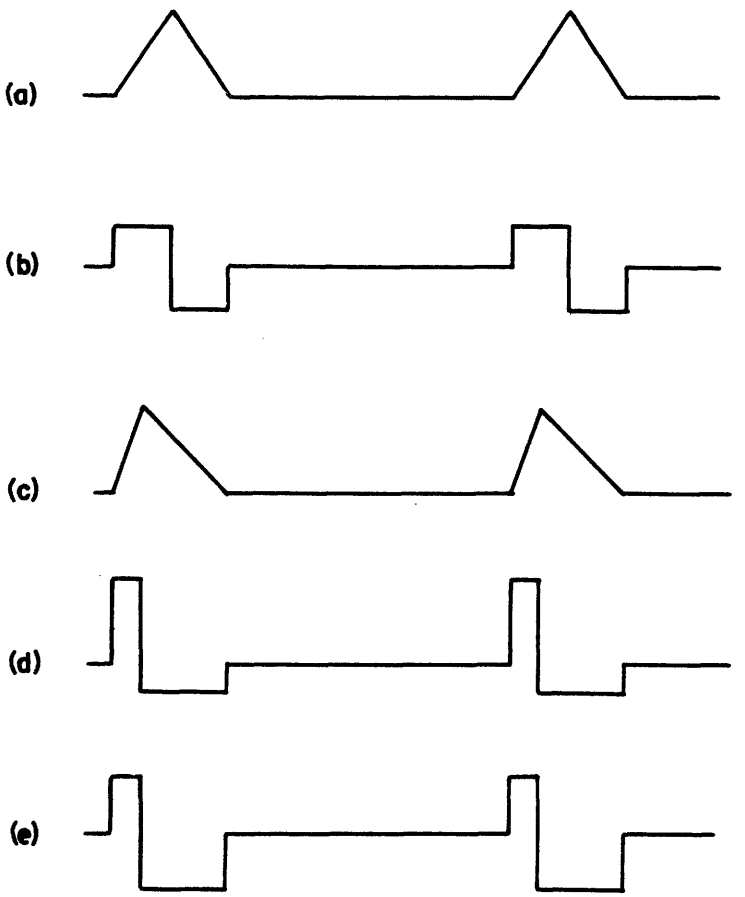

Fig. 6.1. Differentiator-limiter performance.

a. Input pulse with equal rise and fall times.
b. Input pulse differentiated.
c. Input pulse with unequal rise and fall times.
d. Pulse of (c) differentiated.
e. Pulse of (d) amplified and amplitude-limited.

will be baseline shift if the pulse is passed through subsequent a-c coupled amplifiers. This is precisely the case in the ion-detector pulse system, except, of course, the pulses do not have such idealized shapes.

Even if the system input pulse has equal rise and fall times, signal degredation caused by the finite frequency response of the amplifiers and differentiator will lead to unequal output lobe widths. For example, if the differentiator is a high-pass resistance-capacitance filter (which it is in the actual pulse system), its effect on an ideal triangular input will be as shown in Fig. 6.2. Again the trailing lobe of the output is wider than the leading one.

The use of differentiation was a fundamental design error. However, at input rates of practical interest ($< 10^7$ counts/sec), the resulting baseline shift lay within the threshold tolerance of the pulse standardizer, so no attempt was made to correct it. In any redesign the differentiator should probably be omitted, and rectifier-and-d-c-feedback-amplifier compensation used immediately before each nonlinear operation, e.g., amplitude limiting and threshold detection.

B. Pulse System

The pulse system is shown in diagrammatic form in Fig. 6.3. The current pulse from the electron multiplier is applied to an input "preamplifier" that drives a chain of alternated broad-band

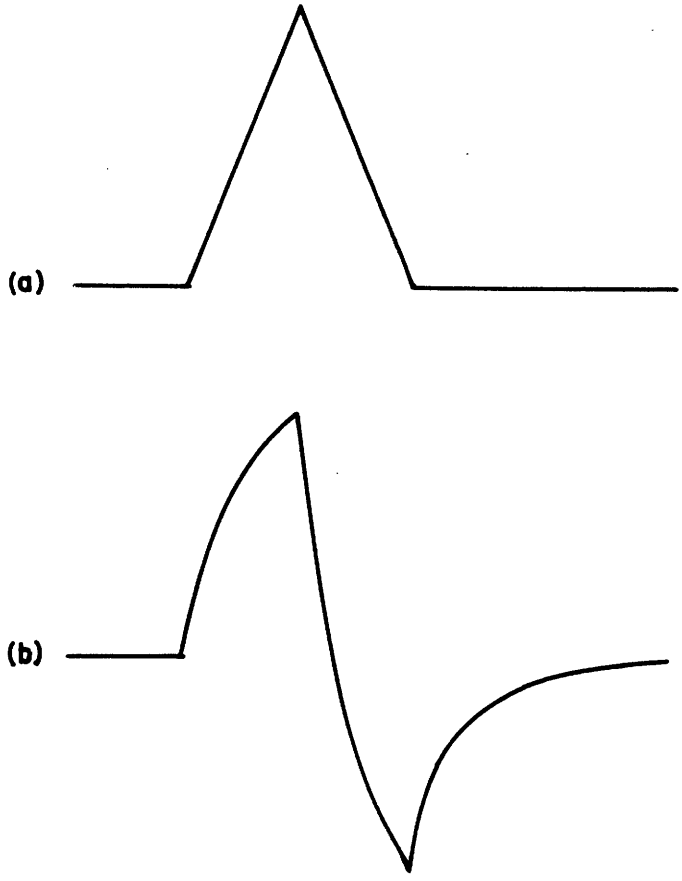

Fig. 6.2. Differentiator response.

a. Ideal triangular input.

b. Output of high-pass R-C filter with time constant equal to 1/4 total input pulse width.

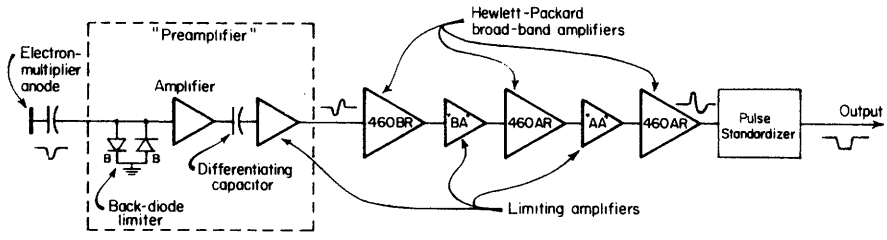

Fig. 6.3. Ion-detector pulse system.

distributed amplifiers and transistor limiting amplifiers. The output of the chain drives a pulse standardizer.

Electron Multiplier

A 20-stage electron multiplier (Chap. III) was constructed for the ion detection system in order to obtain gains high enough to permit the use of amplitude limiters before the first pulse amplifier. The circuit for this multiplier is shown in Fig. 6.4. One power supply provides the electron-mulitplier-stage accelerating voltages by means of a voltage divider. Output pulses are capacitively coupled from the multiplier anode to the preamplifier so the multiplier may be operated at an arbitrary potential with respect to ground. A second power supply establishes the ion accelerating voltage independently of the multiplier voltage.

The dynode structure of the RCA 6810A photomultiplier was chosen for the 20-stage multiplier because it provides low dispersion in electron transit times and so a short output pulse for a single ion incident on the first dynode. The 14-stage 6810A is rated at a rise time, between the 10% and 90% points, of 3 nsec. If, for ease of computation, the multiplier impulse response is assumed to be a Gaussian function of time, and if all 20 stages of the mass-spectrometer multiplier are assumed to have the same dispersion time, so that the 20-stage rise time is $\sqrt{20/14}$ of that of the 6810A, the impulse response for 20 stages is a Gaussian with full width at half maximum amplitude of 3.3 nsec.

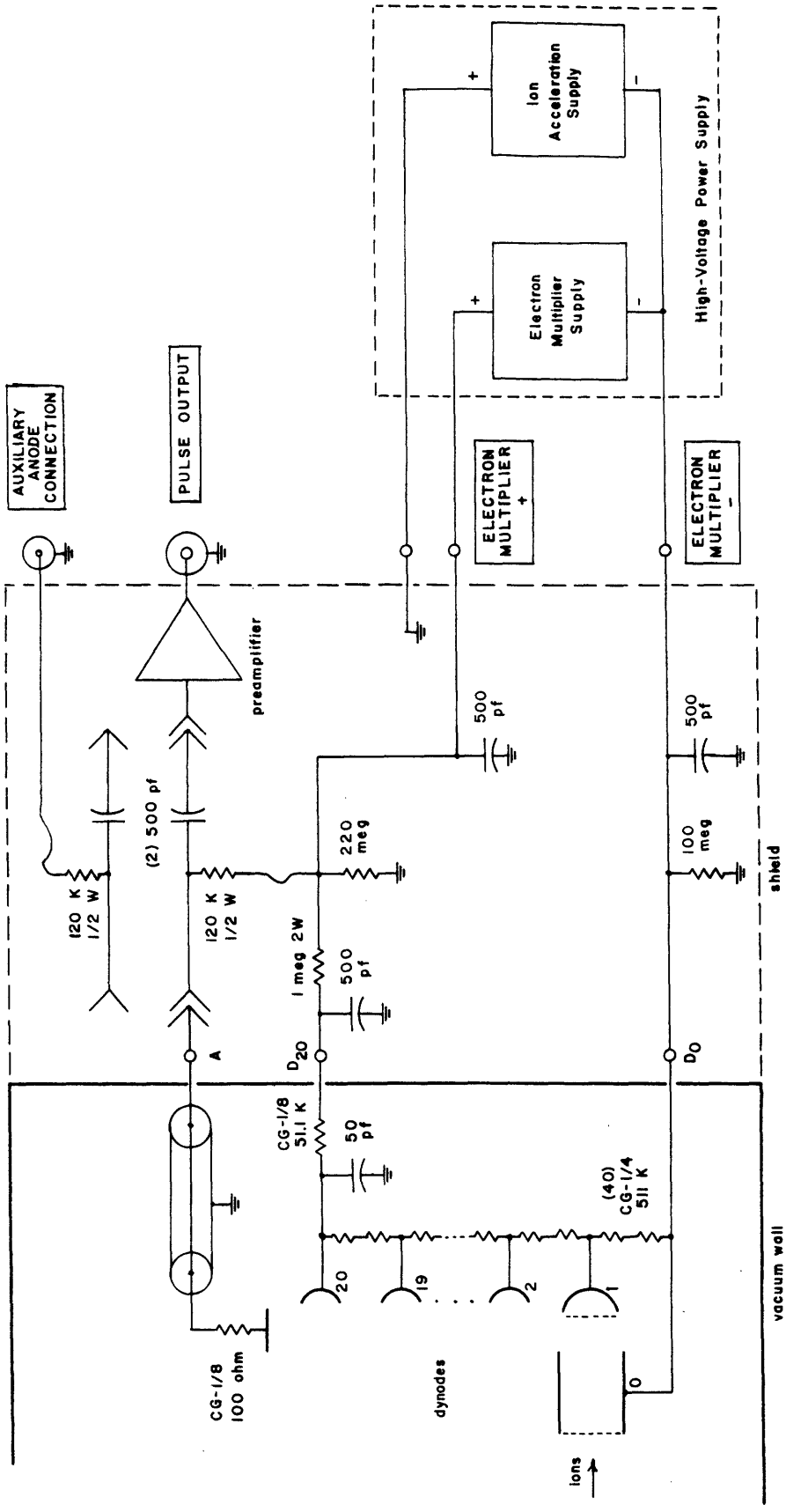

Fig. 6.4. Electron-multiplier circuit. Resistors inside vacuum wall are Texas Instrument, hard-glass sealed. 500 pf capacitors are Centralab TV-20.

The peak amplitude of the response to a single ion is then

$$i_m = 4.6 \times 10^{-11} K \quad [\text{amperes}],$$

where K is the multiplier gain.

The mass spectrometer multiplier is, strictly speaking, not a 20-stage device because of the presence of the ion-extraction tube that serves as a zeroth dynode. This may cause far greater pulse-width degredation than would be expected by the mere addition of a single dynode. The first dynode of the multiplier was made large for effective ion collection. No particular care was given to variation in first-to-second-dynode transit time for electrons emitted from various points on the first-dynode surface, because all electrons from an incident ion would come from the same point, and so suffer little time dispersion. With the addition of the zeroth dynode, however, the first dynode becomes an electron-to-electron multiplier as well as an ion-to-electron one. Each ion incident on the zeroth dynode produces several electrons that may travel to different points on the second dynode. The transit-time dispersion of their secondaries can be substantial.*

---

* The zeroth dynode also brings into the realm of possibility two or more pulses for an incident ion. Those ions that strike the zeroth dynode do so at an oblique angle. It is possible that some of them could produce secondary electrons there, but themselves be reflected to cause still another ion-to-electron conversion at the first dynode. The transit time of electrons from the zeroth dynode to the first would be on the order of nanoseconds, while the transit time of the reflected ion would be several hundred times as long. One ion could then produce two output pulses separated a fraction of a microsecond.

The overall pulse performance of an electron multiplier is, of course, much more than a matter of the dispersion time. Any stray reactance in the multiplier output circuit causes ringing, or at least pulse broadening, that represents a post-pulse noise that can only be enhanced in a subsequent limiting operation. Every element of the output circuit must therefore be designed for optimum response to nanosecond pulses.

To minimize stray reactance, the multiplier anode lead should be as short as possible, but shortness was not easy to achieve with the existing system. Because the vacuum chamber was not specifically designed for this mass-filter and multiplier assembly, the electron-multiplier anode is some 18 cm from the vacuum wall; there is also an additional 6 cm to the end of the high-voltage anode-feed-through insulator. In order to minimize the effect of the inductance of a 24-cm wire for nanosecond pulses, the anode lead was shielded inside the vacuum system, in an approximation to a coaxial line. However, because of the non-constant load impedance presented by the limiter input of the preamplifier, and line impedance changes associated with changes in dimensions and dielectric material at a number of points, a sizable amount of ringing persisted. This could be only partially damped by a resistor at the anode. Any future system should have the anode as close to the vacuum wall as possible.

Capacitance between the anode and last dynode can lead to out-

put-pulse degredation unless the dynode voltage is held constant. The last dynode and anode have an equivalent circuit for pulses shown in Fig. 6.5a. Each element has a capacitance to ground, C_d and C_a respectively, and a mutual capacitance C_{ad}. An electron current I_a flows from the anode to the last dynode, and a current I_a/k from the last dynode to the previous one (k is stage gain). A Norton equivalent circuit (Fig. 6.5b) of all sources driving the anode shows that there is substantial reduction in effective anode current by displacement current - by a factor of 0.7 for a stage gain of 2.5 and $C_{ad} = C_d$. The cure is a large C_d - a 50 pf capacitor mounted inside the vacuum system, right at the multiplier structure.

The circuit originally had no resistor in the dynode lead. The dynode capacitance then combined with the inductance of the lead to constitute a resonant circuit that was excited by multiplier current pulses. The resulting lightly damped sinusoidal oscillation was capacitively coupled to the anode and amplified and quantized by the pulse electronics, providing multiple output pulses for a single input ion. The resistor eliminated this ringing.

In so far as the probability of emission of n electrons from a dynode is described by a Poisson distribution of mean λ, the probability of zero output is $e^{-\lambda}$ and the standard deviation of the distribution, relative to the mean, is $1/\sqrt{\lambda}$. In order to obtain the smallest possible gain dispersion and lowest probability of

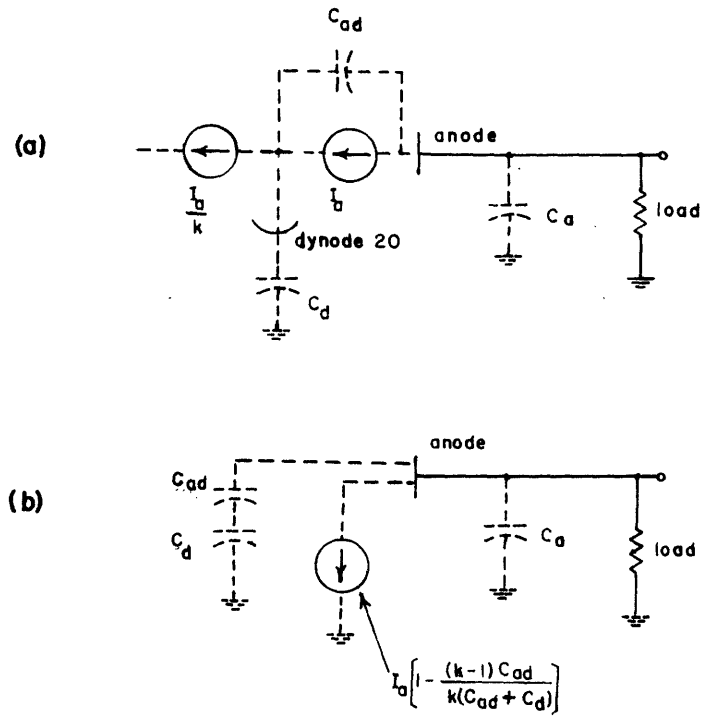

Fig. 6.5. Electron-multiplier anode circuit.

a. Circuit for pulses.

b. Norton equivalent of anode circuit.

missed counts, it is advantageous to operate the multiplier with the highest possible mean yield per ion. Because yield from an ion-to-electron dynode increases monotonically with voltage (for all practical voltages),[23] it is desirable to operate the first dynode at the highest possible voltages. It was intended that normal multiplier operation be with the first dynode at -15 kv, the power-supply limit, with the multiplier voltage adjusted to the value between 5 and 10 kv that gave optimum mean overall gain. Unfortunately, breakdown occurs from the first dynode when it is more than 12 kv from ground, and from the anode and last dynode when they are more than 6 or 7 kv from ground. Operation must therefore always be at restricted voltages.

To minimize the overall amplitude dispersion of multiplier gain, it might also be advantageous to operate each of the first few stages at the voltage giving the highest yield no matter what overall multiplier gain was desired: 500 volts for beryllium-copper dynodes. This could easily be accomplished by use of a corona voltage regulator across the divider string of the first few stages.

The possibility of operation as either a 20- or 21-stage multiplier, depending upon whther ions strike the first or zeroth dynode, enhances overall gain dispersion by the electron-to-electron gain of the first stage, probably about 2.5.

Electron multipliers are usually operated from electronical-

ly regulated, low-ripple, high-stability power supplies, because regulation and ripple modulate multiplier gain, and ripple can also be electrostatically coupled to the output. However, in particle-detector operation gain modulation is absorbed in the dynamic-range capability of the pulse system, and any ripple is attenuated to negligibility in the high-pass coupling networks of the pulse amplifiers. Hence much less sophisticated power supplies are required. Unregulated commercial supplies with substantial 60-cps ripple (2%) were used, although additional R-C filtering was added to reduce ripple an order of magnitude and lower the dynamic-range requirements of the pulse system.

The electron multiplier may be used simultaneously as a current amplifier and a particle detector. In this mode the anode is at ground potential and a single power supply furnishes the electron-multiplier voltage, so the ion acceleration potential is equal to the multiplier voltage.

The electron multiplier circuit was not especially designed for combined operation, so many difficulties arise in addition to gain variations common to all current-amlifier multipliers. First of all, there is a problem of excessive anode and dynode current for the multiplier divider string. Nominal divider currents are some 300 to 500 μa, so to prevent excessive dynode voltage regulation, the d-c anode current must be held below 50 μa. The ion count rate in terms of anode current and multiplier gain is

$$N = \frac{i_a}{Ke} ,$$

where e is electron charge. With the mean gain normally used in particle-detector operation, $\approx 5 \times 10^7$, the maximum count rate is about 6×10^6/sec, which corresponds rather closely to the upper limit for practical operation of the pulse system. However, the usual reason for operation of the multiplier as a current amplifier is to be able to handle ion count rates beyond the pulse-system capability. To do this, the mean multiplier gain must be reduced by lowering the voltage. This also lowers the ion acceleration voltage and so increases problems in collection of skew-trajectory ions coming from the mass filter.

The unregulated power supplies are, primarily because of ripple, not adequate for most current-amplifier applications of the electron multiplier, so an electronically regulated supply must be used.

Finally, low multiplier voltage coupled with the existence of two ion dynodes can cause an undesirable gain variation. Ions of low mass require low mass-filter voltages and so have exit trajectories with low skewness; most of them are collected on the first dynode. High-mass ions, on the other hand, have exit trajectories of higher skewness; many of them are collected on the zeroth dynode. The mean multiplier gain for heavy ions may be higher than for light ions by as much as the gain of a multiplier stage, a factor of about 2.5. This gain variation is, of course, in addition to the usual variation introduced by difference in electron yields for different

ions incident on the initial dynode.

Preamplifier

The "preamplifier" (Fig. 6.6) consists of an input limiter, a linear amplifier and differentiator, and a limiting amplifier.

The input limiter is a pair of germanium back diodes (low-current tunnel diodes) connected in parallel opposition across the preamplifier input. For small signals (below 100 μa) the diodes have a constant impedance of about 200 ohms, but for large signals an increasing conductance limits the voltage applied to the linear amplifier. At d-c, the diodes in parallel with 220 ohms (the input resistance of the linear amplifier) give a 200:1 range in output voltage for an input-current range of 10 μa to 10 ma. The limiting effect is somewhat smaller for pulses because of L di/dt voltage developed in the stray circuit inductance in series with the diodes. (The contribution of the inducatance in the diode itself is negligible.)

One nonperformance aspect of this limiter severely reduces system reliability. The back diodes, which are easily damaged by current overloads, are coupled to an anode at a high voltage (several kilovolts) by a capacitor large enough to provide appreciable energy storage. Any voltage breakdown to ground of the anode discharges the coupling capacitor through the diodes, inevitably degrading their voltage-current characteristics so as to make them unusable. Operation of the electron multiplier with the anode at other than

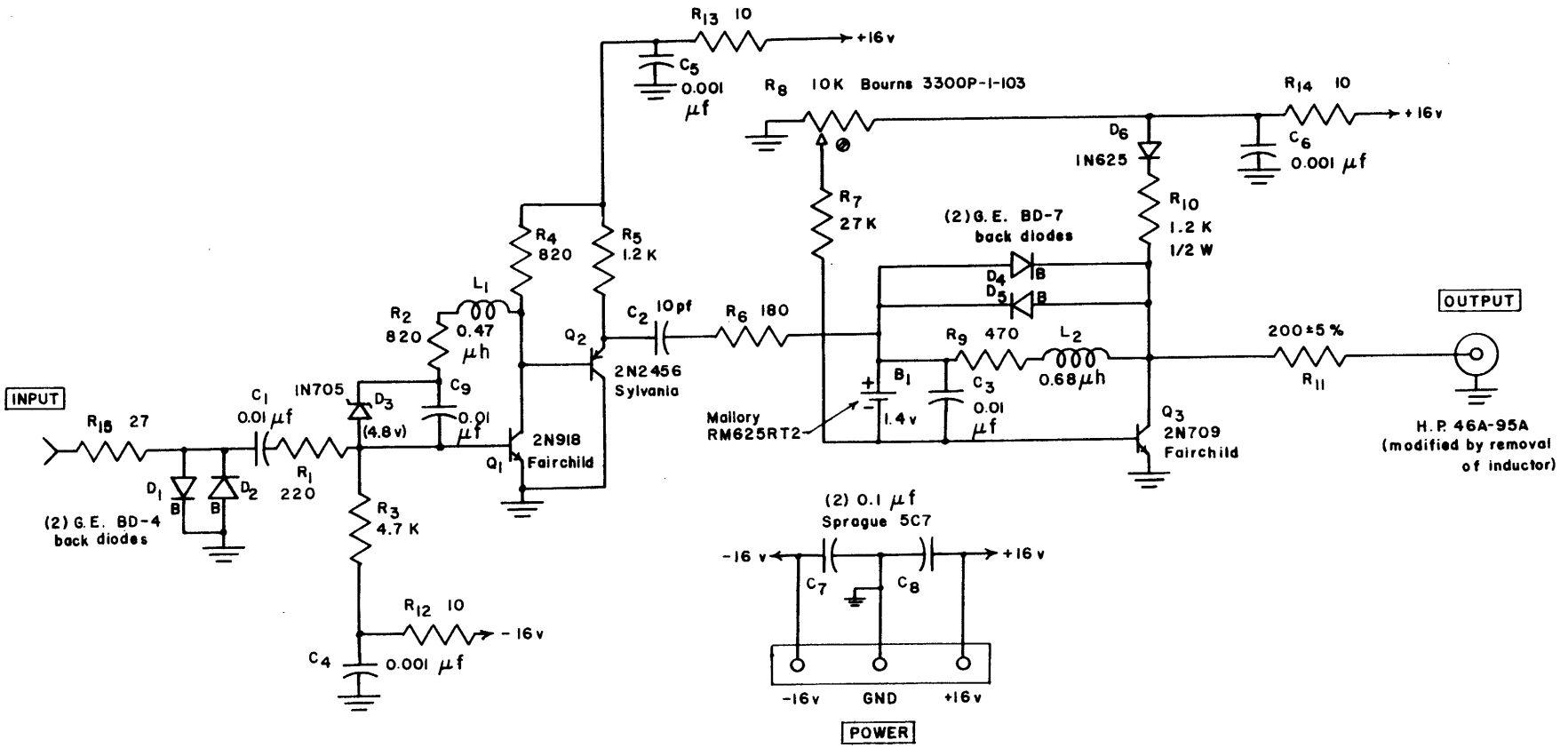

Fig. 6.6. Preamplifier circuit. R_8 is adjusted for zero voltage across D_4 and D_5. Unless otherwise noted: (1) resistances in ohms, ± 10%, 1/4 w; (2) 0.01 μf capacitors, Erie Y5U; (3) 0.001 μf capacitors, Vitramon VK20C; (4) inductors, Delevan 1840.

ground potential is therefore fraught with peril.

The linear amplifier is a conventional collector-to-base-feedback transistor amplifier with inductive peaking applied according to the technique developed by Reddi,[45] followed by an emitter follower to drive the differentiating capacitor. Design voltage gain is about 3.7, design rise time (10% to 90% points) somewhat better than 2 nsec.

The positive pulse output of the amplifier is differentiated by capacitor C_2. Resistor R_6, in series with C_2, necessarily degrades differentiation action, but is necessary to prevent ringing; the output impedance of the emitter follower is inductive, and would constitute a resonant circuit with C_2 without this damping.

The differentiated pulse is applied to the limiting amplifier, another inductively peaked, collector-to-base-feedback transistor amplifier. Small-signal current gain is about unity, the design rise time about 3 nsec. Limiting action is provided by a pair of germanium back diodes in parallel opposition in the feedback network. Ideally, for very small signals diode conduction is negligible and the circuit functions as a linear amplifier, but large signals cause diode conduction and so increase feedback and lower the amplifier gain. (Actually the back diodes always provide some shunt conduction in the feedback path, and so reduce amplifier gain even for small signals.) One significant advantage of this limiter is its constant output impedance (about 200 ohms) that mini-

mizes mismatch reflections in the input line of the distributed amplifier that it drives.

The preamplifier has a doublet response to test pulses (Fig. 6.7a; Appendix E). Figure 6.7b shows the response to an input pulse of about 3×10^7 electrons, Fig. 6.7c the response to a pulse 10 times as large. Limiting action is demonstrated by an output amplitude ratio of 2:1 for an input ratio of 10:1.

The leading or negative lobe of the output is substantially narrower than the trailing lobe, in part because of a slightly steeper leading edge of the input pulse, but more because of imperfect differentiation. The differentiator is actually a high-pass R-C filter with time constant of about 2 nsec, half the 4-nsec transition times of the triangular input pulse. This corresponds closely to the hypothetical situation for which the response was drawn in Fig. 6.2.

Amplifier-Limiter Chain

The bulk of the amplification of the pulse system is provided by three commercial, vacuum-tube, distributed amplifiers with individual rise times of about 3 nsec: Hewlett-Packard 460AR and 460BR, with gains of 20 db and 15 db, respectively. Both have an approximately Gaussian frequency response, and so an approximately Gaussian impulse response, and (at least compared to an amplifier with flatter frequency response) relative freedom from ringing.

The output of any distributed amplifier for a short pulse input

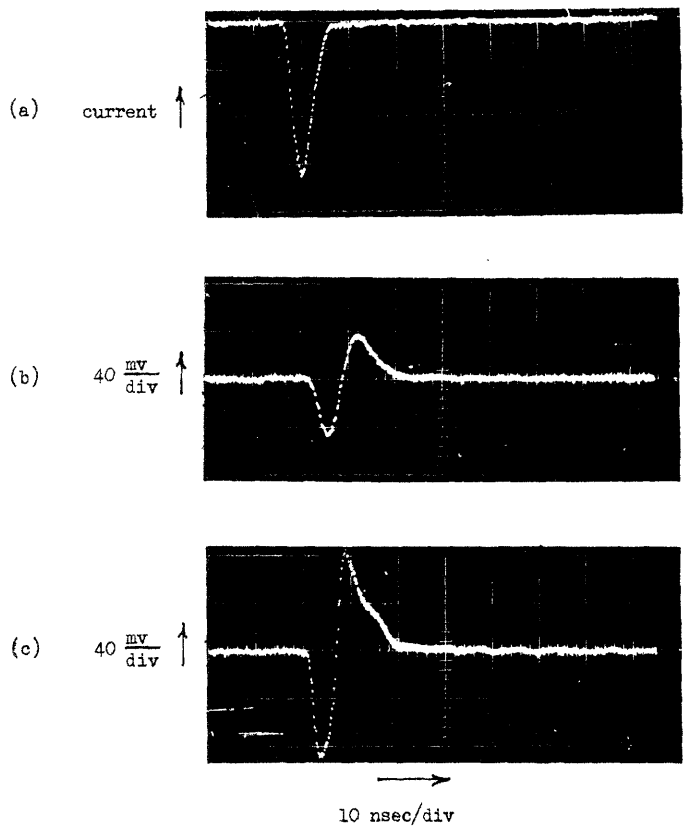

Fig. 6.7 Preamplifier performance.

a. Test pulse.

b. Response to pulse of 3×10^7 electrons.

c. Response to pulse of 3×10^8 electrons

contains mismatch reflections at double multiples of the delay times of the internal transmission lines, some 10 to 15 nsec in this case. These reflections can, if of sufficient amplitude, constitute post-pulse noise at the system output, so it is necessary to take every precaution to minimize them. The 460BR was chosen for the first amplifier in the chain, the most sensitive position, because it was found to have greater freedom from these reflections. All amplifiers except the last were terminated at both input and output in their nominal characteristic impedance: 200 ohms at all inputs and at the 460BR output, 270 ohms at the 460AR output. In addition, it was found that reflections in the 460BR were reduced if a small capacitance (2 pf) was placed across its load. The last 460AR drives the nonlinear load of a trigger circuit in the pulse standardizer, and so suffers substantial output mismatch, but at this high-level point reflections are of little importance.

The metal cabinets of the Hewlett-Packard amplifiers give the appearance of providing electrostatic shielding. However, paint on all joined surfaces prevents bonding of the various parts of the cabinet into an effective shield. Leakage from the r-f rod driver was, under some circumstances, picked up by these amplifiers and caused false outputs of the pulse system; cabinet modifications were therefore necessary.

The two interstage limiting amplifiers, the BA and AA

(Fig. 6.8), are of the same type as the limiting output amplifier of the preamplifier; a single-transistor, collector-to-base-feedback, inverting amplifier with parallel-opposed diodes in the feedback network to provide limiting action. Here advantage is taken of the fact that both input and output impedance are essentially constant, independent of limiting action, so that mismatch reflections of the associated distributed amplifiers are minimized.

The BA limiter, used between the 460BR and first 460AR amplifier, has back diodes as limiting elements in order to hold signal amplitudes as low as possible at this early stage. The AA limiter, on the other hand, uses point-contact silicon diodes, because it is necessary only to keep the output of the last 460AR, which it drives, below the 4-volt maximum specified by the manufacturer.

The BA kimiter is designed for nominal small-signal insertion gain of 1.0, the AA limiter for 1.25. Measured small-signal rise times are approximately 2 and 3 nsec, respectively. The faster response of the BA limiter, despite the handicap of a higher parasitic shunt conductance and capacitance in its feedback element, can be attributed to the peaking effect of the capacitor across its input resistor, plus the fact that the actual amplifier element of the AA limiter must operate at reduced bandwidth because it has to provide appreciably greater gain in order to perform a transformation from a high-impedance (270-ohm) source to a low-impedance (200-ohm) load.

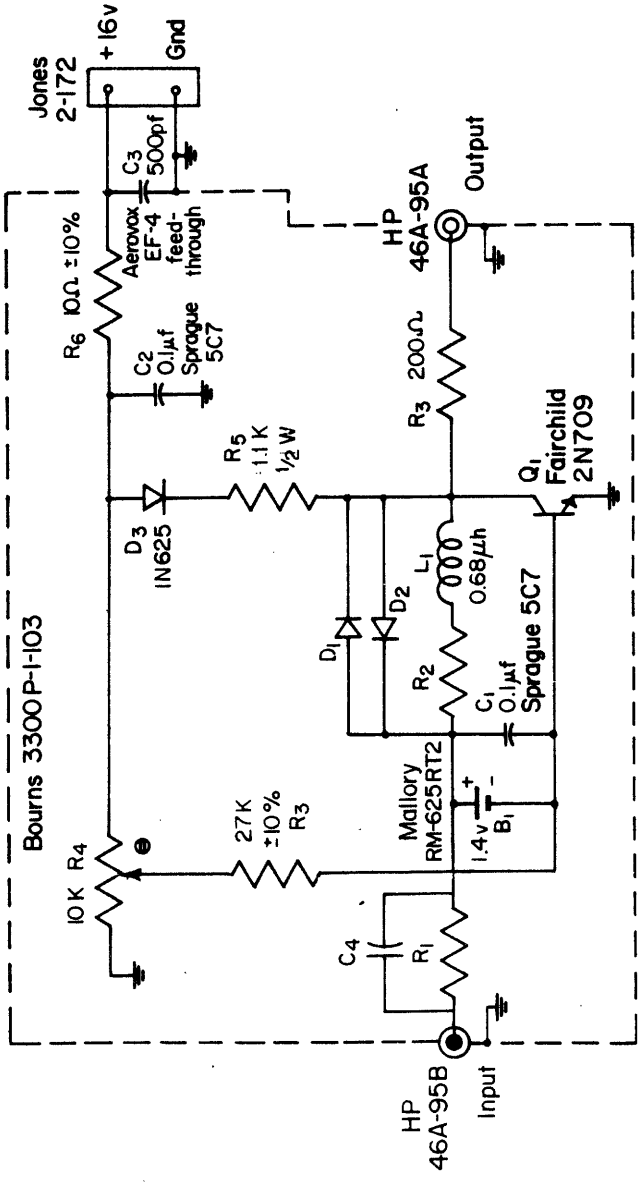

Type	BA	AA
R_1	200Ω	270Ω
R_2	560Ω	680Ω
D_1 and D_2	Gen. Elec. BD-7	Micr. Assoc. MA-4121
C_4	2 pf	0

Fig. 6.8. Interstage limiting amplifiers. Potentiometer R_4 is adjusted for equal input and output d-c voltages. All resistors 1/4 w, ±5%, unless otherwise noted.

The amplifier-limiter chain provides an overall small-signal gain of about 600 with a rise time of about 6 nsec. Its performance when driven by the preamplifier is shown in Fig. 6.9. For a small (3×10^6-electron) preamplifier input the output is a reasonably symmetric doublet confined to about 25 nsec. For larger inputs, however, as more and more limiting action occurs, the trailing lobe of the doublet lengthens ("post-pulse noise"), finally extending total doublet length to about 70 nsec. This is, of course, undesirable in a system intended to have a total response time of 20 nsec, but is not quite as bad as it might seem. First, the post-pulse noise is entirely negative; there is no positive overshoot that could cause double-pulse output from the pulse standardizer. Second, the system is not prevented from detecting a second pulse during the long trailing-lobe period; pulses of effective amplitude greater than the negative-lobe voltage can carry the net voltage positive, past the pulse-standardizer threshold.

The pulse baseline shift arising from such markedly unsymmetric outputs must be considered. The integral over all time of each pulse must be zero; because the negative lobe of each pulse is larger than the positive, the voltage between pulses must go slightly positive. If the repetition rate is high enough, this positive level might possibly cause false triggering of the pulse standardizer. A quantitative study shows that this cannot happen: The output pulse for an input of 3×10^8 electrons has a positive lobe

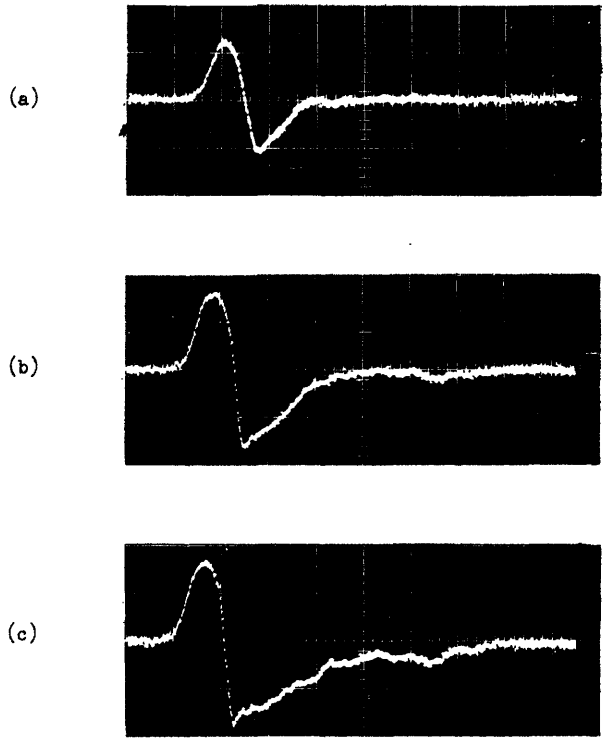

Fig. 6.9. Response of preamplifier-amplifier-limiter chain to test pulses of (a) 3×10^6, (b) 3×10^7, and (c) 3×10^8 electrons. Scales: vertical, 0.8 v/major div; horizontal, 10 nsec/major div.

of about 1×10^{-8} volt-sec, a negative lobe of about 2.8×10^{-8} volt-sec, for a net negative integral of -1.8×10^{-8} volt-sec. An input of a sequence of such pulses at a mean rate of 10^7 counts/sec would produce a positive shift of the pulse baseline of only 0.18 volts, well below the 0.5-volt threshold of the standardizer. In actual operation, of course, there would be a statistical spread in input pulse amplitudes; 3×10^8 electrons would be near the top of that spread. For an assumed xe^{-x} distribution of input pulse amplitudes, and an assumed mean amplitude of 6×10^7 electrons, the mean pulse integral is -9×10^{-9} volt-sec, just half the maximum value. For pulse rates practical for this system, the effect of pulse baseline shift is negligible.

Pulse Standardizer

The pulse standardizer (Fig. 6.10) consists of an input threshold element, a timing unit, and an output current switch.

The input threshold element is a 1-ma tunnel diode, TD_1, that switches to a high-voltage state whenever the input pulse rises above +0.5 volt, and returns to a low-voltage state when the input goes negative. This threshold element discriminates against noise and provides limiting action to prevent spurious responses to large input signals.

The performance of this threshold detector was somewhat less than ideal, primarily because it was driven from a relatively low-

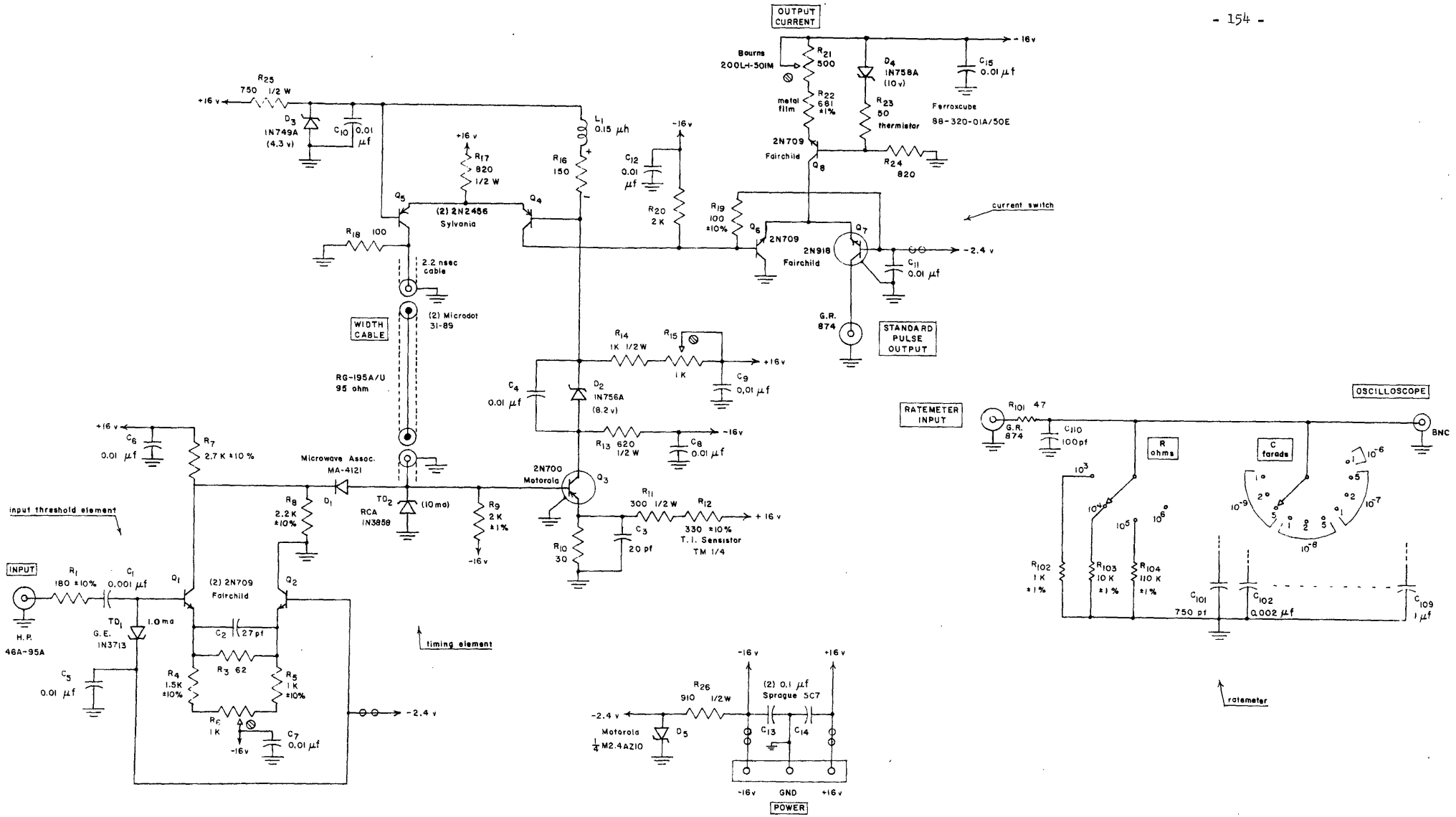

Fig. 6.10. Pulse standardizer. Input threshold = +0.5 v. Output = -10 ma pulse; width = 5 nsec + "width cable." Potentiometer R_6 is adjusted for 0 v across R_8, R_{15} for 0.4 v across R_{16}. Unless otherwise noted: (1) resistances are ohms, ± 5%, 1/4 w; (2) potentiometers Ohmite AS; (3) 0.01 μf capacitors Erie Y5U; (4) power-lead beads Ferroxcube 56-590-65/4B.

impedance (450-ohm) source - the amplifier output plus a series resistance. There is marked difference in rise time for signals barely over the 0.5-v threshold end for those much larger in amplitude. This eventually manifests itself as a slightly narrower standardizer output pulse for very small inputs than for very large ones. The rise-time shift could easily be reduced by driving the tunnel diode with a common-base transistor amplifier, whose high output impedance would lead to much faster transitions for the smaller input pulses.

The tunnel-diode voltage is amplified by the differential amplifier consisting of transistors Q_1 and Q_2. The differential arrangement was chosen for d-c stability, but it also makes it easy to modify the standardizer to trigger on negative-going signals; it would be necessary only to place a tunnel diode in the Q_2 base circuit and couple the input to that diode, instead of to TD_1.

The timing unit, an almost exact copy of a "discriminator" used in nuclear instrumentation,[46] is centered about the 10-ma level-sensing tunnel diode TD_2. A negative signal from the input-threshold amplifier turns TD_2 on. The resulting negative voltage is amplified by Q_3, whose output switches a current from transistor Q_4 to Q_5 of a "long-tailed pair" (a differential-sensitive pair of transistors with emitters driven from a common current source). This current is sent through a timing cable to the 10-ma tunnel diode. At a time equal to the cable delay plus the delay in the

two transistor stages, this current turns off the tunnel diode and holds it off (to prevent a second pulse) for a time equal to the original delay time.

The other output of the Q_4-Q_5 long-tailed pair is used to drive the output current switch. The standardizer therefore has an output pulse of width equal to the delay time and a dead time just twice as long.

Because the output pulse width should be as independent as possible of changes in circuit elements with time and temperature, the design of the timing unit emphasized high-speed operation for each element, so that the total loop delay time would be, as much as possible, determined solely by the timing cable. Nevertheless, 2.8 nsec was contributed by the amplifier and switching elements. An additional 2.2-nsec delay was deliberately incorporated in an internal cable, so that the output pulse width would be 5 nsec longer than the delay time of the external width cable.

The output current switch consists of a long-tailed pair of silicon transistors, Q_6 and Q_7, fed at the emitters by 10 ma from a current source (transistor Q_8). The output current from the collector of Q_7 is switched from a leakage current of about 10^{-10} amp to 10 ma by the pulse from the timing unit. Rise and fall times are on the order of 1 nsec (Fig. 6.11).

The ringing shown in Fig. 6.11 is inherent in the output of a long-tailed pair, as conventional small-signal analysis of the

(a)

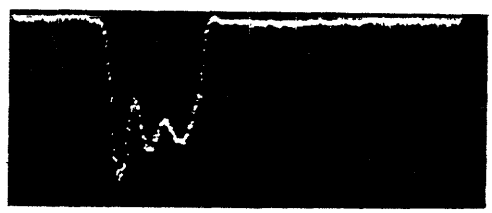

(b)

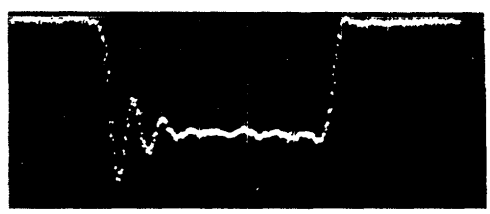

Fig. 6.11. Pulse standardizer output into 50 ohms:
(a) 10-nsec pulse, (b) 25-nsec pulse.
Scales: vertical, 4 ma/major div; horizontal, 5 nsec/major div.

transistor that is passing current shows: The base is held at a fixed voltage, so the impedance at the emitter is the input impedance of a common-base amplifier. The "intrinsic" transistor, i.e., the transistor treated as a pure conduction-by-diffusion device, with no external reactances or resistances, has an inductive input impedance.[47] The capacitance of the emitter-base junction, plus that of the same junction of the nonconducting transistor and circuit strays, resonates with the inductance. The abrupt change of current in this resonant circuit causes ringing, which then appears in the output of the amplifier, the transistor collector circuit.

While it is esthetically displeasing, ringing has no deleterious effect in this application, because it does not cause variation in the total amount of charge in the output pulse.

The thermistor in the current source for the output switch was intended to hold output current constant by compensating for variations in breakdown-diode and transistor voltages and in transistor current gains. In a test with the standardizer counting a steady input pulse rate, after 3 hours operation in the equipment racks of the mass spectrometer, the output current increased by about 1% with a 6°C rise in standardizer temperature. An additional 10°C increase, produced by an external heater, caused another 1% increase in output. These current drifts, which may have resulted from either inexact compensation of d-c component variations

or a change in effective pulse width with temperature, were considered too small to warrant investigation.

Performance with Test Pulses

The performance of the pulse system as the output element of the mass spectrometer can in part be predicted by its performance in response to signals from a test source (Appendix E). The minimum input to trigger the standardizer is a pulse of about 10^6 electrons. The average output current of the pulse standardizer depends slightly on input pulse amplitude, dropping 3% as the input is reduced from 6×10^8 electrons to 10^6 electrons; this probably results from amplitude sensitivity of the standardizer threshold detector.

The resolving time, or minimum spacing that permits detection of the second of two pulses, depends on the amplitudes of both pulses (Table 6.1). For a large pulse following a small one, the resolving time is less than the nominal standardizer dead time because of the "memory" effect of a level-sensing standardizer following a pulse-stretching amplifier. For a small pulse following a large one the resolving time tends to be longer than standardizer dead time because of the blocking effect of post-pulse noise produced in the amplifier chain.

The effect of rapid sequences of pulses was investigated by measuring average output currents for widely spaced (40 μsec) pulses and for pulses in closely spaced pairs (15 to 30 nsec) with

Table 6.1. Pulse-system resolving times.

1st pulse amplitude (electrons)	2nd pulse amplitude (electrons)	minimum spacing for 10-nsec standardizer pulse (nsec)	minimum spacing for 25-nsec standardizer pulse (nsec)
10^6	10^6	19	47
	10^7	19	49
	10^8	21	50
10^7	10^6	27	44
	10^7	15	44
	10^8	17	44
10^8	10^6	80	80
	10^7	14	42
	10^8	14	44

the same mean rate. A pair consisting of a large pulse following a small one causes an increase in mean current of up to 3% over that of the first pulse alone, simply because the larger pulse yields a larger output. On the other hand, a pair consisting of a large or small pulse following a large one causes a decrease in mean current of up to 1.5%, probably because the effective amplitude of the second pulse is diminished by post-pulse noise from the first.

C. Output Processor

Linear Count-Rate Meter

The output current of the pulse system is fed to a simple resistance-capacitance count-rate meter mounted on the pulse-standardizer panel. Resistance can be switched by decades, and capacitance in a 1:2:5 pattern over three orders of magnitude, so it is possible to adjust the R-C time constant to an optimum value for the signal being observed.

Recording Oscilloscope

The small commercial oscilloscope (Tektronix 503) used as a recording device has, except for a tendency to drift, proven highly satisfactory. Its convenience for observation of the wide range of spectral-line amplitudes could be enhanced, however, by an apparatus that rapidly switches (say at a 100-kc rate) between two (or more) sensitivity values differing by a power of 10, or by some other convenient factor. There would then be visible two mass spectra at different sensitivities. (This would be a trivial problem for a so-called "dual-trace" oscilloscope - the two inputs could be connected in parallel, and different channel gains selected.)

D. Ion-Detector Performance

Pulse Response

Waveforms at the output of the preamplifier-amplifier-limiter chain were observed with a sampling oscilloscope. To obtain a dis-

cernible waveform line, rather than a smeared envelope, the oscilloscope trigger level was adjusted so only the largest pulses of the amplitude distribution were detected. The output produced by a 20-stage multiplier (Fig. 6.12a) closely resembles that produced by a test-pulse input (Fig. 6.9), but that produced by the 21-stage multiplier (Fig. 6.12b,c,d) has a lower amplitude, as well as a flatter top and slightly wider positive lobe. The differences may in part be caused by the higher gain of the 20-stage multiplier. (The gain of the 21-stage multiplier had been only partly restored after being lowered by contamination.) However, the difference in pulse shape indicates something more significant, possibly a broader output pulse from the 21-stage multiplier. Because only the largest output pulses were observed, there is a good chance that most of them arose from ions incident on the zeroth dynode. The possibility of greater transit-time dispersion in such a case was discussed in Section B.

It was necessary to operate at relatively high ion count rates (perhaps 10^5/sec) to obtain data with the 21-stage multiplier, because of a high background-count rate (10^4/sec). Therefore a number of second counts were recorded as randomly scattered dots in the waveform photos.

Ion-Detection Operation

The mass spectrometer was used successfully with the particle-detection ion collector, but a number of performance aspects must

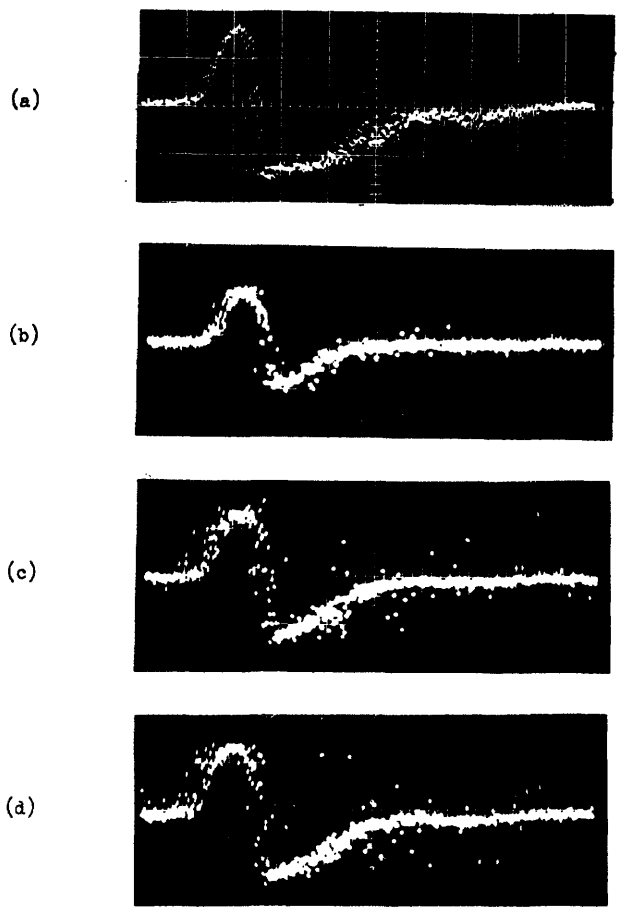

Fig. 6.12. Response of preamplifier-amplifier-limiter chain to electron-multiplier output pulses: (a) 20-stage multiplier, 8 kv ion-acceleration and electron-multiplier voltages, ions of mass 18; (b) 21-stage multiplier, 6 kv, ions of mass 28; (c) same, 8 kv; (d) same, 10 kv. Scales: vertical, 0.8 v/major div; horizontal, 10 nsec/major div.

be checked before operation can be said to be proven. These include: tolerance to electron-multiplier gain variations, lost counts by coincidence at high input rates, multiple counts, and background count rate. Unfortunately, the operation of the spectrometer system was never adequate to perform tests for any but the last of these. For example, tests of coincidence losses require: operative pulse electronics, an electron multiplier with adequate gain (5×10^7) and negligible background-count rate ($< 10^3$/sec), and a source of ions with an output rate high enough to drive the system near saturation ($> 10^7$ ions/sec). All of these requirements were met at one time or another, but never simultaneously.

Tolerance to multiplier gain variations represents the most questionable aspect of pulse-system performance. The electronic circuits responded to a test-pulse dynamic range of almost three orders of magnitude, but it is not obvious that they would respond as well to multiplier output pulses under the high-repetition-rate and random-arrival-time conditions of an ion collector. The inability to perform definitive tests is in this respect most unfortunate.

A test of coincidence-count losses would have provided a calibration curve for true ion count rate in terms of standardizer output current. In the absence of such a test, a first-order correction can be obtained from one of the count-rate equations of Chapter V. The pulse system does not correspond exactly to any of

the models postulated there, but, provided standardizer resolving time is chosen to be about as long as the output doublet of the amplifier chain - say 50 nsec - it probably comes closest to the pulse-stretching amplifier with level-sensing standardizer (Eq. 5.30). The "stretch" of the amplifier is the pulse width from the first +0.5-v point to approximately the zero crossing between lobes, or about 10 nsec (Fig. 6.12). Output count rate is therefore down 20% at input rates of 5×10^6/sec, a performance inferior to the design goal by a factor of two. Coincidence loss could be reduced by use of shorter standardizer resolving time, perhaps 20 nsec, but at the price of greater inapplicability of Eq. 5.30 and the possibility of substantial dependence of coincidence loss on electron-multiplier gain.

It seems unlikely that the electron multiplier would produce multiple outputs for a single input ion, except as a consequence of the "zeroth" dynode expedient (Section B); however, statistical examination of the randomness of the pulse-standardizer outputs would be advisable.

Background count rates ranged from a few hundred counts/sec to almost 10^5 counts/sec for electron-multiplier voltages high enough (8 kv) for proper pulse-system operation. These high rates, which apparently resulted from field emission from the mulitplier structure, could probably be reduced by careful attention to smoothness of multiplier surfaces.

VII. MASS-SPECTROMETER PERFORMANCE

Precise measures of mass-spectrometer performance were made impossible by the two defects of the metallized-ceramic quadrupole rods: crookedness and obstruction of the regions beyond the electrode ends. Nevertheless, some minimal observations were made of line shape, resolving power, and background-gas mass spectra.

A. Line Shape

The shape of the mass lines of the quadrupole mass spectrometer ideally should be either trapezoidal or triangular, depending on the chosen resolution, with the more gradual slope on the low-mass edge. In a practical instrument one would also expect long, low-amplitude "wings" on the lines, caused by inadequate rejection of ions just outside the stable region of the a-q diagram. In this instrument, however, the line shape proved much more complex. For one thing, there was fine structure on the lines, as demonstrated by a series of spectra centered about mass 28 (Fig. 7.1). Fine structure of similar form has been observed with both the original stainless-steel quadrupole lens[51] and with all modifications of the ceramic lens. Originally it was attributed to the nonconstant quadrupole cross section caused by the crooked stainless-steel rods. When the supposedly straight ceramic rods were installed, faulty ion collection caused by rod end problems was blamed. Improvement of ion collection and discovery that the ceramic rods are also crooked

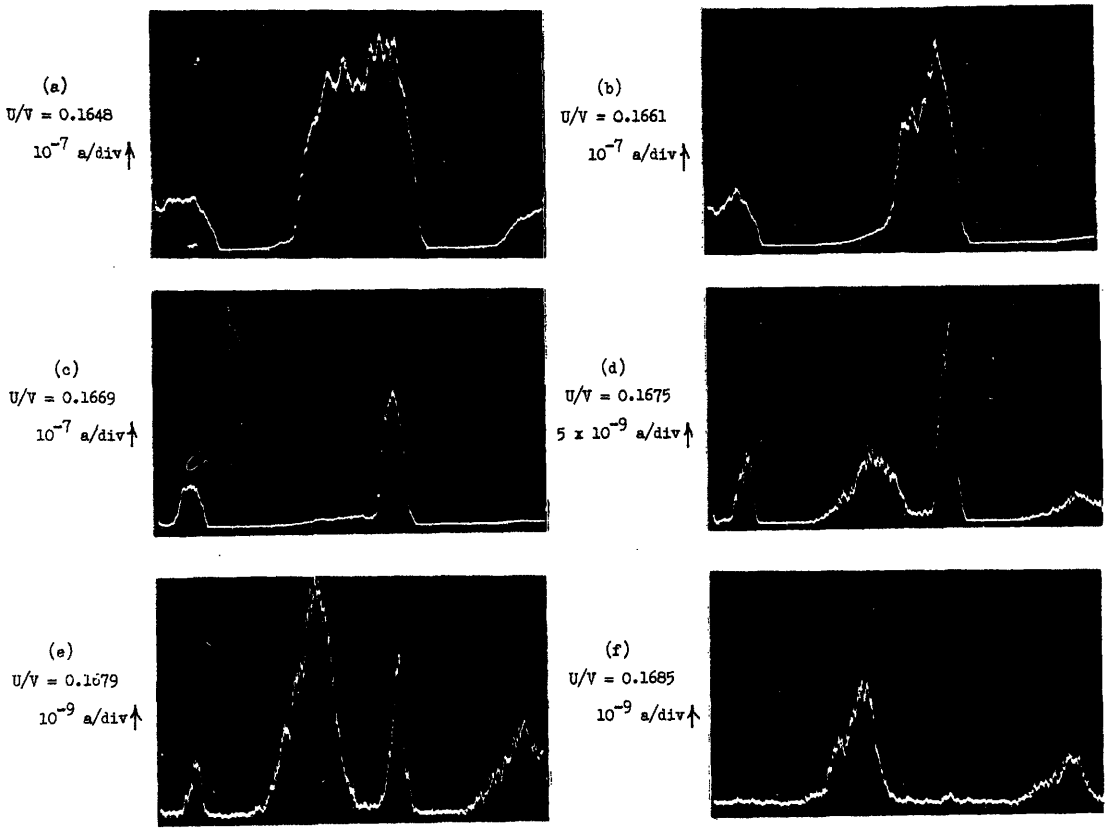

Fig. 7.1. Spectral line shape as a function of voltage ratio. Scales: horizontal, 27 to 29 amu; vertical, as indicated. Currents are anode currents of electron multiplier with gain $\simeq 10^5$. Operating conditions: Source electron current = 7 ma, other source conditions as shown on Fig. 3.3. Mass filter on 0-50 range, operating in constant $m/\Delta m$ mode. Ions were background gas: total pressure increased from 2×10^{-6} to 3×10^{-6} torr during run from (a) through (f).

has once more shifted the blame to the rods.

It is possible to explain fine structure simply on the basis of a change in inscribed radius (r_o) along the quadrupole. The simplest model is a step change in r_o. In effect, ions then pass through two cascaded mass filters with overlapping pass bands. If the transition point corresponds to a null in the standing wave of ion amplitudes along the first filter, the second filter has low entrance displacements and velocities, hence high transmission. However, if the transition point is at a loop in the first-filter standing wave, second-filter entrance conditions are unfavorable, and transmission is lowered. Because the lengths of the standing waves change during the sweep of a mass line, the overall transmission also changes, and a ripple or fine structure appears in the output ion current.

Because crookedness of the rods not only changes r_o but also destroys the symmetry of the electric field, low-order non-quadrupole field terms are generated that also can cause line fine structure.[12]

With increase in U/V the spectral line shows a long, low-amplitude leading edge (Fig. 7.1c) that breaks away to become an apparent separate line - a "precursor" line (Fig. 7.1d). The precursor does not decrease in amplitude as rapidly with increasing U/V as does the actual line, so it eventually predominates (Fig. 7.1e). In fact, when the U/V ratio is high enough

to essentially extinguish the actual line, the precursor still has appreciable amplitude: Fig. 7.1f shows only the precursor lines for masses 28 and 29.

The precursor line has, like the fine structure, been observed with all mass filters used on this project. Its cause is not known, but is assumed to be connected with the crookedness of the rods.

Both the actual line and the precursor persist at nominal U/V ratios higher than the supposed extinction value of 0.16784 (Fig. 7.1e,f). It should therefore be mentioned just how the nominal U/V ratios were determined. U is directly proportional to the setting of the DC/AC RATIO potentiometer in the d-c rod driver. A plot of extrapolated width Δm of the mass 28 line was made against the control settings. The low-resolution points (Fig. 7.1a,b,c) lay along a straight line, as the theory (Eq. 2.37) predicts. The intersection of this line (as extended) with the axis was assumed to correspond to U/V = 0.16784. This may not be precisely correct for this somewhat anomalous system, so the nominal values of U/V may be high.

B. Resolving Power

Three numbers are required to describe the resolving power of a quadrupole mass spectrometer: (1) The highest attainable resolution at unity transmission, which theoretically depends upon the entrance aperture relative to the size of the quadrupole lens, and

upon entrance transverse momenta relative to the applied voltages. (2) Ultimate resolution of a distinguishable line, which depends upon the mechanical precision of the quadrupole lens and the stability of the applied voltages during the measurement period. (3) Relative transmission at the ultimate resolution, which, like unity-transmission resolution, depends upon entrance conditions.

The best agreement with theory is obtained with mass line width Δm defined as the width between axis intersections of straight lines extrapolated from the sides of the mass line. On the other hand, comparison with other types of spectrometers is best made by the standard definition of Δm as the width between the points at 1% of maximum amplitude. In most intruments these two figures correspond closely, but in this one, because of the line shape, they differ widely.

Resolution measurements were made at mass 28 with the 0-50 range of the spectrometer. The entrance aperture was 1.5 mm, so by Eq. 2.38 the theoretical maximum resolution for unity transmission was $m/\Delta m = 19$. The measured resolutions for unity transmission were approximately 60 and 30, based on extrapolated line width and on 1% amplitude, respectively. That both exceed the theoretical resolution would seem to indicate that the ion source was focussing the ions so that they used only the central portion of the entrance aperture, while maintaining transverse momentum well below the $U_{to} = 0.8$ volt that Eq. 2.49 allows. This seems

unlikely, particularly in light of the conclusions about transverse momentum in the next section.

Maximum resolution based on extrapolated line width was 200 at a relative transmission of 10%. This is actually better than one would predict from the measured crookedness of the rods. However, because of the precursor line, the maximum resolution based on 1% amplitude was only 40, at a relative transmission of 70%; resolution actually declined at lower values of transmission.

It can be concluded that, because of quadrupole lens defects, the design goal of a maximum resolving power of 500 was not even approached. Indeed, resolution was too low for the intrument to be of practical service in analytical work.

C. Mass Spectra

A series of background-gas spectra obtained on the three lower mass ranges in both the constant-$m/\Delta m$ and constant-Δm modes are shown in Fig. 7.2. Resolution was adjusted so that the mass 44 line was 0.88 amu wide (extrapolated width) in each spectrum.

It can be deduced from Fig. 7.2 that the transverse entrance momentum is not negligible. The amplitude of the mass 44 varies as 1.00:0.67:0.48 on the 0-50, 0-100, and 0-200 ranges, respectively. From Eq. 2.49 one must conclude that at least 33% of entering ions must have a transverse momentum equivalent to more than 0.7 volt, and 52% greater than 0.35 volt.

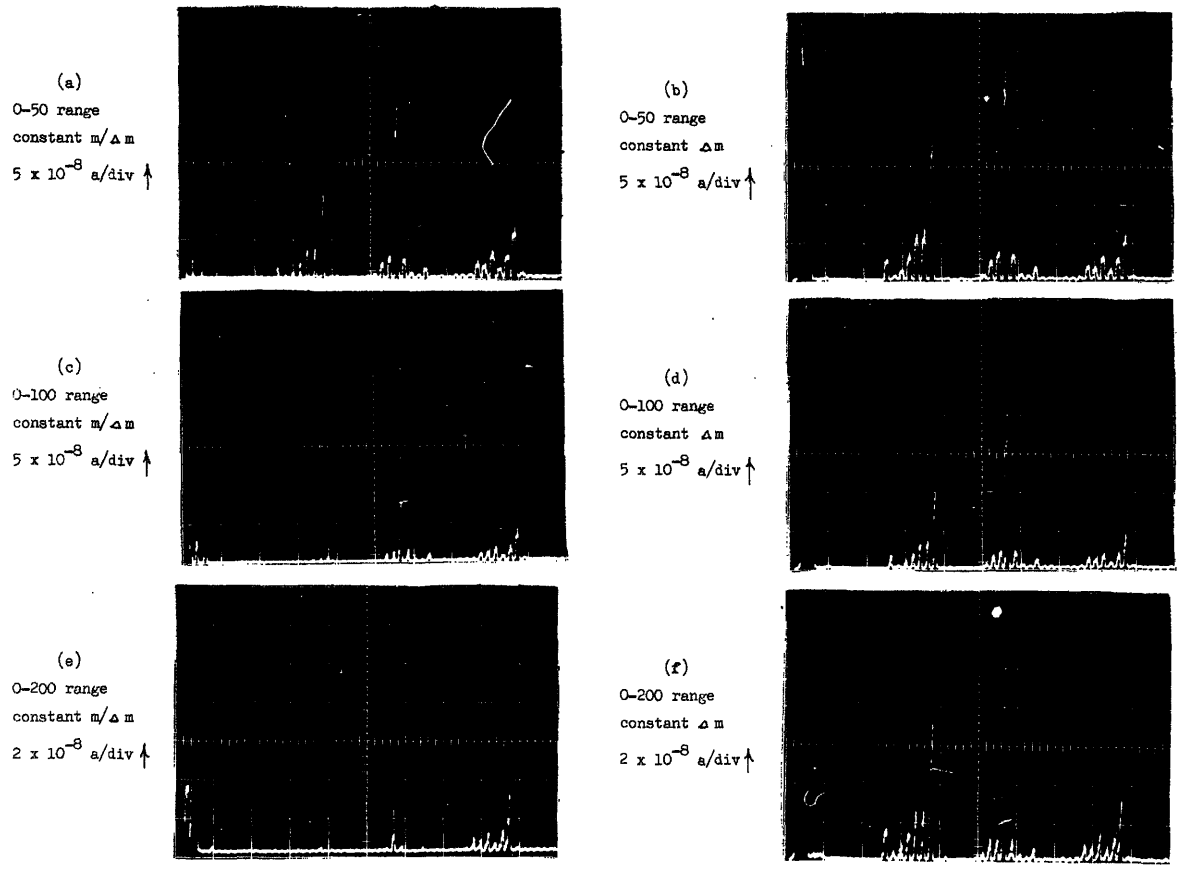

Fig. 7.2. Background-gas mass spectra. Scales: horizontal, 0-50 amu; vertical, indicated currents are anode currents of electron multiplier with gain $\sim 10^5$. Operating conditions: Source electron current = 5ma, other source conditions as shown on Fig. 3.3. Mass filter adjusted for $\Delta m = 0.88$ amu at mass 44 on all ranges. All mass spectra swept in one second. Background-gas total pressure $\sim 2 \times 10^{-6}$ torr. Spectra taken in the sequence b-a-d-c-f-e.

The constant-m/Δm spectra demonstrate the inadequacy of nonlinearity compensation in the ratio of d-c to r-f voltage. In the 0-100- and 0-200-range spectra the amplitudes of lines between 10 and 40 amu are relatively low because r-f voltage V is slightly high with respect to d-c voltage U, a consequence of overcompensation. On the other hand, lines 1 and 2 display excessive amplitudes, because compensation is inadequate at the very lowest masses.

The constant-Δm mode should (and does) exhibit greater tolerance to both nonlinearity of r-f voltage and transverse entrance momenta. Even so, apparent ion abundances depend on mass range; Table 7.1 shows a substantial change in amplitude ratios of the mass 18, 28 and 44 lines with change in mass range.

Table 7.1. Relative amplitudes of mass 18, 28 and 44 spectral lines.

Mass range	Constant m/Δm	Constant Δm
0-50	1.7 : 3.8 : 1.0	2.8 : 4.6 : 1.0
0-100	0.44 : 3.2 : 1.0	2.4 : 5.2 : 1.0
0-200	0.07 : 0.73: 1.0	2.4 : 3.9 : 1.0

Mass lines 1 and 2 in the constant-Δm spectra are substantially wider than 0.88 amu; in fact, they merge into a single line. This is in part a result of r-f control nonlinearity, but is more a consequence of the failure at low resolution of the approximations on which the constant-Δm equation (Eq. 2.46) was based.

An apparent mass line occurs at m = 0 in the constant-$m/\Delta m$ spectra because some of the injected ions traverse the filter on the basis of their own longitudinal injection momentum and negligible deflecting voltage.

Spectrometer output ion current I_i is proportional to the partial pressure of the corresponding molecule, p_m, and the ionizing electron current, I_e. Instrument sensitivity can be estimated from the spectrum of Fig. 7.2a, along with the known total background pressure (as determined from ion-pump current) and the known electron current:

$$I_i \approx 10^{-3}\, p_m(\text{torr})\, I_e\,(\text{amp}) \quad \text{ampere} \quad .$$

With a maximum practical electron current of 10 ma, and a minimum detectable ion current of perhaps 10^{-16} amp, the minimum detectable partial pressure is 10^{-11} torr.

VIII. CONCLUSIONS

A. Summary of Work

The work of this thesis was divided into two broad categories: the electronic circuits that provide voltages for the quadrupole mass filter, as well as some associated theory of the filter itself; and circuits associated with a particle-detection ion collector, including some associated signal and noise problems.

Quadrupole Filter

Extension of the theory of the quadrupole filter showed that the transverse momenta of ions leaving the filter were high enough to pose serious collection problems for an electron-multiplier ion detector.

Quadrupole drive circuits that are capable of rapid sweeps of wide-range mass spectra were designed and constructed. However, their stability was inadequate for long-term, high-resolution ($m/\Delta m = 500$) operation, and the nonlinearity of the r-f control precluded the sweep of wide spectral ranges at anything but the lowest resolution. A compensation scheme that reduced r-f nonlinearity was demonstrated, but even its performance was inadequate for high-resolution operation.

The ultimate resolving power of the mass filter fell short of the design goal of 500 by more than an order of magnitude because of some unfortunate errors in the manufacture of the quadrupole lens.

Ion Collector

The theory of coincident-count losses in particle-detection system was extended to a model resembling a practical pulse system - a pulse-stretching amplifier followed by a nonparalyzable standardizer. An analysis of the signal and noise requirements on the linear circuit, or ratemeter, that processes the output of a particle-counting system, showed that an idealized "dealy-line" ratemeter had some advantages over the conventional R-C circuit, but that these essentially disappeared when the practical limitations of delay lines were considered. An expression for the minimum sweep time for a mass spectrometer with particle-detecting ion collector and R-C ratemeter was developed.

The electronic circuits necessary for particle-detection operation of an electron-multiplier at count rates substantially higher than those reported in the literature were designed and constructed. The most significant problem was to maintain minimum pulse width, and so maximum count-rate capability, while simultaneously accepting the wide range of pulse amplitudes from an electron multiplier. It had been hoped that a system could be built with resolving time controlled by a single system element (the pulse standardizer) and low enough so that only 10% of input counts would be lost by coincidence at a mean rate of 5×10^6/sec. System resolving time actually depends in a complicated way on both the standardizer and associated amplifiers; operation so that the standardizer had predominant control

of the resolving time resulted in 20% coincidence loss at a mean rate of 5×10^6/sec.

Some practical problems were encountered in application of the particle-detection ion collector: Electron-multiplier background noise caused by field emission was always intolerably high. It is impossible to overcome this problem by lower-voltage operation, because high voltage (> 10 kv) is required to prevent loss of ion counts by zero electron yield on the first dynode. There may be significant difficulty in constructing an adequately noise-free multiplier.

Difficulty was also experienced with multiplier gain stability. The high-speed pulse system requires a high-gain ($> 5 \times 10^7$) multiplier. The original 20-stage multiplier constructed with unsensitized dynodes yielded adequate gain over an extended period of time (several months) that included a number of exposures at the atmosphere. However, when a sensitization process was used to restore gain lowered by severe contamination, the gain became sensitive to exposure to the atmosphere. This bodes ill for the practical application of such a system, for it had been hoped that only an occasional resensitization by baking and oxygen exposure would be necessary to maintain multiplier gain at adequate levels.

B. Suggestions for Future Work

Mass-Filter Theory

Despite extensive early work by the group at Bonn, many gaps remain in the theory of the quadrupole mass filter. An extensive study of ion orbits, with particular attention to the orbits of rejected ions, is needed. It has been noted that the empirical maximum longitudinal entrance velocity for satisfactory resolution is appreciably less than that predicted from the length of standing waves of stable orbits.[10,52] This is probably because the velocity is determined not by the behavior of selected ions, but by the behavior of nominally rejected ions; ions of improper mass must stay in the filter long enough to be rejected.

The effects of multipole fields that arise both from inadvertent field asymmetry and from the circular approximations to hyperbolic electrodes also need further investigation.[12] A determination of the optimum ratio of rod radius to inscribed field radius for full circular rods would be useful.

End effects in the quadrupole filter should also be investigated. At the entrance end some questions to be answered include: What is the effect of the input transition field on ion motion? Should the ion injection be from an aperture in a flat plate, or from a small canal, or from some other geometry? At the output end questions to be answered include: What is the ion trajectory as it leaves the field? Should an exit grid be placed over the

end of the quadrupole? If so, at what potential should it be operated?

Mass-Filter Design

It is possible that the performance of the mass filter could be improved by some fundamental modifications of its design. For example, it is possible that the filter would show greater tolerance for entrance displacement and velocity if ion injection were confined to a certain phase of the r-f cycle. Or, it might be advantageous to use short entrance and exit quadrupole sections to which only r-f voltage is applied, which would act as orbit-stabilizing high-pass filters. (This has been tried experimentally by several groups, with inconclusive results; a theoretical investigation is needed.) Alternatively, it might be advantageous to apply r-f voltage to a set of rectilinear deflection plates placed ahead of the quadrupole, in order to impart some optimum entrance velocity to each entering ion.

Mass-Filter-Voltage Circuits

Two major improvements are needed in the circuits that provide the quadrupole-rod voltages: greater stability and more precise r-f amplitude control. The stability problem requires only straightforward changes involving more drift-free operational amplifiers in all control circuits. The amplitude-control problem is much more difficult. Some improvement could be obtained with more elaborate

nonlinearity compensation, combined with an improved scheme for compensation adjustment. However, a much more fundamental approach - a more linear rectifier - is desirable. This is a problem that defied solution in the course of this thesis work. Two possible schemes were devised too late to be tested: both involve compensation for the forward drop of the diode rectifier, the principal source of rectifier nonlinearity. The first (Fig. 8.1a) involves two diode rectifiers, D_1 and D_2. Both conduct at the same phase of the r-f cycle, and, to first order at least, pass equal currents. If the diodes have matched conduction characteristics, the forward drops cancel, and the output of D_1 is a linear function of r-f amplitude.

The second scheme (Fig. 8.1b) involves measuring the forward drop of D_1 through D_2 and subtracting it from the output. That there is accurate compensation for D_1 forward drop is not obvious, for only peak drop is measured, and that through another diode. However, because this scheme is relatively easy to implement it might merit investigation.

The Quadrupole as a Voltmeter

The extreme sensitivity of quadrupole performance to the ratio of r-f to d-c voltage suggests the possibility of its use as a precision r-f voltmeter. The r-f voltage to be measured would be applied to a high-resolution quadrupole mass filter, and the applied d-c voltage adjusted for "infinite" resolution.

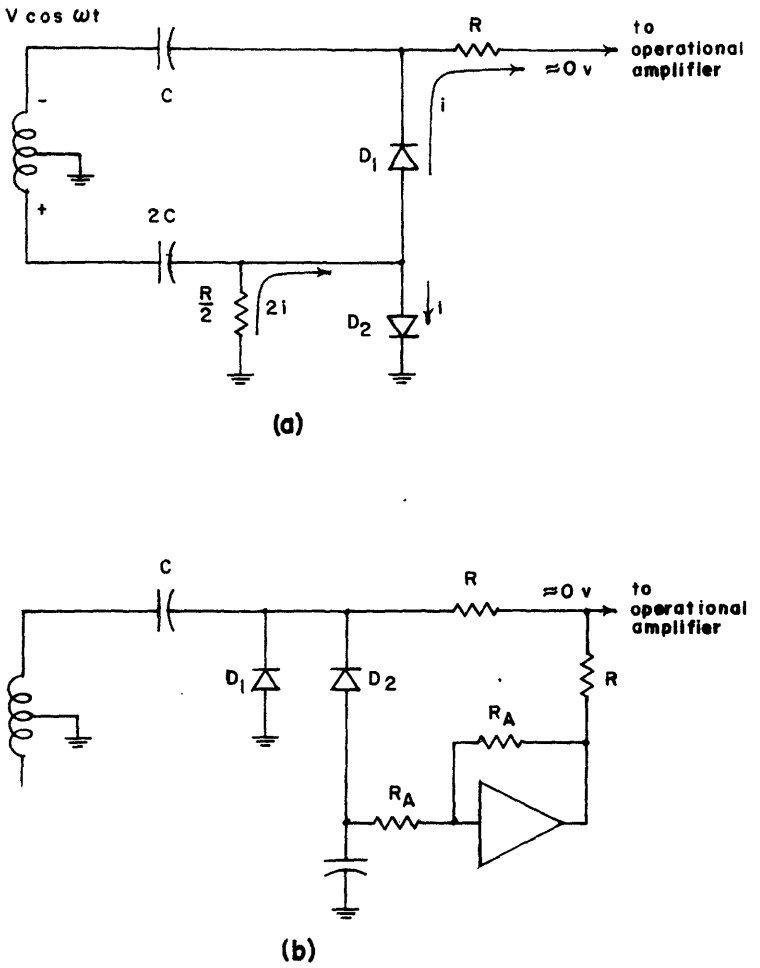

Fig. 8.1. Proposed high-linearity rectifiers.

Measurement of the d-c voltage would, by Eq. 2.36, determine the r-f voltage. Obviously this a highly inconvenient process. Its only value is in calibration of other voltmeters, and then only if the accuracy exceeds that attainable by such simpler means as heater-thermocouple combinations.

Ion-Collector Pulse Circuits

Although no clear-cut directions for improvement of the ion-collector pulse circuits can be given, their overall performance can undoubtedly be substantially improved by further development work. In particular, the scheme of signal differentiation might well be abandoned and one of the alternative methods of handling pulse baseline shift employed.

It should be noted that since thesis work was begun nuclear-instrumentation circuits that might well satisfy all requirements of the pulse system have become commercially available.*

---

* E.g., Edgerton, Germeshausen and Grier, Inc., M100 Modular Counting System.

APPENDIX A

Coefficients in Series Expansion of Solutions of Mathieu's Equation

y-Direction Coefficients

Equation 2.16 is based on the assumption that the two coefficients c_2 and c_{-2} in the series solution for ion motion are nearly equal. The proof of that assumption is as follows: The series coefficients may be evaluated from continued-fraction expansions:[48*]

$$\left(\frac{c_{2m}}{c_{2m-2}}\right)_y = \frac{-q/(2m+\beta_y)^2}{1 + a/(2m+\beta_y)^2} - \frac{q^2/(2m+\beta_y)^2(2m+2+\beta_y)^2}{1 + a/(2m+2+\beta_y)^2} - \cdots \quad (A.1)$$

$$\left(\frac{c_{2m-2}}{c_{2m}}\right)_y = \frac{-q/(2m-2+\beta_y)^2}{1 + a/(2m-2+\beta_y)^2} - \frac{q^2/(2m-2+\beta_y)^2(2m-4+\beta_y)^2}{1 + a/(2m-4+\beta_y)^2} - \cdots \quad (A.2)$$

If it is assumed that $c_o = 1$, $\beta_y \ll 1$, $q \lesssim 0.7$, $a \lesssim 0.23$, expansions for c_2 and c_{-2} may be terminated with the first term, so

$$c_2 \lesssim \frac{-q/(2+\beta_y)^2}{1 + a/(2+\beta_y)^2} = \frac{-q}{(2+\beta_y)^2 + a} , \quad (A.3)$$

$$c_{-2} \lesssim \frac{-q(-2+\beta_y)^2}{1 + a/(-2+\beta_y)^2} = \frac{-q}{(2-\beta_y)^2 + a} . \quad (A.4)$$

---

* Consideration is taken of the fact that "-a" of the y-equation (Eq. 2.10) equals "+a" of the canonical Mathieu equation (Eq. 2.11).

If $\beta_y = 0$, the two coefficients are exactly equal. For non-zero β_y one may write

$$c_2 - c_{-2} \approx \frac{-q\left[(2 - \beta_y)^2 - (2 + \beta_y)^2\right]}{\left[(2 + \beta_y)^2 + a\right]\left[(2 - \beta_y)^2 + a\right]} = \frac{-c_2 8\beta_y^2}{(2 - \beta_y)^2 + a} \quad . \quad (A.5)$$

According to Paul, et al.,[6] after a straight-line approximation to the stability region and constant-β lines, β_y can be approximated at $q = 0.706$ by

$$\beta_y^2 = \frac{0.23699 - a_{0.706}}{0.79375} \quad . \quad (A.6)$$

Equation 2.23 can be used to eliminated $a_{0.706}$ from Eq. A.6 to give

$$\beta_y^2 = 0.224 \frac{\Delta m}{m} \quad , \quad (A.7)$$

which, in turn, can be applied to Eq. A.5 to give, approximately,

$$c_2 - c_{-2} \approx -0.45 \left(\frac{\Delta m}{m}\right) c_2 \quad . \quad (A.8)$$

This shows that for any reasonable resolution, say $m/\Delta m$ 10, the difference between c_2 and c_{-2} is small.

x-Direction Coefficients

The continued-fraction expansions for the series-solution coefficients (Eqs. A.1 and A.2) may be applied to the x solution as well as to the y, but the signs of a and q in the expansions must be changed, to correspond to the reversed signs in the original Mathieu's equation (Eq. 2.9). The first coefficients may again be evaluated by terminating the expansion with the first term, but

this time with the assumption $1 - \beta_x \ll 1$, or $\beta_x \quad 1$. Then

$$c_2 \simeq \frac{q/(3)^2}{1 - a/(3)^2} = \frac{q}{9(1 - a/9)} \simeq \frac{0.7}{9(1 - 0.03)} \ll 1 \qquad (A.9)$$

and

$$c_{-2} \simeq \frac{q/(1)^2}{1 - a/(1)^2} = \frac{q}{1 - a} \quad . \qquad (A.10)$$

The second coefficient is approximately unity, as may be observed from

$$1 - c_{-2} \simeq 1 - \frac{q}{1 - a} = \frac{1 - a - q}{1 - a} \simeq \frac{1 - 0.7 - 0.23}{1 - 0.23} \ll 1 \; .$$

APPENDIX B

Tank Coil Design

The two sets of r-f transformers used in the r-f rod driver, the output tank coils and the interstage transformers, are similar in many essentials. In each case a transformer is driven from a high-impedance source, tuned with a single variable capacitor in the secondary circuit, and required to have a predetermined secondary-to-primary voltage ratio. The circuit theory common to both sets of transformers and the design techniques used for each is presented in this Appendix.

Circuit Theory of Single-Tuned Transformers

If coil losses are ignored, a reasonable equivalent circuit for a coupling transformer is that of Fig. B.1. Capacitor C_p represents stray capacitance of the circuits associated with the primary coil, plus distributed capacitance of the primary itself. Capacitor C_s includes stray and distributed capacitance associated with the secondary, plus the tuning capacitor used to obtain resonance.

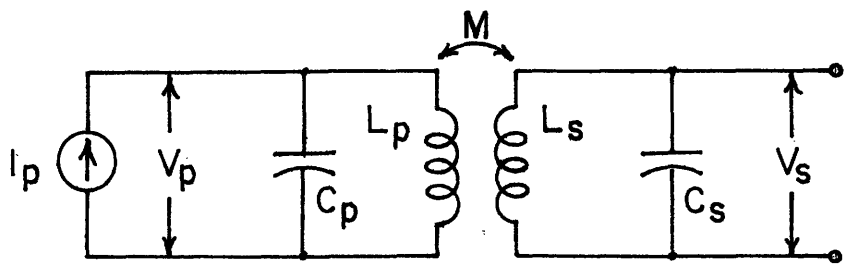

Fig. B.1. Tuned coupling-transformer circuit.

Solution of the loop equations for the circuit gives, for a frequency ω, the following equations for transfer impedance and voltage ratio:

$$\frac{V_s}{I_p} = \frac{j\omega M}{\omega^4 C_p C_s (L_p L_s - M^2) - \omega^2 (C_p L_p + C_s L_s) + 1} \qquad (B.1)$$

$$\frac{V_s}{V_p} = \frac{M}{L_p - \omega^2 (L_p L_s - M^2) C_s} \quad . \qquad (B.2)$$

The first equation shows that the circuit has two resonant frequencies, the two pairs of roots of

$$\omega^4 C_p C_s (L_p L_s - M^2) - \omega^2 (C_p L_p + C_s L_s) + 1 = 0. \qquad (B.3)$$

If C_p is negligible, this resonance equation reduces to

$$\omega^2 = \frac{1}{C_s L_s} \quad , \qquad (B.4)$$

and the voltage-ratio equation becomes

$$\frac{V_s}{V_p} = \frac{L_s}{M} \quad . \qquad (B.5)$$

In the general case the primary capacitance is, however, not negligible. It is then necessary to develop tractable design equations for the inductances in terms of known or assumed quantities: the capacitances C_p and C_s, the voltage ratio V_s/V_p, and the frequency ω. As a first step, the primary inductance L_p can be eliminated from the resonance

equation (Eq. B.3), by use of Eq. B.2, to give

$$\omega^2\left(L_s C_s + M C_p \frac{V_p}{V_s}\right) = 1. \qquad (B.6)$$

Then the definition of coefficient of coupling, k, for two coils, expressed as

$$L_p = \frac{M^2}{k^2 L_s} \qquad (B.7)$$

can be used to eliminate L_p from the voltage-ratio equation, which becomes

$$\frac{V_s}{V_p} = \frac{L_s}{M\left[\frac{1}{k^2} - \omega^2 L_s C_s\left(\frac{1}{k^2} - 1\right)\right]} . \qquad (B.8)$$

The mutual inductance M can be eliminated between Eqs. B.6 and B.8 to give an expression for the secondary inductance in terms of the capacitances, the frequency, and the unknown coefficient of coupling:

$$L_s^2\left(\frac{1}{k^2} - 1\right)C_s^2\omega^4 - L_s\omega^2\left[C_s\left(\frac{2}{k^2} - 1\right) + C_p\left(\frac{V_p}{V_s}\right)^2\right] + \frac{1}{k^2} = 0. \qquad (B.9)$$

The coefficient of coupling varies slowly as a function of coil structure; for design purposes a reasonable value may be assumed and Eq. B.9 solved for

$$L_s = \frac{\frac{2}{k^2} + \left[\frac{C_p}{C_s}\left(\frac{V_p}{V_s}\right)^2 - 1\right] - \sqrt{\left[\frac{C_p}{C_s}\left(\frac{V_p}{V_s}\right)^2 - 1\right]^2 + \frac{4}{k^2}\frac{C_p}{C_s}\left(\frac{V_p}{V_s}\right)^2}}{2\omega^2\left(\frac{1}{k^2} - 1\right)C_s} . \qquad (B.10)$$

There are, of course, actually two solutions for L_s, for each of which there will be two circuit resonant frequencies. Only the smaller value of L_s (for which the desired resonant frequency is the lower one) is used, because the smaller coil is more easily fabricated.

Equation B.8 may be rewritten to give the mutual inductance in terms of the value of L_s determined from Eq. B.10:

$$M = \frac{L_s\left(\frac{V_p}{V_s}\right)}{\frac{1}{k^2} - \omega^2 L_s C_s\left(\frac{1}{k^2} - 1\right)} \quad . \qquad \text{(B.11)}$$

A final design equation is a solution of Eq. B.3 for C_s:

$$C_s = \frac{1 - L_p C_p \omega^2}{\omega^2\left[L_s - C_p(L_s L_p - M^2)\omega^2\right]} \quad . \qquad \text{(B.12)}$$

Output Tank Coil Design

Four balanced-primary, balanced-secondary plug-in output tank coils are needed, one for each operation frequency. The secondary winding is opened at the center to allow application of d-c voltages to the quadrupole rods. The primary capacitance, consisting of two 4-65A output capacitances in series (about 1 pf) and the distributed capacitance of the coil, is negligible, so the simple approximations of Eqs. B.4 and B.5 are adequate for design computations.

The minimum voltage ratio for the transformer is determined

by the required maximum output voltage for the quadrupole, about 2500 v peak measured across one half of the secondary, and the permissible plate-voltage swing on the tetrodes. For maximum energy transfer and minimum plate dissipation the tetrode plate swing should be as large as possible, or the secondary-primary voltage ratio as small as possible. The limitation is that on negative r-f peaks, when the plate voltage is substantially lower than that of the screen, cathode current is diverted from the plate to the screen, limiting peak plate current and presenting the possibility of overdissipation of the screen. It was found experimentally that for a plate supply of 1800 v and a screen voltage of 300 v the maximum permissible plate voltage swing was about 1500 v, or roughly the amount for which the lowest instantaneous plate voltage equalled the screen voltage.

There is, however, another factor that makes it desirable to make the secondary-primary voltage ratio as large as possible: the introduction of symmetric-mode signals into the secondary because of the difference in mutual inductance from one half of the primary to the corresponding half of the secondary and that from one half of the primary to the opposite side of the secondary (see Appendix C). Any scheme for cancellation of this effect by special windings, such as, for example, a bifilar-wound primary, seems fraught with difficulties involving interwinding capacitance. The simplest method to reduce the difference in mutual inductances to a minimum is to

compress the primary winding to a minimal length located at the center of the secondary. In practice, this means a small value of overall mutual inductance, M, and a high secondary-to-primary voltage ratio.

There is still one more benefit in the increase in voltage ratio: the Class C tetrode driver amplifier operates with longer conduction times and so lower harmonic distortion.

When all factors are considered, the secondary-to-primary voltage ratio is therefore a compromise between high output capability and low symmetric-mode distortion.

A configuration of coaxial, concentric solenoids, with the high-inductance secondary the outer coil was chosen for the tank coil. Low-loss "air-wound" coils were used for the three highest frequencies. The lowest frequency required more inductance than could be obtained from a mechanically rigid air-wound coil, so a structure supported on phenolic tubing was used. Primary and secondary solenoids were wound in the same sense, that of a right-hand screw, so that adjacent ends would have the same r-f polarity and energy storage in interwinding capacitance would be minimized. An even number of turns was used on both coils so that the center tap could be brought out in the same radial direction as the end leads of the coil; a gap between the two halves of the secondary permitted the primary center-tap lead to be brought out. Finally, high-melting-point Lexan supporting insulation was used for the two

highest-frequency coils because of coil heating; even with a 100 cfm cooling blower, the coil temperature rises to 75°C after several minutes of full output at 3.3103 Mc.

Coil design involves datisfying the specific requirements on L_s and M. The most simple equation for a practical solenoid is adequate for calculation of the secondary inductance:[49]

$$L = \frac{n^2 r^2}{9r + 10\ell} \quad , \tag{B.13}$$

where n is the total number of turns, r the coil radius and ℓ the coil length, measured in inches. This equation is solved for the number of turns (n) in terms of the specified L_s and arbitrarily selected r and ℓ.

The applicable equation for mutual inductance for coaxial, concentric coils with the outer coil the longer is

$$M = 0.0501 \frac{r_s^2 r_p^2}{\sqrt{r_s^2 + \frac{\ell_s}{4}}^2} (1 + c) \quad , \tag{B.14}$$

where

$$c = \frac{r_s^2 r_p^2}{8\left(r_s^2 + \frac{\ell_s^2}{4}\right)^2} \left(3 - \frac{\ell_p^2}{r_p^2}\right) \tag{B.15}$$

and n_p and n_s are primary and secondary turns, r_p and r_s are primary and secondary coil radii, and ℓ_p and ℓ_s are primary and secondary coil lengths, respectively, with all dimensions in inches.[50] The correction term c is usually small with respect to unity.

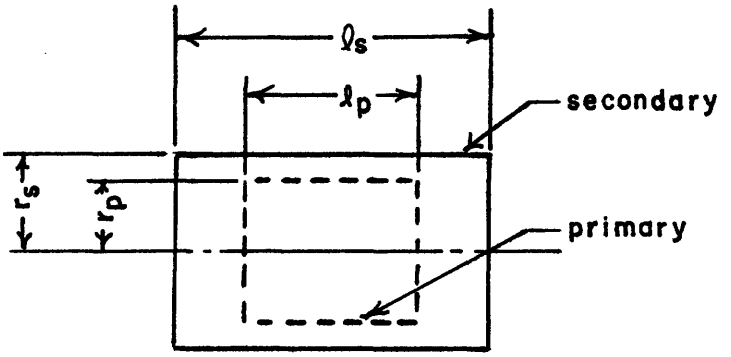

Fig. B.2. Coupled-coil configuration.

Equation B.14 is used to design the primary. All secondary parameters are established by the design based on the required L_s. The radius of the primary coil is assumed, the correction term c assumed zero and Eq. B.14 solved for the number of primary turns, n_p. A suitable length for the primary is then determined by mechanical considerations, a value of c determined from Eq. B.15 and Eq. B.14 solved again for a new value of n_p. This process converges rapidly, usually within one iteration.

The secondary coil must resonate at 3.2103, 2.27, 1.6051, or 1.135 Mc with the end-to-end value of quadrupole, cable, and circuit capacitance. Quadrupole capacitance is 81 pf, cable capacitance (for $3\frac{1}{2}$ ft RG-11/U between the driver output and the quadrupole) 35 pf, mean tuning capacitance 32 pf, and miscellaneous stray and circuit capacitance 7 pf, for a total of 155 pf at the mid position of the tuning capacitor, with a possibility of a $\pm$17 pf adjustment.

It was experimentally determined that, for operation at

3.2103 Mc, power considerations required the secondary-to-primary voltage ratio to be its minimum value of 2500/1500 = 1.7. Higher voltage ratios were used to minimize harmonic distortion at the less demanding lower frequencies: 1.8 at 2.27 and 1.6051 Mc, 2.0 at 1.135 Mc.

The design procedure for the output tank coils can be illustrated by the design of the 3.2103 Mc coil. The secondary must, by Eq. B.4, resonate with 155 pf, which requires $L_s = 15.8\ \mu h$. To minimize losses and heating the coil should be as large as possible, a requirement that leads to a diameter of 3 inches, the largest available in commercial coil stock, and a length of 3 inches, fixed by the plug strip on which the coil is mounted. Solution of Eq. B.13 then gives 18 turns for the coil, or a pitch of 6 turns/inch. With this rather coarse pitch a 1-turn gap in the center is an adequate space in which to bring out the primary center-tap lead. The calculation for number of turns on the coil is repeated with a more accurate estimate of coil length, $\ell = (n + 1)/6$, and again it is found that 18 turns is required. Final inductance calculations show that an 18-turn coil 3 inches in diameter and $3\frac{1}{6}$ inches long has an inductance $L_s = 16.1\ \mu h$.

By Eq. B.5 a voltage ratio of 1.7 requires a mutual inductance $M = 9.48\ \mu h$. To minimize symmetric-mode coupling the primary must be as short as possible. It is therefore made with the largest diameter, $2\frac{1}{2}$ inches, that will fit inside the secondary with the

tightest winding pitch available, 10 turns/inch. Use of Eq. B.14 with c = 0 gives n_p = 14.7 turns. The nearest even integer, 14, makes c = 0.034. A second solution of Eq. B.14 with this value of c gives n_p = 14.2 turns. A value n_p = 14 turns is then assumed and M computed from Eq. B.14: M = 9.33 μh.

Interstage Transformer Design

Two switch-selected interstage transformers are used, one for the two lower operation frequencies, one for the two upper frequencies. Each has an unbalanced primary, a balanced, center-tapped secondary, and a Faraday shield between (to prevent inter-winding capacitance from introducing an unbalanced signal in the output). The secondary is tuned by a variable capacitor and switched fixed capacitors. The primary capacitance, which consists of the output capacitance of the buffer amplifier, coil distributed capacitance, and stray circuit capacitance, is not negligible, so the more involved design equations must be used.

The transformer voltage ratio is determined by the requirement that for fixed output voltage the pentode plate swing be at the highest possible level without excessive screen conduction on the negative r-f peaks. For the required output voltage of 450 volts peak, measured from end to end of the secondary, and a buffer d-c plate supply of 300 v, screen supply of 160 v, it was found experimentally that the optimum secondary-to-primary voltage ratio was about 2.3:1.

A systematic design procedure for an interstage transformer is as follows:

(1) Assumption of parameters. The upper of the two frequencies at which the transformer will operate is taken as the design frequency. The appropriate voltage ratio V_s/V_p is selected. A secondary capacitance, C_s (which consists of the tuning capacitance, driver-amplifier input capacitance, monitoring capacitances, coil distributed capacitance and stray circuit capacitance), and a primary capacitance, C_p are assumed. The coil coefficient of coupling is estimated. (A rough estimate is the square root of the ratio of the volumes of the primary and secondary.)

(2) The secondary inductance, L_s, is calculated from Eq.B.10 with the parameter values assumed in step (1).

(3) The mutual inductance, M, is calculated from Eq. B.11.

(4) The primary and secondary coils are designed for the determined values of L_s and M by means of Eqs. B.13 through B.15 and the technique employed in the design of the output tank coils.

(5) As a check, the actual C_s necessary to tune the coils and the actual voltage ratio V_s/V_p are computed by means of Eqs. B.12 and B.2, respectively.

(6) Equation B.12 is used to compute the C_s necessary for resonance and Eq. B.2 to check the voltage ratio for operation at the lower of the two frequencies.

The technique used to design the 3.2103 and 2.27 Mc inter-

stage transformer provides an example. The design voltage ratio is $V_s/V_p = 2.3$. It is assumed that the secondary capacitance C_s = 60 pf, the primary capacitance C_p = 30 pf. This rather high primary capacitance has been found a reasonable estimate in light of the high distributed capacitance in the coils used. A first estimate for coefficient of coupling for coils of the type used in the interstage transformer is k = 0.7. At 3.2103 Mc these values substituted in Eq. B.10 give L_s = 37.6 μh, and substituted in Eq. B.11 give M = 15.1 μh.

Commercial coil stock $1\frac{1}{4}$-inch in diameter and 32 turns/inch is assumed for the secondary coil. Use of a design procedure similar to that employed for the output tank coil secondary gives n_s = 42 turns, L_s = 36.7 μh. The primary is assumed to be 32-turn/inch, 1-inch-diameter commercial coil stock. Again a design procedure similar to that previously employed gives n_p = 26 turns, M = 15.2 μh, L_p = 13.4 μh, and k = 0.68. These values inserted in the check equations give C_s = 61.2 pf, V_s/V_p = 2.22. At 2.27 Mc the required tuning capacitance is C_s = 128 pf, the voltage ratio V_s/V_p = 2.32.

APPENDIX C

Symmetric Signals in Balanced, Inductively Coupled Circuits

Elementary theory, which assumes a transformer with unity coupling between primary and secondary, predicts no inductive coupling of symmetric-mode signals into the output of a balanced circuit such as that used in the output of the r-f rod driver. However, there is inductive coupling caused by flux leakage in the transformer.

A good representation of the output tank coil and associated circuits for symmetric signals is that shown in Fig. C.1. The primary consists of two mutually coupled coils driven by two current sources; an equivalent circuit is a single coil driven by one current source, as in Fig. C.2. The secondary likewise consists of two mutually coupled coils, with one side of each going to the output and the other to ground through an impedance Z_s that represents the impedance of chokes L_{13} and L_{14} in the rod-driver circuit (Fig. 4.4) and the stray capacitance to ground from the rather bulky "transmitting" mica capacitor, C_{20}; an equivalent circuit is a single coil connected to ground through Z_s. There are four primary-to-secondary mutual inductances: two inductances M_1 between adjacent sides of the primary and secondary, two inductances M_2 between opposite sides of the primary and secondary; these are equivalent to a single mutual inductance equal to half the difference between M_1 and M_2. It is this mutual

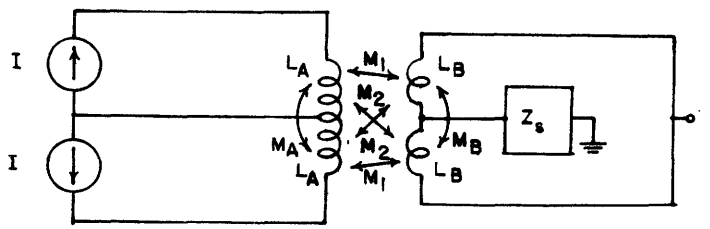

Fig. C.1. Rod-driver output equivalent circuit for symmetric signals.

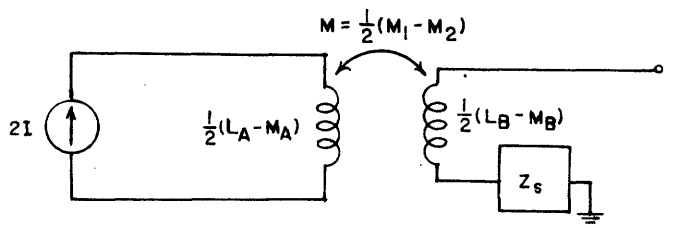

Fig. C.2. Output circuit of Fig. C.1 collapsed into simpler form.

inductance that provides the coupling for symmetric signals between primary and secondary. Because coils in which $M_1 = M_2$ are impractical, and it is impossible to completely eliminate the current path through Z_s, Fig. C.2 shows that there will be symmetric, even-order harmonic signals inductively coupled into the rod-driver output.

APPENDIX D

Self-Checking Balance Detector Algorithm

"Self-checking" balance detectors are used on both the d-c and r-f rod drivers to ensure the balance, or antisymmetry, of the d-c and r-f voltages. An algorithm for adjustments of the detectors is presented in this Appendix.

Either balance detector can be represented by the flow graph of Fig. D.1. The balance-detector output (V_z) is, within the constant k, the sum of its two inputs multiplied by the factors $1 + \delta$ and $1 - \delta$. Perfect balance of the detector corresponds to $\delta = 0$. The detector is connected through a reversing switch to the two rod-driver outputs, v_+ and v_-. It shall be assumed that the rod-driver outputs are antisymmetric, except for multiplicative error factors $1 + \epsilon$ and $1 - \epsilon$, that is

$$v_+ = V_A(1 + \epsilon) \quad \text{and} \quad v_- = -V_A(1 - \epsilon).$$

Then $\epsilon = 0$ is the condition of perfect antisymmetry.

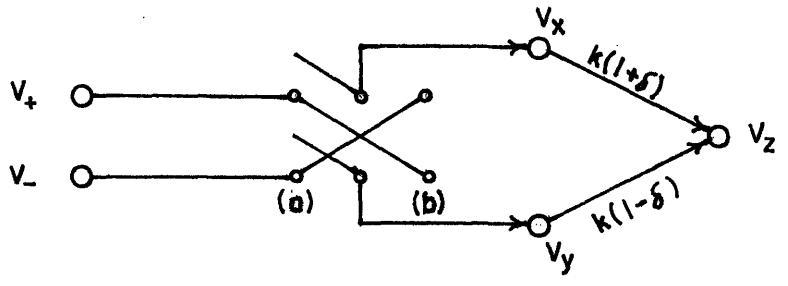

Fig. D.1. Balance-detector flow graph.

According as the reversing switch is in position (a) or (b) the balance-detector output is

$$v_z(a) = 2k(\epsilon + \delta)V_A$$

or

$$v_z(b) = 2k(\epsilon - \delta)V_A$$

respectively. Clearly $v_z(a) = v_z(b) = 0$ implies $\epsilon = \delta = 0$, and perfect balance.

The balance algorithm is as follows:

(1) Assume the switch is initially in position (a), and that $\epsilon = \epsilon_o \neq 0$ and $\delta = \delta_o \neq 0$. Then the initial output voltage is

$$\left[v_z(a)\right]_o = 2k(\epsilon_o + \delta_o)V_A \quad .$$

The detector balance, characterized by δ, is adjusted until the output voltage is zero:

$$\left[v_z(a)\right]_1 = 0 = 2k(\epsilon_o + \delta_1)V_A .$$

Therefore,

$$\delta_1 = -\epsilon_o \quad .$$

(2) The switch is thrown to position (b). The output voltage is then

$$\left[v_z(b)\right]_2 = 2k(2\epsilon_o)V_A \quad .$$

(3) The rod-driver balance, characterized by ϵ, is adjusted until the output voltage is one half $\left[v_z(b)\right]_2$:

$$\left[v_z(b)\right]_3 = 2k(\epsilon_3 + \epsilon_o)V_A = \frac{1}{2}(2k)(2\epsilon_o)V_A \quad .$$

Therefore,

$$\epsilon_3 = 0.$$

(4) The detector balance is again adjusted until the output vanishes:

$$\left[v_z(b)\right]_4 = 0 = 2k(0 - \delta_4)V_A \ .$$

Therefore

$$\delta_4 = 0,$$

and the balance is complete.

In practice, a fifth step is added to the balance process:

(5) As a check, the switch is again thrown to position (a) and the output observed. If it is not zero, there is some maladjustment, and the adjustment algorithm is continued by adjustment of the rod driver, as in step (3), except with switch positions (a) and (b) interchanged.

It should be noticed that the algorithm depends upon measurements of only the magnitude of the detector output voltage, $|v_z|$, and so is equally applicable to the r-f and d-c rod drivers.

There is one complicating factor in the case of the r-f rod driver. The output contains a number of harmonics, primarily in a symmetric mode. This means that even with both the rod driver and the detector adjusted for perfect balance there is still a residual detector output. Experimentally, it has been found best to modify the algorithm in two ways: (1) Each time the algorithm specifies adjustment for zero output, adjustment is instead made to minimum output. (2) Each time the algorithm specifies adjustment for half the previous output voltage, adjustment is instead made to the arithmetic mean of the previous output and the minimum output.

APPENDIX E

Pulse-System Test Apparatus

Special apparatus is necessary to provide pulses with which to test the circuits of the ion-detector pulse system. The use of a Tektronix Type N Sampling Unit as the basic pulse measuring device places two special requirements upon this apparatus: (1) It must provide a trigger signal for the sampling unit. (2) For convenience in observation, the source repetion frequency must be high enough to make possible a sample of a complete waveform in less than one second. These two requirements on the basic pulse generator were met by a Tektronix 111 Pulse Generator, which uses an avalanche transistor to generate fast (nanosecond rise) pulses at repetition rates up to 100 kc.

Certain requirements on the nature of the output pulses have to be met: (1) The pulse width should approximate that of an electron multiplier, some 4 nsec at half amplitude. (2) The pulse should come from an effective current source, to approximate an electron-multiplier anode. (3) The pulse should be free of any "tail" that would appear as post-pulse noise in the ion-detector system output. (4) Pulse amplitude should be variable over a wide range. (5) It should be possible to obtain two or more pulses, of different amplitudes, in quick succession - within nanoseconds.

A system that meets all these requirements is shown in Fig. E.1. The output pulse of the Tektronix 111 Pulse Generator

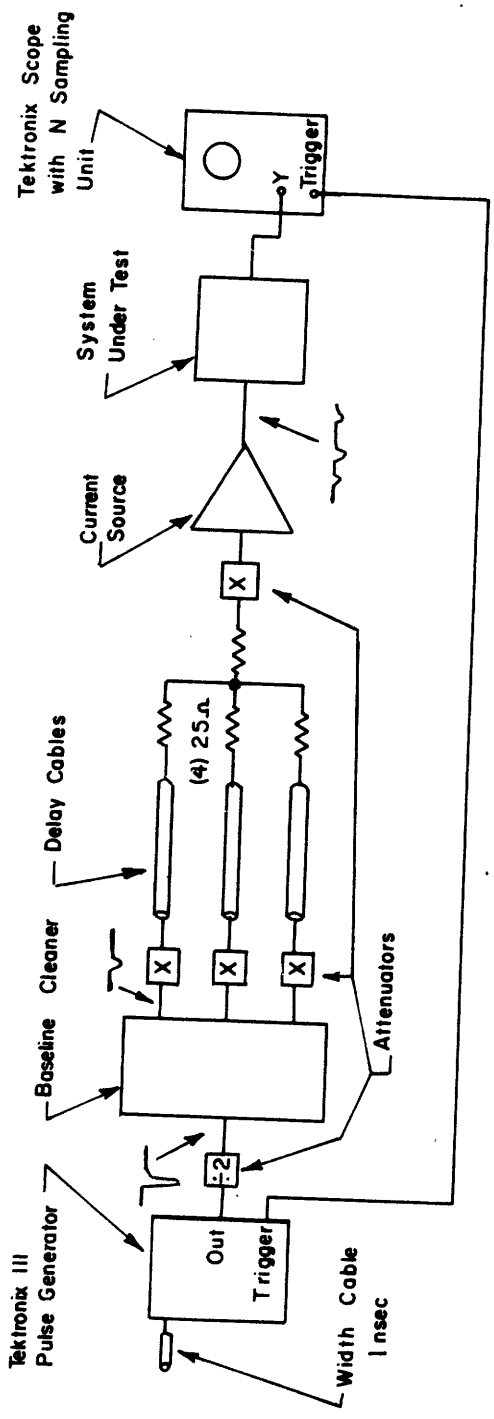

Fig. E.1. Pulse-system test apparatus.

has a long, slowly decaying tail that extends more than 50 nsec, so it is necessary to pass it through a "pulse baseline cleaner" (Fig. E.2), actually two cascaded diode clippers that pass only the negative peak of the input pulse to three parallel outputs. The resulting pulse is carried over as many as three cables of different lengths to yield three pulses that are combined in a mixer and applied to the pulse current source, actually a grounded-base transistor amplifier (Fig. E.3). The output of the current source drives the preamplifier of the ion-detector system.

The test apparatus has a maximum output pulse of about 6×10^8 electrons with an essentially triangular shape: amplitude 2 ma, full width at half maximum 5 nsec (Fig. 6.7). A narrower pulse, which may correspond more closely to an electron-multiplier output, can be obtained by eliminating the external timing cable of the Tektronix 111. This shortened pulse is obtained, however, at the price of reduced total charge.

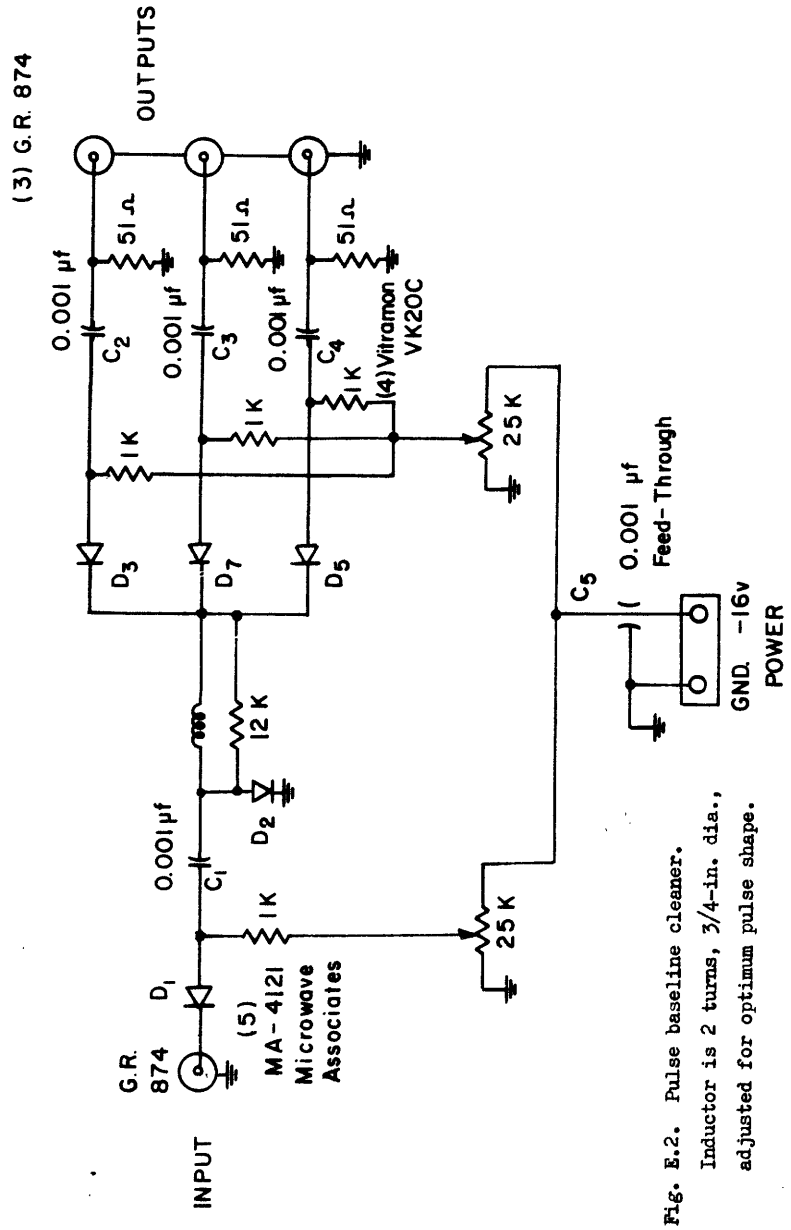

Fig. E.2. Pulse baseline cleaner. Inductor is 2 turns, 3/4-in. dia., adjusted for optimum pulse shape.

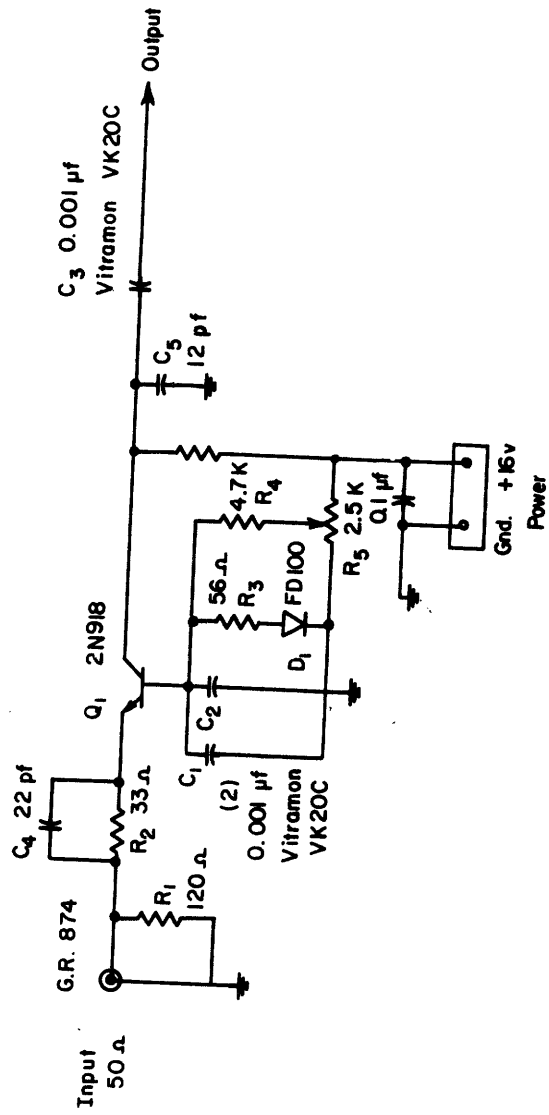

Fig. E.3. Test current source. Capacitor C_5 is chosen to approximate electron-multiplier anode capacitance. R_5 is adjusted for +5 v on Q_1 collector.

REFERENCES

1. W. Paul and H. Steinwedel, Z. Naturforschung 8a, 448 (1953).

2. W. Paul and M. Raether, Z. Physik 140, 262 (1955).

3. W. Paul and H. Steinwedel, German Patent 944,900 (1956).

4. U. von Zahn, Z. Physik 168, 129 (1962).

5. H. Matsuda, J. Phys. Soc. Japan 11, 183 (1956).

6. W. Paul, H.P. Reinhard and U. von Zahn, Z. Physik 152, 143 (1958).

7. K. Günther, Vacuum 10, 293 (1960).

8. C.K. Crawford and C.E. Woodward, Tech. Rep. 175, Lab. Ins. Res., Mass. Inst. Tech., November, 1962.

9. N.W. McLachlan, "Theory and Application of Mathieu Functions," Oxford University Press, London, 1947, p. 10.

10. W.M. Brubaker, unpublished, Bell and Howell Research Center, Pasadena, California, December 14, 1960.

11. C.E. Woodward and C.K. Crawford, Tech. Rep. 176, Lab. Ins. Res., Mass. Inst. Tech., January, 1963, p. 8.

12. F. von Busch and W. Paul, Z. Physik 164, 588 (1961).

13. H.G. Bennewitz and R. Wedemeyer, Z. Physik 172, 1 (1963).

14. I.E. Dayton, F.C. Shoemaker and R.F. Mozley, Rev. Sci. Instr. 25, 485 (1954).

15. J. Millman and H. Taub, "Pulse and Digital Circuits," McGraw-Hill Book Co., New York, N.Y., 1956, p. 221.

16. C.E. Woodward and C.K. Crawford, op. cit., p. 16.

17. J. Truxal, "Automatic Feedback Control System Synthesis," McGraw-Hill Book Co., New York, N.Y., 1955, p. 221.

18. J.S. Allen, Phys. Rev. 55, 966 (1939).

19. A.I. Akishin, Soviet Phys. - Uspekhi 66,(1) 113 (1958).

20. P.I. Richards and E.E. Hays, Rev. Sci. Instr. 21, 99 (1950).

21. E. Schönheit, Z. Naturforschung 11a, 819 (1956).

22. F.D.S. Butement and N.P. Finkelstein, J. Sci. Instr. 37, 328 (1960).

23. C.F. Barnett, G.E. Evans and P.M. Stier, Rev. Sci. Instr. 25, 1112 (1954).

24. T. Sugiura, Bull. Chem. Soc. Japan 35, 1257 (1962).

25. F.A. White and T.L. Collins, Applied Spectroscopy 8, 17 (1954).

26. K. Koyama and R.E. Connally, Rev. Sci. Instr. 28, 833 (1957).

27. L. Cathey, AEC Report DP-498, 1960.

28. G.W. Barton, Jr., L.E. Gibson and L.F. Tolman, Anal. Chem. 32, 1599 (1960).

29. W. Shockley and J.R. Pierce, Proc. IRE 26, 321 (1938).

30. R.E. Barrington and J.M. Anderson, Proc. Phys. Soc. 72, Pt. 5, 717 (1958).

31. R.F. Tustin, Q.A. Kerns, and H.K. Knudsen, IRE Trans. Nuc. Sci. NS-9, No. 3, 118 (1962).

32. F.J. Lombard and F. Martin, Rev. Sci. Instr. 32, 200 (1961).

33. W.H. Johnston, AEC Report JLI-650-8-8, 1962.

34. W.B. Davenport,Jr., and W.L. Root, "Random Signals and Noise," McGraw-Hill Book Co., New York, N.Y., 1958, p. 122.

35. W.B. Davenport, Jr., and W.L. Root, loc. cit., p. 144.

36. R.D. Evans, "The Atomic Nucleus," McGraw-Hill Book Co., New York, N.Y., 1955, p. 787.

37. R.D. Evans, loc. cit., p. 786.

38. R. Jost, Helv. Phys. Acta 20, 173 (1947). Unfortunately this paper is marred by numerous typographical errors, so all results must be checked before use.

39. H. Richter, Math. Ann. 118, 145 (1942).

40. Y.W. Lee, "Statistical Theory of Communication," John Wiley and Sons, New York, N.Y., 1960, Chapts.14-16.

41. C.H. Vincent, Nucl. Inst. and Meth. 23, 193 (1963).

42. Z.H. Fröhner, Nukleonik 5, 82 (1963).

43. J. Millmand and H. Taub, op. cit., p. 120.

44. H. Verweij, Nuc. Instr. Meth. 24, 39 (1963).

45. V.G.K. Reddi, Fairchild Semiconductor Application Data, APP-32/2, Sept. 1961.

46. R. Sugarman, F.C. Merritt and W.A. Higinbotham, AEC Report BNL-711 (T-248, Brookhaven National Laboratory, February, 1962).

47. R.D. Middlebrook, "Junction Transistor Theory," John Wiley and Sons, New York, N.Y., 1957, p. 220.

48. N.W. McLachlan, op. cit., p. 106.

49. F.E. Terman, "Radio Engineer's Handbook," McGraw-Hill Book Co., New York, N.Y., 1943, p. 55.

50. F.E. Terman, op. cit., p. 71.

51. C.E. Woodward and C.K. Crawford, op. cit., p. 29.

52. U. von Zahn, Rev. Sci. Instr. 34, 1 (1963).

BIOGRAPHICAL NOTE

Charles E. Woodward

Born: Harvard, Nebraska, March 31, 1931.

Eduation: Iowa State College, 1953 to 1957, B.S. in Electrical Engineering (1957).

Massachusetts Institute of Technology, 1957 to 1964, S.M. in Electrical Engineering (1960).

Professional Experience: (1) Staff Member, M.I.T. Lincoln Laboratory, 1957 to 1960. Designed circuits for digital computers.

(2) Research Assistant, M.I.T. Department of Electrical Engineering, 1957 to 1958. Wrote digital-computer utility programs.

(3) Teaching Assistant, M.I.T. Department of Electrical Engineering, 1960. Taught one laboratory course in electronic circuits.

(4) Research Assistant, M.I.T. Laboratory for Insulation Research, 1961 to 1964. Designed circuits for quadrupole mass spectrometer.

Professional Society: Member, Institute of Electrical and Electronics Engineers.